

UNCLASSIFIED

AD NUMBER

AD832007

LIMITATION CHANGES

TO:

Approved for public release; distribution is unlimited.

FROM:

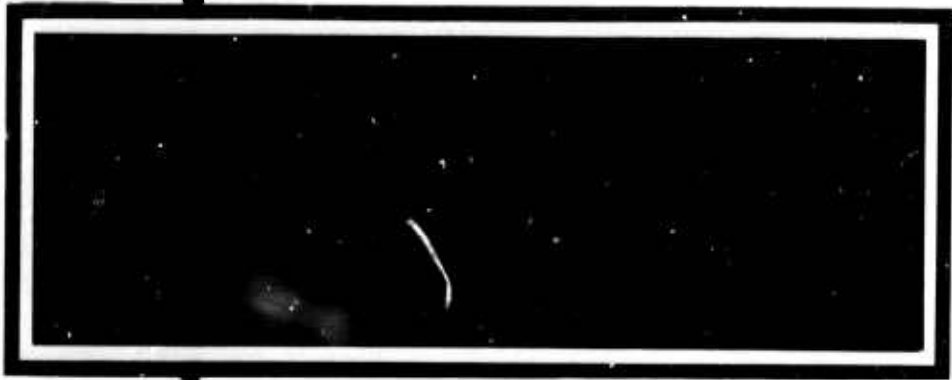
Distribution authorized to U.S. Gov't. agencies and their contractors; Critical Technology; FEB 1968. Other requests shall be referred to Air Force Technical Application Center, Washington, DC 20333. This document contains export-controlled technical data.

AUTHORITY

usaf ltr, 25 jan 1972

THIS PAGE IS UNCLASSIFIED

AD832007



DDC
RECEIVED
MAY 15 1968
B



TEXAS INSTRUMENTS

SCIENCE SERVICES DIVISION



This document is subject to special export controls and each transmittal to foreign governments or foreign nationals may be made only with prior approval of Chief, AFTAC.

attn: vsc Wash, DC 20333

VELA T/7701

PREDICTION ERROR AND
ADAPTIVE MAXIMUM-LIKELIHOOD PROCESSING

ADVANCED ARRAY RESEARCH
Special Report No. 10

Prepared by

Aaron H. Booker Ronald J. Holyer

John P. Burg, Project Scientist
George D. Hair, Program Manager
Telephone: 1-214-238-3473

TEXAS INSTRUMENTS INCORPORATED
Science Services Division
P.O. Box 5621
Dallas, Texas 75222

Contract No.: F33657-67-C-0708-P001
Contract Date: 15 December 1966
Amount of Contract: \$625,500
Contract Expiration Date: 14 December 1967

Sponsored by

ADVANCED RESEARCH PROJECTS AGENCY
Nuclear Test Detection Office
ARPA Order No. 624
ARPA Program Code No. 7F10

28 February 1968

science services division



ACKNOWLEDGMENT

This research was supported by the
ADVANCED RESEARCH PROJECTS AGENCY
Nuclear Test Detection Office

under
Project VELA UNIFORM
and accomplished under the technical direction of the
AIR FORCE TECHNICAL APPLICATIONS CENTER
under Contract No. F33657-67-C-0708-P001



ABSTRACT

Adaptive multichannel prediction-error filtering is compared with conventional optimum Wiener filtering for 10 types of array data. An actual signal, an artificial signal with varying strength and velocity, and the design of filters for a composite of noise data are considered for three sets of data in the comparison of adaptive maximum-likelihood signal extraction with Wiener filtering. Comparison of the two methods is based on total mean-square-error and the distribution of the error power over frequency.

Online adaptive processing solves problems with slowly time-varying noise fields such as UBO road noise. The adaptive method also is simpler and more economical than the Wiener method as an offline filter-design procedure for array data known to be approximately time stationary.

Both methods produce essentially equivalent filters with respect to total mean-square-error; however, relatively large differences in the actual filter-response characteristics are possible.



SYMBOLS AND ACRONYMS

CPO	Cumberland Plateau Seismological Observatory
k_s	Rate of convergence parameter of adaptive algorithm
LASA	Large-Aperature Seismic Array
MCF	Multichannel filter
MLF	Maximum-likelihood filter
NSA	Noise sample A
NSB	Noise sample B
rms	root-mean-square
SDL	Seismic Data Laboratory
SNR	Signal-to-noise ratio
TI	Texas Instruments Incorporated
UBO	Uinta Basin Seismological Observatory



TABLE OF CONTENTS

Section	Title	Page
	ABSTRACT	iii
I	INTRODUCTION AND SUMMARY	I-1
II	PREDICTION-ERROR FILTERING	II-1
	A. UBO ROAD NOISE	II-3
	B. UBO NORMAL NOISE	II-11
	C. UBO NOISE NORTHEAST	II-19
	D. LASA SUBARRAY B1	II-22
	E. ARRAY DATA	II-40
	F. VERTICAL ARRAY A	II-49
	G. VERTICAL ARRAY B	II-50
	H. LASA SUBARRAY B1, RING-STACKED	II-53
	I. LASA LONG-PERIOD 3339	II-69
	J. LASA LONG-PERIOD 1196	II-71
III	MAXIMUM-LIKELIHOOD FILTERING	III-1
	A. LASA SUBARRAY C1, ALEUTIAN ISLANDS EVENT	III-2
	B. CPO NOISE SAMPLE	III-3
	1. Case 1 — Noise Rejection	III-7
	2. Case 2 — Infinite-Velocity Signal (SNR = 1.0)	III-9
	3. Case 3 — Infinite-Velocity Signal (SNR = 10.0)	III-13
	4. Case 4 — 12 km/sec Signal (SNR = 1.0)	III-13
	5. Case 5 — 12 km/sec Signal (SNR = 10.0)	III-13
	C. DESIGN PROBLEM FOR FIVE SAMPLES	III-13
	1. Summary	III-13
	2. Method	III-17
	3. Discussion	III-19
IV	REFERENCES	IV-1

TABLE

II-1	Summary of Prediction-Error Processing	II-2
------	--	------



ILLUSTRATIONS

Figure	Description	Page
II-1	Prefiltered and Resampled UBO Road Noise	II-3
II-2	Prefiltered, Resampled, and Whitened UBO Road Noise	II-5
II-3	Mean-Square-Error Vs k_s for UBO Road Noise	II-6
II-4	Wiener and Adaptive Filter Outputs for UBO Road Noise	II-7
II-5	Wiener and Adaptive Filter Outputs for Whitened UBO Road Noise	II-8
II-6	Power Spectra of Channel 10, Wiener Errors, and Adaptive Errors for UBO Road Noise	II-9
II-7	Power Spectra of Channel 10, Wiener Errors, and Adaptive Errors for Whitened UBO Road Noise	II-10
II-8	Prefiltered and Resampled UBO Normal Noise	II-12
II-9	Prefiltered, Resampled, and Whitened UBO Normal Noise	II-13
II-10	Mean-Square-Error Vs k_s for UBO Normal Noise	II-14
II-11	Wiener and Adaptive Filter Outputs for UBO Normal Noise	II-15
II-12	Wiener and Adaptive Filter Outputs for Whitened UBO Normal Noise	II-16
II-13	Power Spectra of Channel 10, Wiener Errors, and Adaptive Errors for UBO Normal Noise	II-17
II-14	Power Spectra of Channel 10, Wiener Errors, and Adaptive Errors for Whitened UBO Normal Noise	II-18
II-15	Original UBO Noise Northeast Data	II-20
II-16	Whitened UBO Noise Northeast Data	II-21
II-17	Mean-Square-Error Vs k_s for UBO Noise Northeast	II-23
II-18	Wiener and Adaptive Outputs for UBO Noise Northeast	II-24
II-19	Wiener and Adaptive Outputs for Whitened UBO Noise Northeast	II-25



ILLUSTRATIONS (CONTD)

Figure	Description	Page
II-20	Power Spectra of Channel 10, Wiener Errors, and Adaptive Errors for UBO Noise Northeast	II-26
II-21	Power Spectra of Channel 10, Wiener Errors, and Adaptive Errors for Whitened UBO Noise Northeast	II-27
II-22	Prefiltered and Resampled LASA Subarray B1 Center Seismometer and First Ring	II-28
II-23	Prefiltered, Resampled, and Whitened LASA Subarray B1 Center Seismometer and First Ring	II-30
II-24	Mean-Square-Error Vs k_s for Prefiltered and Resampled LASA Subarray B1 Center Seismometer and First Ring	II-32
II-25	Wiener and Adaptive Outputs for Prefiltered and Resampled LASA Subarray B1 Center Seismometer and First Ring	II-33
II-26	Wiener and Adaptive Outputs for Prefiltered, Resampled, and Whitened LASA Subarray B1 Center Seismometer and First Ring	II-34
II-27	Power Spectra of Channel 10, Wiener Errors, and Adaptive Errors for Prefiltered and Resampled LASA Subarray B1 Center Seismometer and First Ring	II-35
II-28	Power Spectra of Channel 10, Wiener Errors, and Adaptive Errors for Prefiltered, Resampled, and Whitened LASA Subarray B1 Center Seismometer and First Ring	II-36
II-29	Mean-Square-Error Vs k_s for LASA Subarray B1, 25 Channels	II-37
II-30	Error Traces for LASA Subarray B1, 25 Channels	II-38
II-31	Power Spectra of Adaptive Error Traces for LASA Subarray B1, 25 Channels	II-39
II-32	Prefiltered and Resampled Array Data	II-41
II-33	Prefiltered, Resampled, and Whitened Array Data	II-42
II-34	Mean-Square-Error Vs k_s for Array Data	II-43



ILLUSTRATIONS (CONTD)

Figure	Description	Page
II-35	Wiener and Adaptive Filter Outputs for Array Data	II-44
II-36	Adaptive Filter Outputs for Whitened Array Data	II-45
II-37	Power Spectra of Channel 1, Wiener Error, and $k_s = 0.0005, 0.00005$ for Array Data	II-46
II-38	Power Spectra of Channel 1 and $k_s = 0.0005, 0.00005$ for Whitened Array Data	II-47
II-39	Vertical Array A Data	II-48
II-40	Mean-Square-Error Vs k_s for Vertical Array A Predicting Surface Seismometer	II-50
II-41	Error Outputs for Vertical Array A Predicting Surface Seismometer	II-51
II-42	Power Spectra for Vertical Array A Predicting Surface Seismometer	II-52
II-43	Mean-Square-Error Vs k_s for Vertical Array A Predicting Top Deep-Well Seismometer	II-53
II-44	Error Outputs for Vertical Array A Predicting Top Deep-Well Seismometer	II-54
II-45	Power Spectra for Vertical Array A Predicting Top Deep-Well Seismometer	II-55
II-46	Vertical Array B Data	II-56
II-47	Mean-Square-Error Vs k_s for Vertical Array B Predicting Surface Seismometer	II-57
II-48	Error Outputs for Vertical Array B Predicting Surface Seismometer	II-58
II-49	Power Spectra for Vertical Array B Predicting Surface Seismometer	II-59
II-50	Mean-Square-Error Vs k_s for Vertical Array B Predicting Top Deep-Well Seismometer	II-60
II-51	Error Outputs for Vertical Array B Predicting Top Deep-Well Seismometer	II-61



ILLUSTRATIONS (CONTD)

Figure	Description	Page
II-52	Power Spectra for Vertical Array B Predicting Top Deep-Well Seismometer	II-62
II-53	LASA Subarray B1 Ring-Stacked Data	II-63
II-54	Mean-Square-Error Vs k_s for LASA Subarray B1, Ring-Stacked	II-64
II-55	Adaptive Prediction Error for LASA Subarray B1, Ring-Stacked	II-65
II-56	Error to Center-Seismometer Power Ratio of Wiener and Adaptive Filtering for LASA Subarray B1, Ring-Stacked	II-66
II-57	LASA Subarray B1 Whitened Ring-Stacked Data	II-67
II-58	Adaptive Prediction Error for LASA Subarray B1 Whitened Ring-Stacked Data	II-68
II-59	LASA Long-Period 3339 Data	II-70
II-60	Mean-Square-Error Vs k_s for LASA Long-Period 3339	II-71
II-61	Error Traces for LASA Long-Period 3339	II-72
II-62	Power Spectra for LASA Long-Period 3339	II-73
II-63	LASA Long-Period 1196 Data	II-74
II-64	Mean-Square-Error Vs k_s for LASA Long-Period 1196	II-75
II-65	Wiener and Adaptive Error Outputs for LASA Long-Period 1196	II-76
II-66	Power Spectra for LASA Long-Period 1196	II-77
III-1	Bandpass-Filtered and Aligned Data for LASA Subarray C1, Aleutian Islands Event	III-4
III-2	Adaptive Design of Maximum-Likelihood Filters	III-6
III-3	Adaptive Processing of a 19-Channel CPO Noise Sample	III-8
III-4	Adaptive Processing of the CPO Noise Sample with Full-Gradient Power Output	III-10
III-5	Adaptive Processing of the CPO Noise Sample with Reduced-Gradient Power Output	III-11



ILLUSTRATIONS (CONTD)

Figure	Description	Page
III-6	Adaptive Processing of a 19-Channel Infinite-Velocity Synthetic Signal Plus Noise (SNR = 1.0)	III-12
III-7	Adaptive Processing of a 19-Channel Infinite-Velocity Synthetic Signal Plus Noise (SNR = 10.0)	III-14
III-8	Adaptive Processing of a 19-Channel 12 km/sec Synthetic Signal Plus Noise (SNR = 1.0)	III-15
III-9	Adaptive Processing of a 19-Channel 12 km/sec Synthetic Signal Plus Noise (SNR = 10.0)	III-16
III-10	Five-Sample Maximum-Likelihood Design Problem	III-18
III-11	Outputs for Compared Filter-Design Techniques, Noise Sample 1	III-21
III-12	Outputs for Compared Filter-Design Techniques, Noise Sample 2	III-22
III-13	Outputs for Compared Filter-Design Techniques, Noise Sample 3	III-23
III-14	Outputs for Compared Filter-Design Techniques, Noise Sample 4	III-24
III-15	Outputs for Compared Filter-Design Techniques, Noise Sample 5	III-25
III-16	Error Power Spectra for Compared Filter-Design Techniques, Noise Sample 1	III-26
III-17	Error Power Spectra for Compared Filter-Design Techniques, Noise Sample 2	III-27
III-18	Error Power Spectra for Compared Filter-Design Techniques, Noise Sample 3	III-28
III-19	Error Power Spectra for Compared Filter-Design Techniques, Noise Sample 4	III-29
III-20	Error Power Spectra for Compared Filter-Design Techniques, Noise Sample 5	III-30
III-21	Fixed Adaptive Maximum-Likelihood Filter Response	III-31
III-22	Wiener Filter Response	III-32



SECTION I

INTRODUCTION AND SUMMARY

Basic reasons for using the adaptive technique are its suitability for hardware implementation as an online operation consisting of simultaneous filter design and application, its numerical simplicity and improved efficiency in filter design, and the fact that it represents a technological breakthrough in processing data with unknown time-varying noise characteristics. Algebraic details of the adaptive algorithm can be found in numerous other reports.^{1,2,3}

This report discusses the application of the adaptive technique to a wide variety of seismic array data, comparing the adaptive technique to the classical methods of designing and applying fixed filters.

A very close approximation to the Wiener mean-square-error was obtained on all data samples examined, using the adaptive technique for sufficiently small filter coefficient rates of change.

The adaptive method applied to time-varying data produced smaller mean-square-error than the Wiener method for intermediate filter change rates. Thus, it can be inferred that an online adaptive multichannel filter (MCF) will always perform almost as well as an up-to-date Wiener filter and possibly better if the data characteristics are varying with time.

Although the adaptive method produces total mean-square-error in close agreement with the Wiener method, large differences in the filter-response characteristics are possible. Power spectra for the Wiener and adaptive error traces in the design of maximum-likelihood filters (Section III-C) agree in total power, but favor the Wiener method at low frequencies.



Unexpected mean-square-error vs rate-of-coefficient-change curves for adaptively processing original data led to the discovery of an interaction between the high rate of adapting the coefficients and the relatively large content of low-frequency energy in the data. Evaluation of this phenomenon has not progressed sufficiently to state its exact significance.

Results of adaptively processing seismic data indicate that the adaptive procedure now can be used for MCF design with the assurance of producing filters equivalent to the Wiener method in total mean-square-error.



SECTION II

PREDICTION-ERROR FILTERING

Prediction-error filtering was performed on a set of 10 different data samples. Included in the set are short-period surface-array data (individual and ring-stacked seismometers), short-period vertical-array data, and 3-component long-period surface-array data. Adaptive and Wiener filtering results from the unwhitened versions of four of these data samples (UBO road noise, UBO normal noise, array data, and LASA B1 center and first ring) were given in a TI special report.¹ These results are presented briefly here for comparison with results from the whitened versions of the same data samples. The remaining six data samples have been processed adaptively in their unwhitened form. In some cases, whitened data were adaptively filtered and the unwhitened and whitened data were Wiener-filtered. Table II-1 is a summary of prediction-error processing for each data sample.

Data for each problem, unless otherwise specified, are normalized in the filtering program by being scaled in each trace by $1/$ (rms value of that trace) so that the sample variance of all data traces is 1. Thus, results of processing the different data samples may be compared directly.

Processing results for each data sample are presented as plots of the actual filter outputs, plots of mean-square-error of prediction vs k_s (the rate of convergence parameter of the adaptive algorithm), and power spectra of the data and prediction-error traces.

False-alarm probability (the frequency of error-trace excursion beyond $\hat{\sigma}$, $2\hat{\sigma}$, $3\hat{\sigma}$, etc., where $\hat{\sigma}$ is the sample variance of the error trace) was computed for Wiener and adaptive error traces for seven of the 10 data samples. Rapidly adapting, slowly adapting, and Wiener error traces showed no consistent difference in false-alarm probabilities.



Table II-1
SUMMARY OF PREDICTION-ERROR PROCESSING

Sample	Date	Time	Data Length after Resampling (points) (sec)		Number of Channels	Channels Used for Prediction	Channel Predicted	Filter Length	Number of Points Ahead Predicted	Unwhitened Data		Whitened Data	
										Wiener	Adaptive	Wiener	Adaptive
UBO Road Noise	9-23-64	16:06:20	1250	90	10	1-9	10	27	-13	X	X	X	X
UBO Normal Noise	9-30-64	21:51:10	1250	90	10	1-9	10	27	-13	X	X	X	X
UBO Noise Northeast	3-25-66	04:26:43	1250	90	10	1-9	10	27	-13	X	X	X	X
LASA Subarray B1			2200	220	25	1, 2, 6, 10, 14, 18, 22	1	25	1	X	X	X	X
LASA Subarray B1	3-25-66	04:26:43	2000	200	25	1-25	1	25	-18				
Array Data	11-20-66	23:14:00	3250	234	13	2-13	1	37	-18	X	X		X
Vertical Array NSA	11-20-66	23:14:00	3000	216	7	2-7	1	37	-18	X	X		
Vertical Array NSA	11-20-66	23:14:00	3000	216	7	3-7	2	37	-18	X	X		
Vertical Array NSB	11-20-66	23:14:00	3000	216	7	2-7	1	37	-18	X	X		
Vertical Array NSB		23:14:00	3000	216	7	3-7	2	37	-18	X	X		
LASA Subarray B1 Ring-Stacked	11-20-66	23:14:00	2000	200	8	2-8	1	35	-17	X	X		X
LASA Long-Period 3339	11-12-66		4500	4500	11	2-11	1	11	- 5	X	X		
LASA Long-Period 1196	12-28-66		4500	4500	10	2-10	1	15	- 7	X	X		



A. UBO ROAD NOISE

Special Report No. 1 gives results of adaptive and Wiener processing of the unwhitened data.¹ The data have since been whitened and processed in a manner similar to that used for the unwhitened data.

Unwhitened data shown in Figure II-1 were prefiltered with an antialiasing, slightly prewhitening filter and resampled to a 72-msec sample period. A 9-point deconvolution prewhitening filter designed from the autocorrelation of channel 10 was applied to all channels.

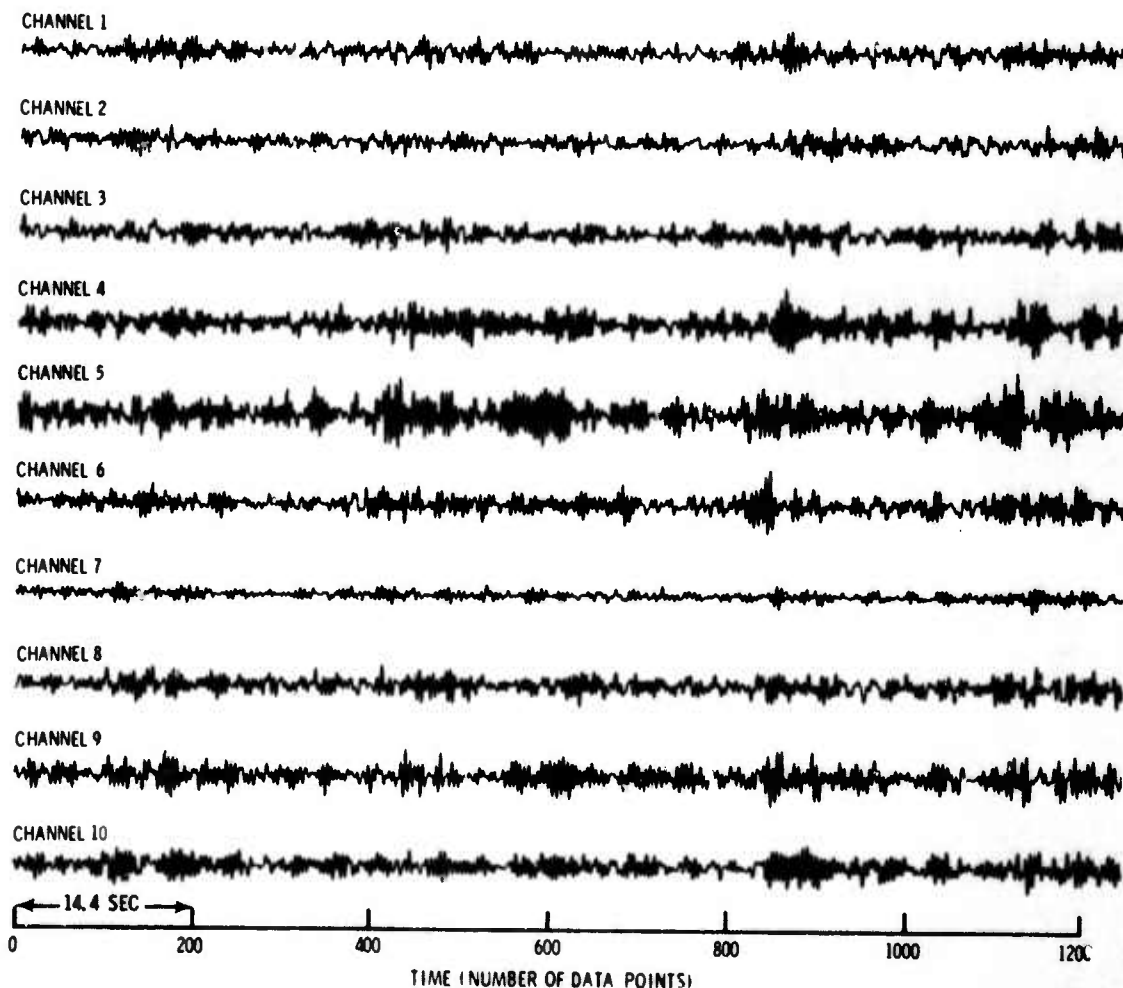


Figure II-1. Prefiltered and Resampled UBO Road Noise



The whitened data shown in Figure II-2 were processed with 27-point Wiener and adaptive filters designed to predict channel 10 at the center of the filter from channels 1 through 9. The Wiener filter, designed from correlation-function estimates computed from the whitened data, gave a mean-square prediction error of 0.414 when applied to the normalized design data. The normalized mean-square prediction error of the Wiener filter designed from and applied to the unwhitened data was 0.147.

Adaptive filtering of the whitened data consisted of nine passes through the data. Values of k_g for the nine passes were 0.0015 (learning), 0.0015, 0.0010, 0.0005, 0.00025, 0.000125, 0.00005, 0.0020, and 0.0025. The filter coefficients were set equal to 0 at the beginning of the first pass; for successive passes, the coefficients initially were equal to their values at the end of the previous pass. Mean-square-error of prediction vs k_g is plotted in Figure II-3 for the unwhitened and whitened data; the Wiener mean-square-errors are shown also.

Adaptive and Wiener predictions and prediction-error traces for the unwhitened and whitened data are shown in Figures II-4 and II-5, respectively. Power spectra of channel 10, Wiener prediction errors, and large and small k_g adaptive prediction errors are given in Figure II-6 for the unwhitened data and in Figure II-7 for the whitened data. Note the linear increase in mean-square-error with increasing k_g for whitened data and the minimum mean-square-error at $k_g = 0.001$ for unwhitened data. Regardless of the degree of whitening, the adaptive procedure gives results equivalent in mean-square-error to the Wiener method for small k_g .

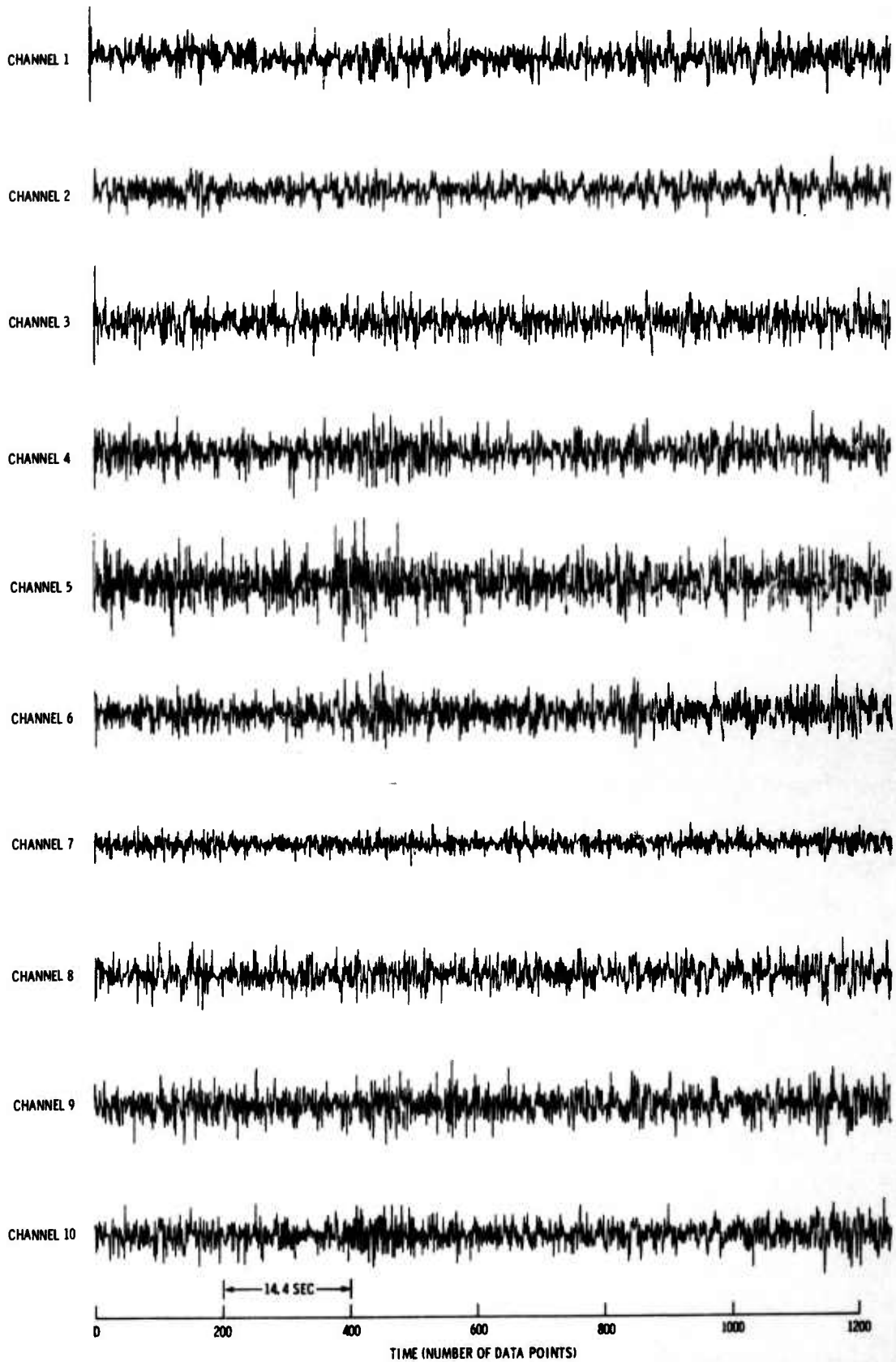


Figure II-2. Prefiltered, Resampled, and Whitened UBO Road Noise

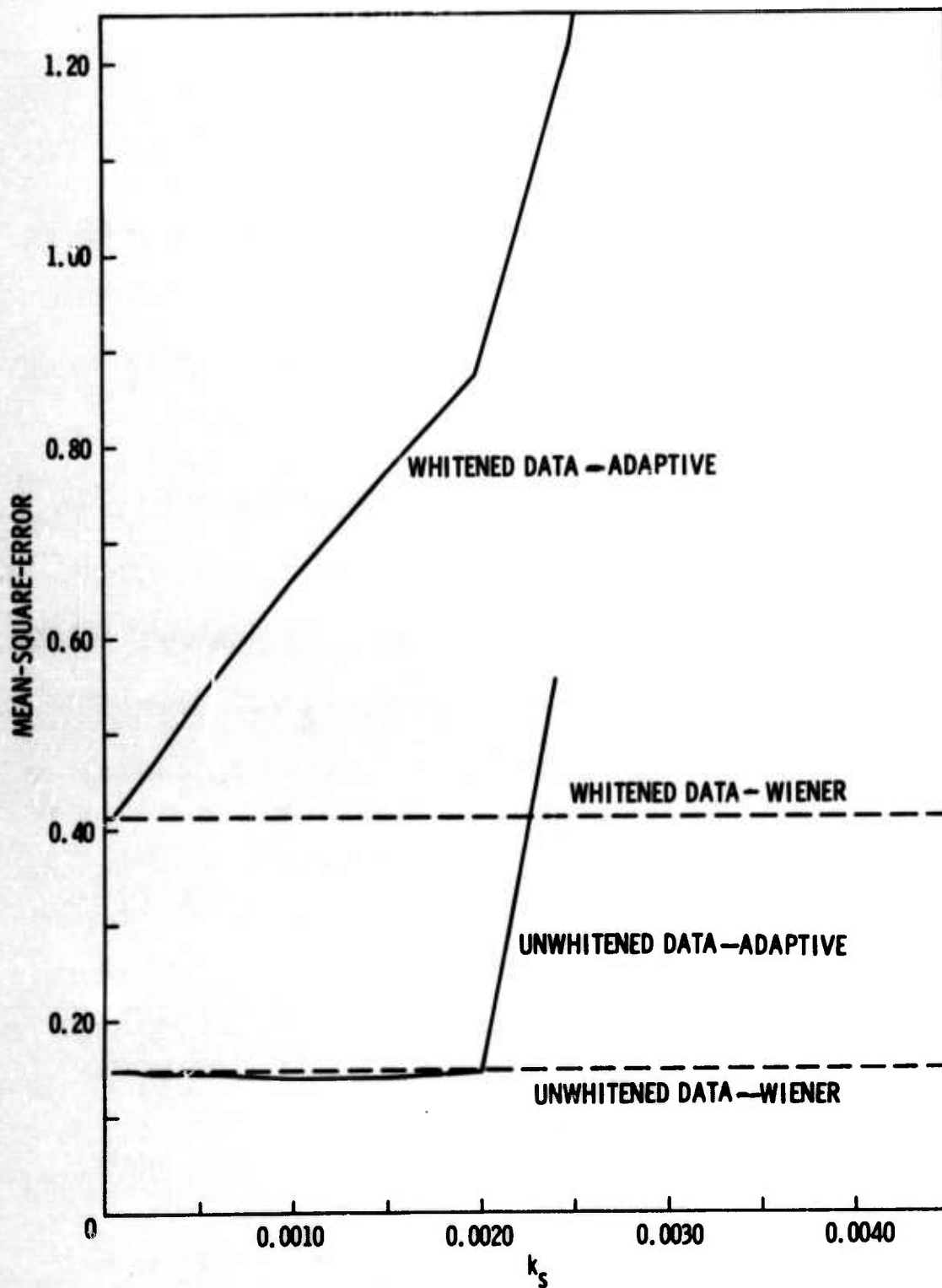


Figure II-3. Mean-Square-Error Vs k_s for UBO Road Noise

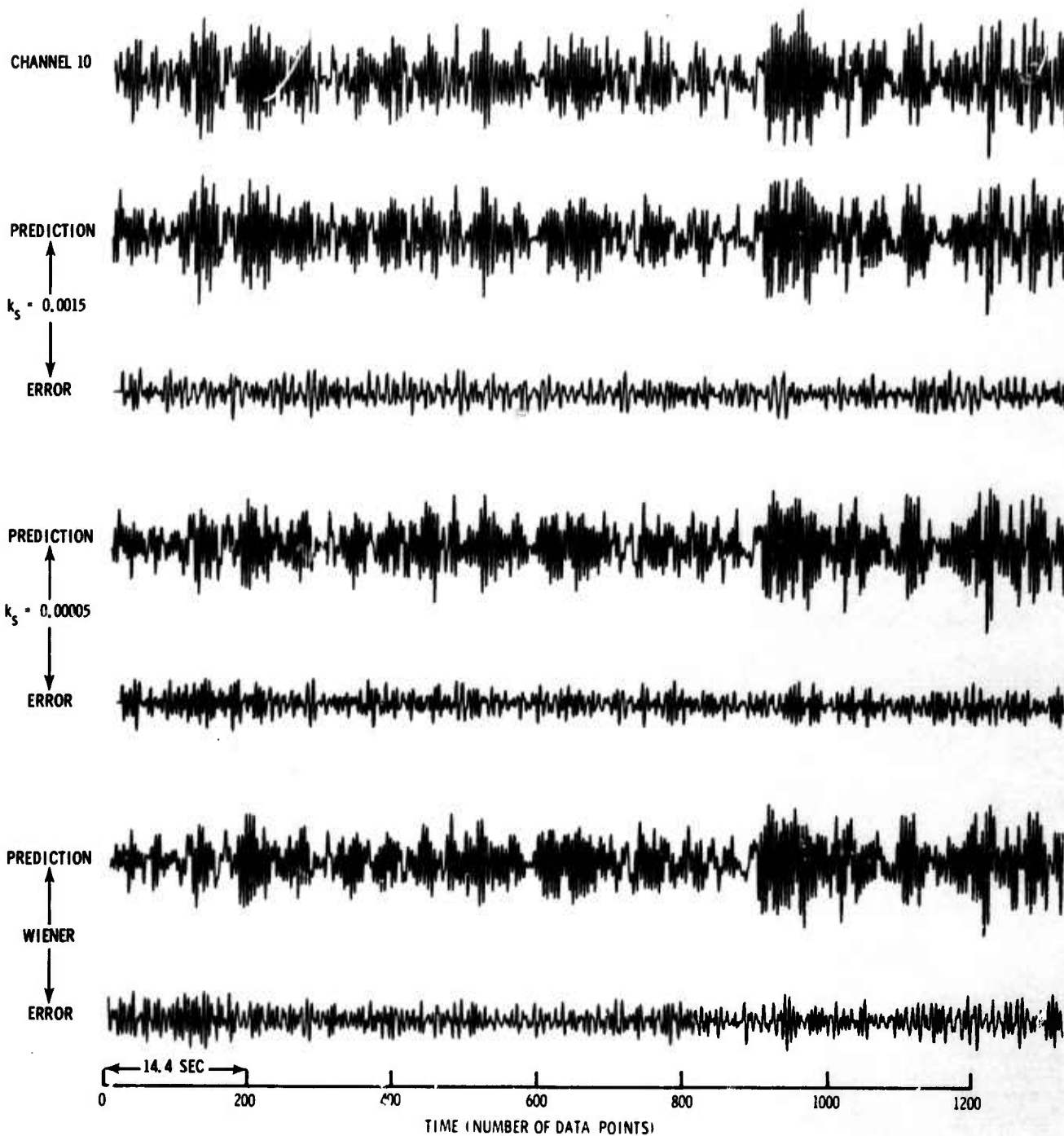


Figure II-4. Wiener and Adaptive Filter Outputs for UBO Road Noise

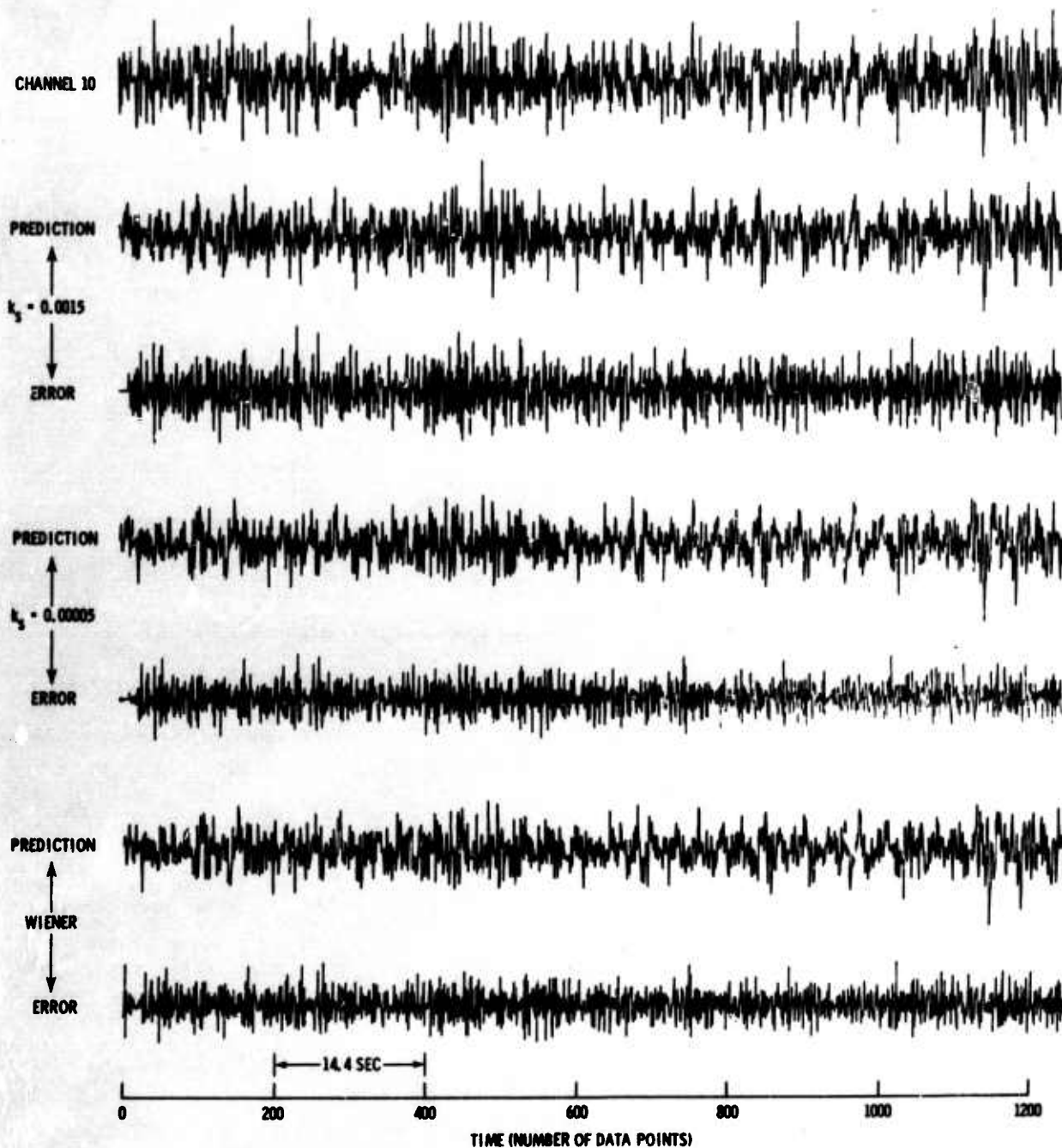


Figure II-5. Wiener and Adaptive Filter Outputs for Whitenened UBO Road Noise

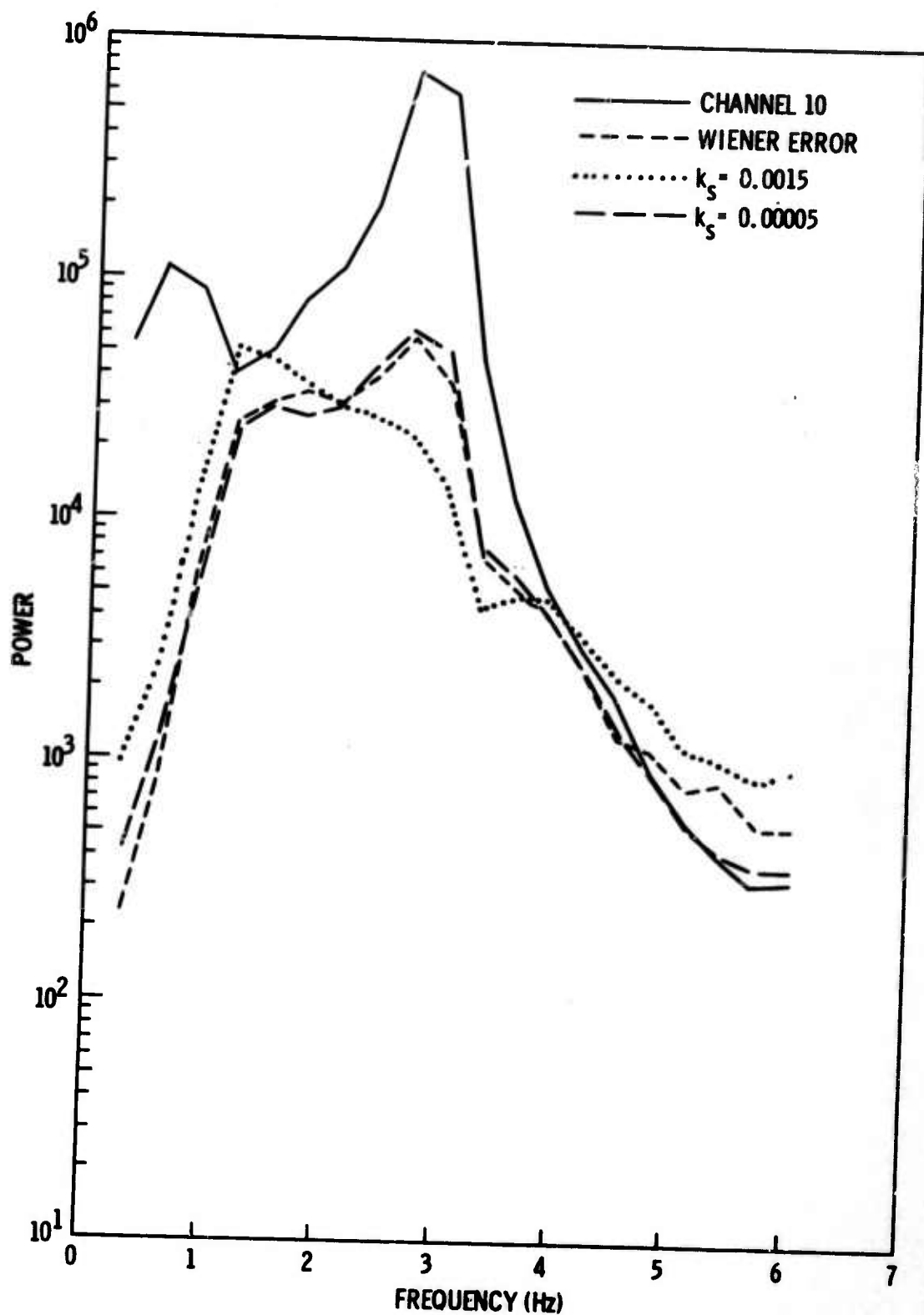


Figure II-6. Power Spectra of Channel 10, Wiener Errors, and Adaptive Errors for UBO Road Noise

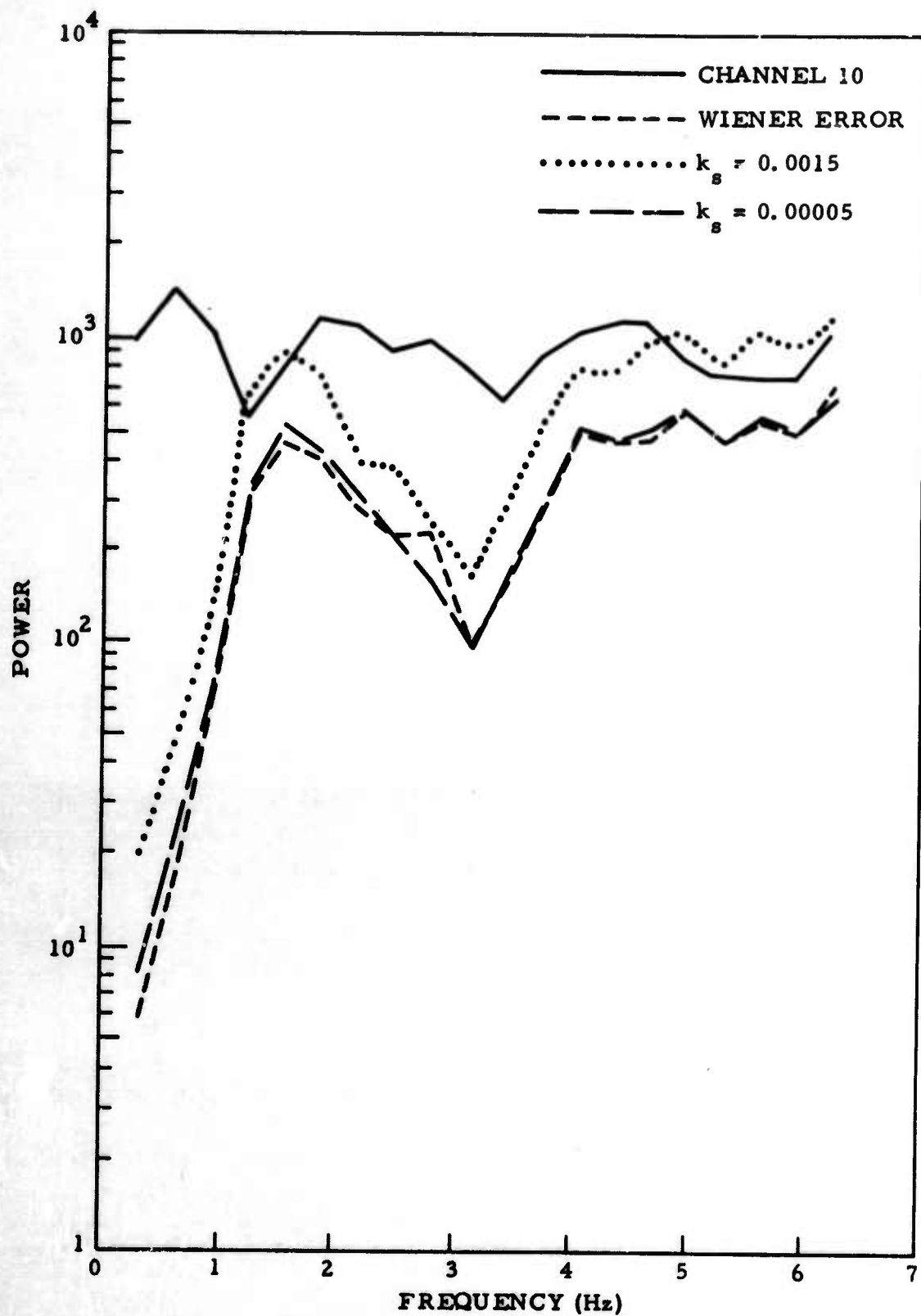


Figure II-7. Power Spectra of Channel 10, Wiener Errors, and Adaptive Errors for Whitened UBO Road Noise



B. UBO NORMAL NOISE

A sample of UBO data, called normal noise because it appears to travel across the array as unattenuated plane waves, is shown in Figure II-8. Discussed in Special Report No. 1, this sample in its unwhitened form was prefiltered, resampled, normalized, Wiener-filtered, and adaptively filtered.¹ A 9-point deconvolution filter designed from the autocorrelation of channel 10 and applied to each trace resulted in the whitened data of Figure II-9. After whitening, the data were renormalized to a variance of 1 for each trace.

Designed were 27-point prediction filters using the whitened data to predict channel 10 at the center of the filter from channels 1 through 9. The Wiener filter gave a mean-square prediction error of 0.408 when applied to the whitened design data. The Wiener filter previously designed from the normal-noise unwhitened data resulted in a normalized mean-square-error of 0.281 when applied to the unwhitened design data.

Ten adaptive filtering passes were made through the whitened data, with k_g equal to 0.0015 (learning), 0.0015, 0.0010, 0.0005, 0.00025, 0.000125, 0.00005, 0.0020, 0.0025, and 0.0030. Each filter coefficient was 0 at the start of the first pass and equal to its value at the end of the previous pass for the beginning of the remaining passes. Figure II-10 shows mean-square-error of prediction vs k_g for unwhitened and whitened data and also shows the corresponding Wiener errors.

Prediction and prediction-error traces for Wiener and adaptive filtering of unwhitened data are shown in Figure II-11. Figure II-12 gives the corresponding results for the whitened data. Figures II-13 and II-14 are power spectra of channel 10, Wiener prediction errors, and adaptive prediction errors for the unwhitened and whitened data, respectively.

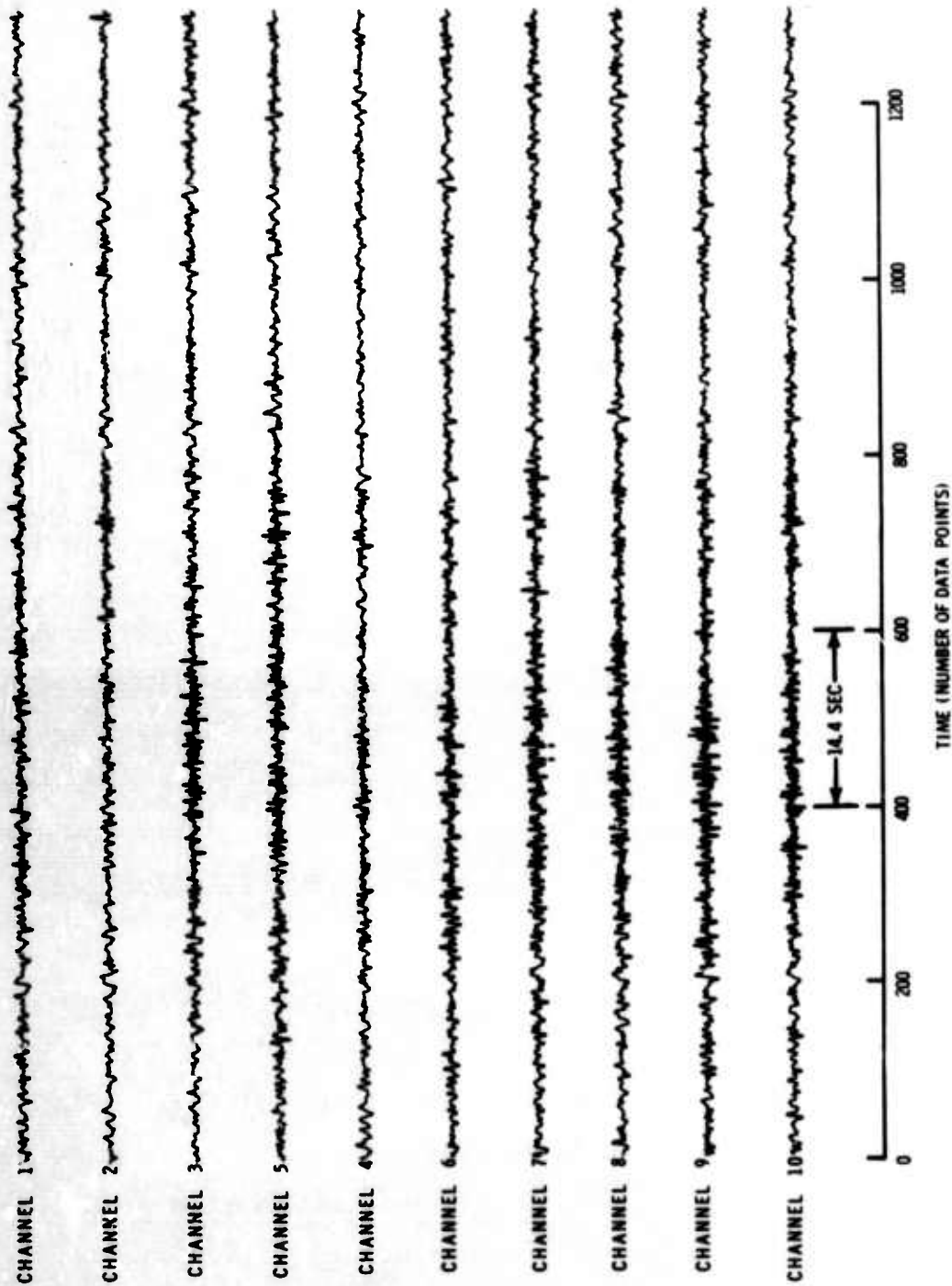


Figure II-8. Prefiltered and Resampled UBO Normal Noise

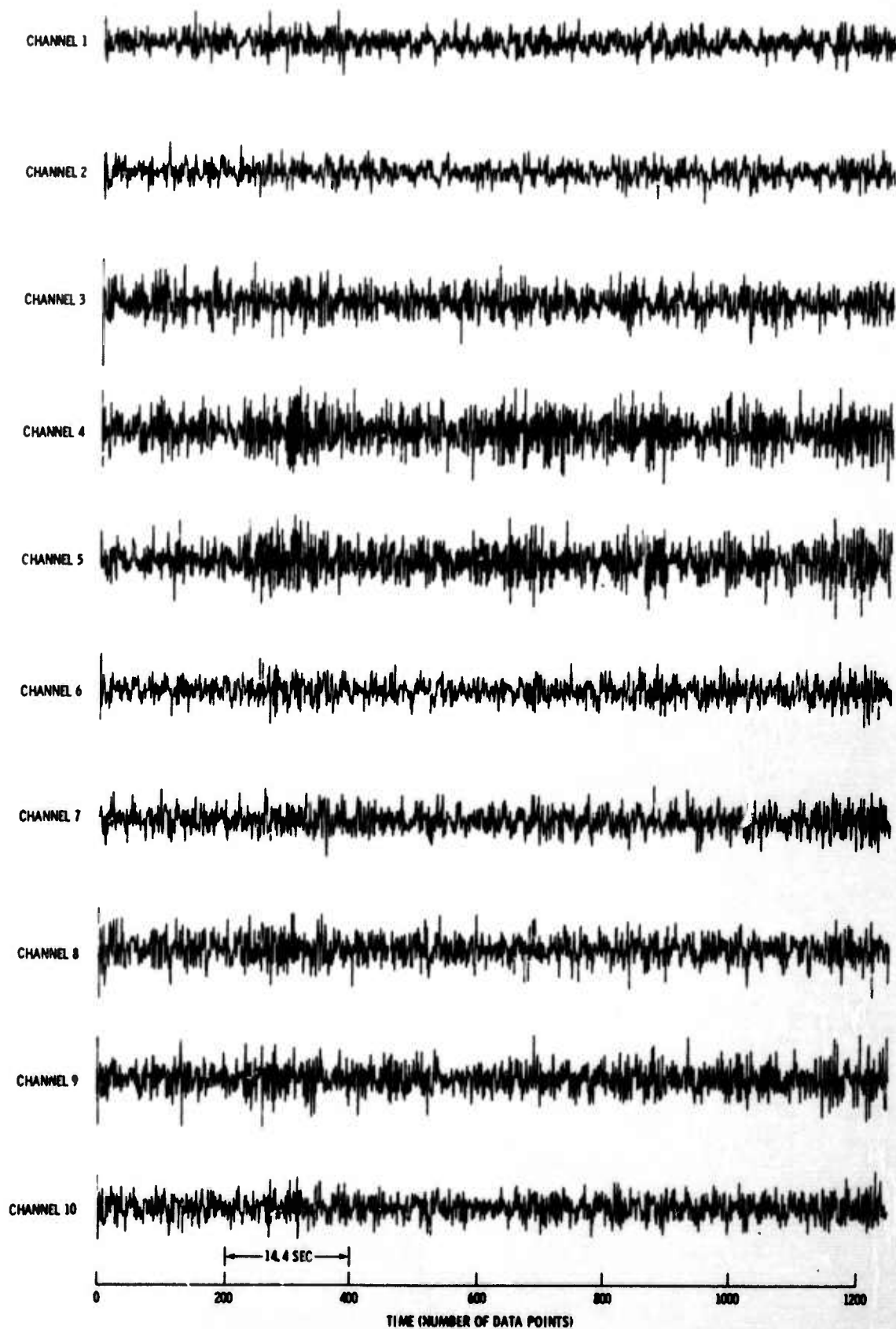


Figure II-9. Prefiltered, Resampled, and Whitened UBO Normal Noise

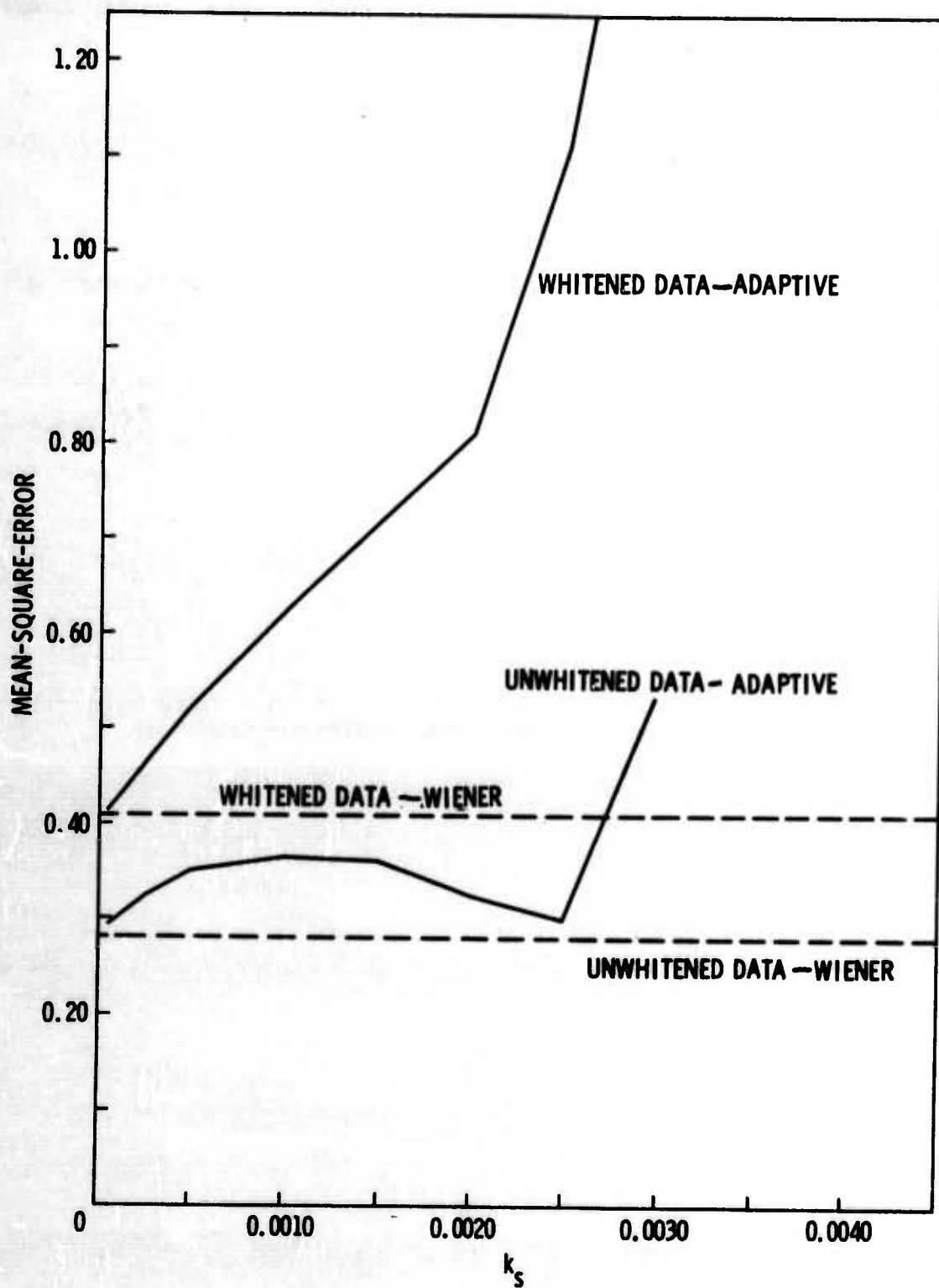


Figure II-10. Mean-Square-Error Vs k_s for UBO Normal Noise

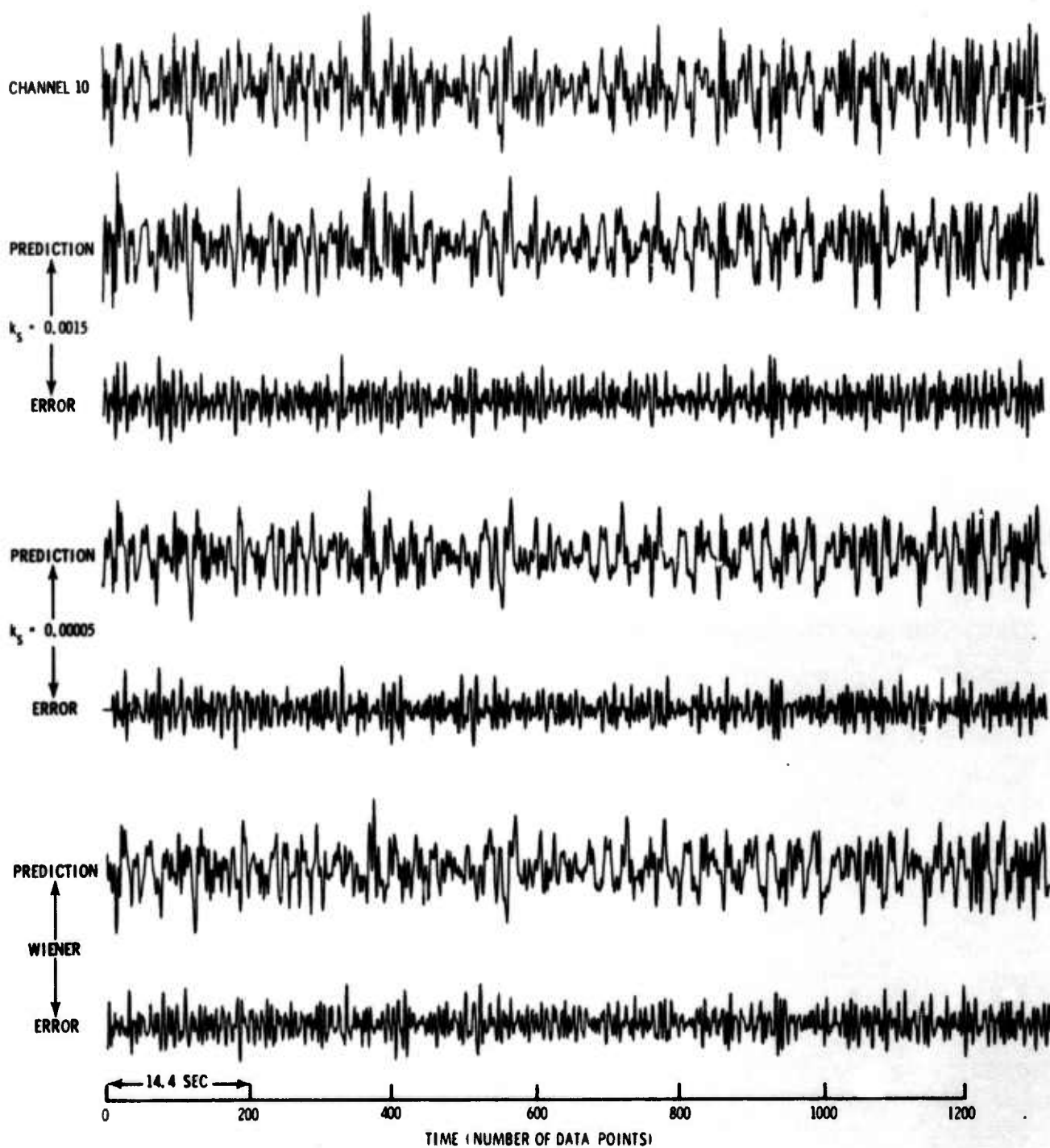


Figure II-11. Wiener and Adaptive Filter Outputs for UBO Normal Noise

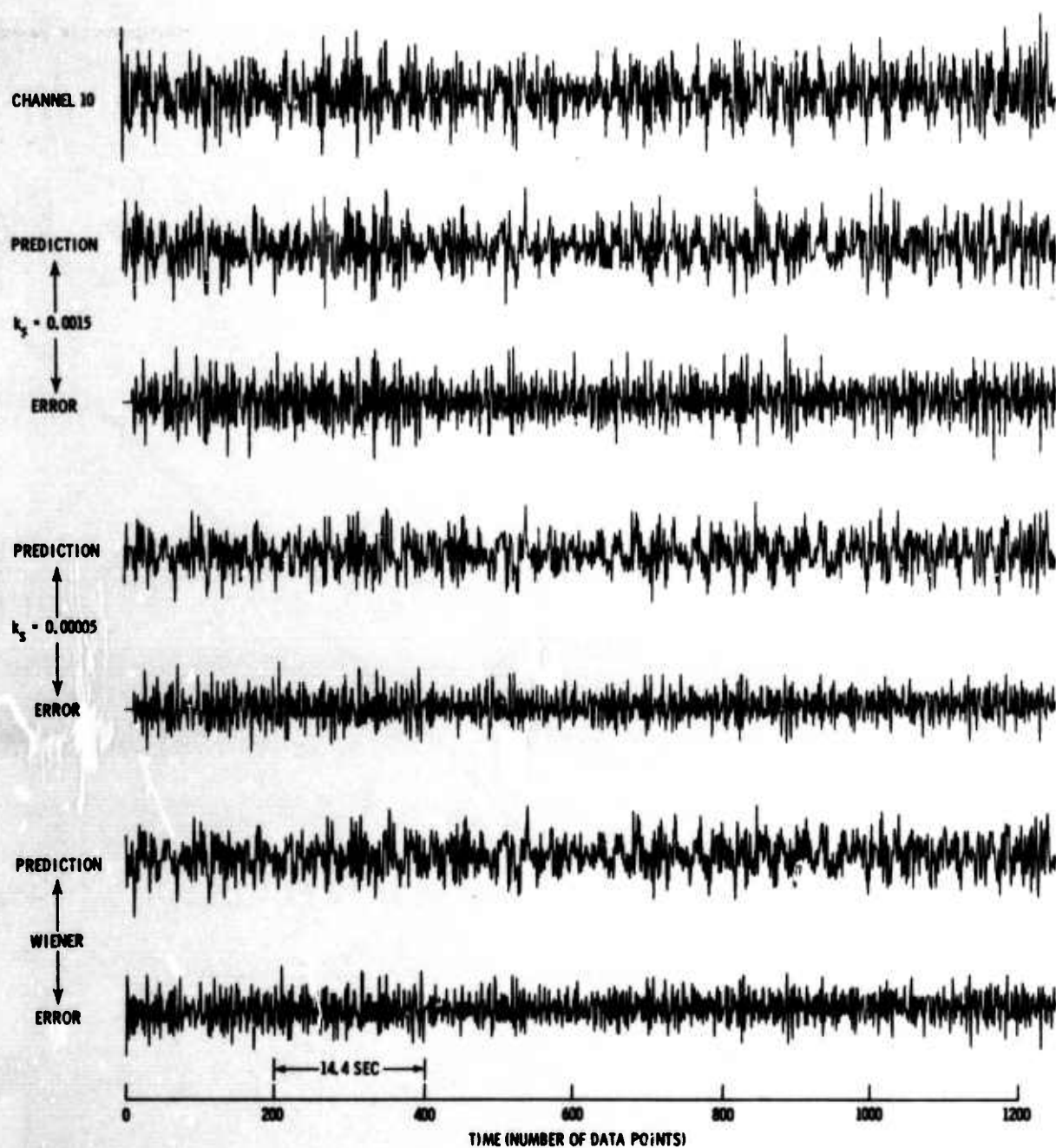


Figure II-12. Wiener and Adaptive Filter Outputs for Whitenened UBO Normal Noise

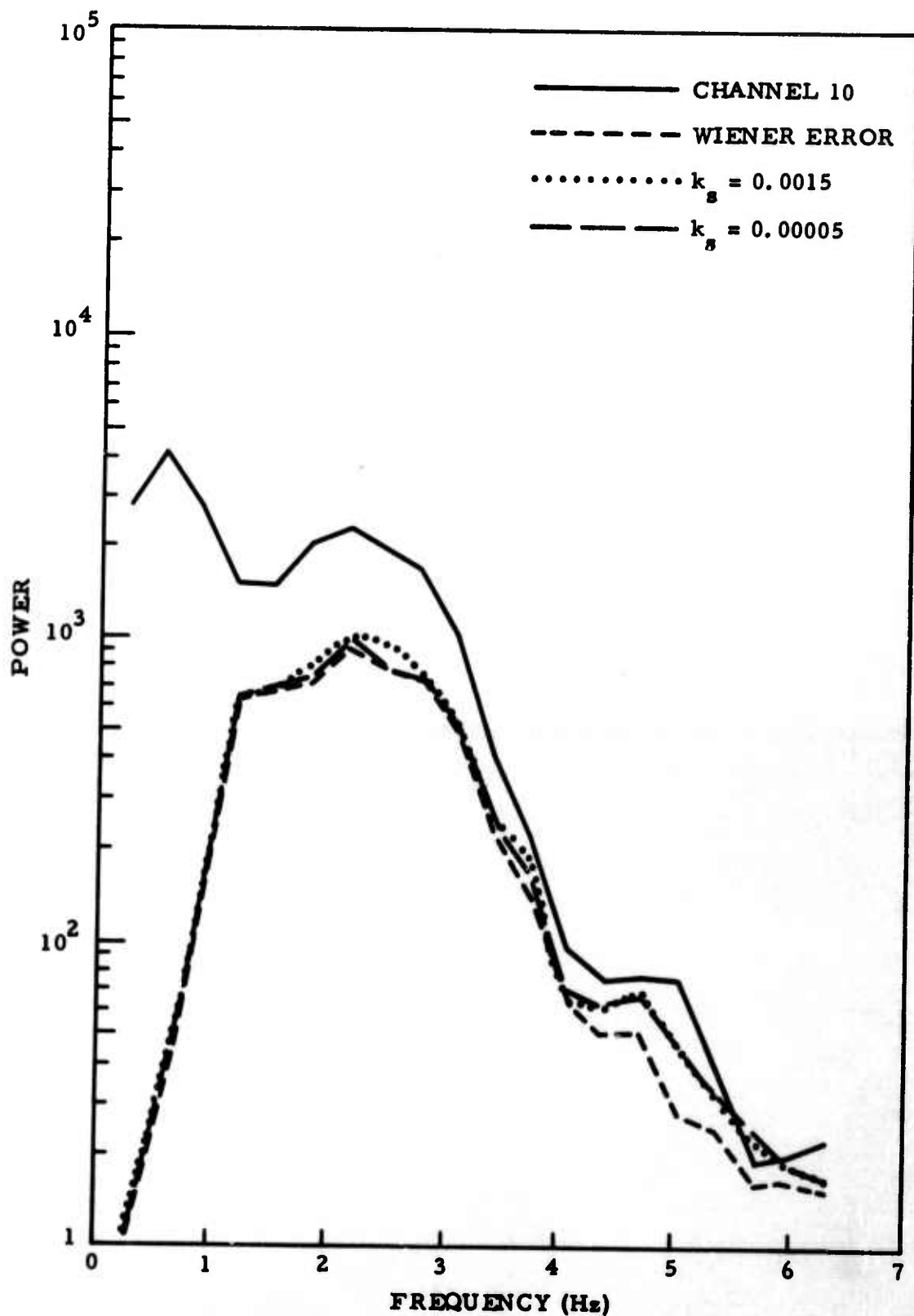


Figure II-13. Power Spectra of Channel 10, Wiener Errors, and Adaptive Errors for UBO Normal Noise

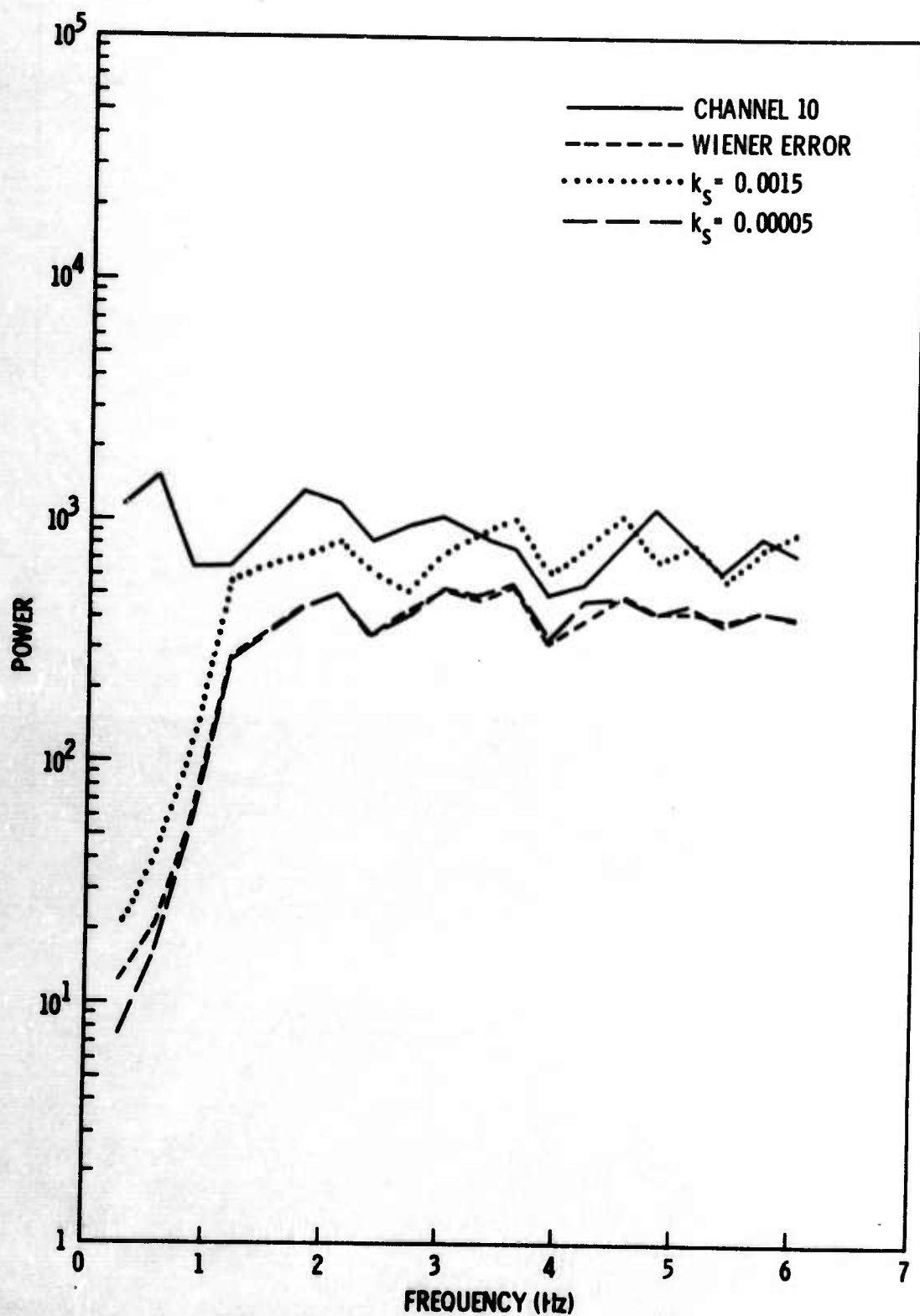


Figure II-14. Power Spectra of Channel 10, Wiener Errors, and Adaptive Errors for Whitened UBO Normal Noise



It is interesting to compare the mean-square-error curves of Figures II-3 and II-10. The curves for whitened normal data and road-noise data are almost equal except that the road-noise data have a slightly larger slope. Shapes of the corresponding curves for unwhitened data are different in a surprising way. Since there are no known time-varying components in the normal data, the mean-square-error curve would be expected to have roughly the same shape as the whitened data curve. The degree to which this situation failed to occur led to a separate study of the phenomenon of false tracking due to the interaction of oversampling and high rate of adaption. Special Report No. 13 discusses the theoretical and empirical investigation of this phenomenon with data of known statistical properties.³

C. UBO NOISE NORTHEAST

A third sample of UBO noise, called UBO noise northeast because $f\text{-}\vec{k}$ analysis of these data indicates a strong component of noise arriving from the northeast, was processed in both unwhitened and whitened forms. The original data, shown in Figure II-15, were prefiltered and re-sampled using the same procedures used for road and normal noise. A 9-point deconvolution filter designed from the autocorrelation of channel 10 and applied to each data channel gave the whitened data shown in Figure II-16.

Designed were 27-point Wiener filters from correlation estimates of the unwhitened and whitened data with the output point at the center of the filter to predict channel 10 from channels 1 through 9. The mean-square prediction error of the filter designed from unwhitened data when applied to the normalized unwhitened design data was 0.27, while the whitened data filter gave a mean-square-error of 0.52 when applied to the normalized whitened data.

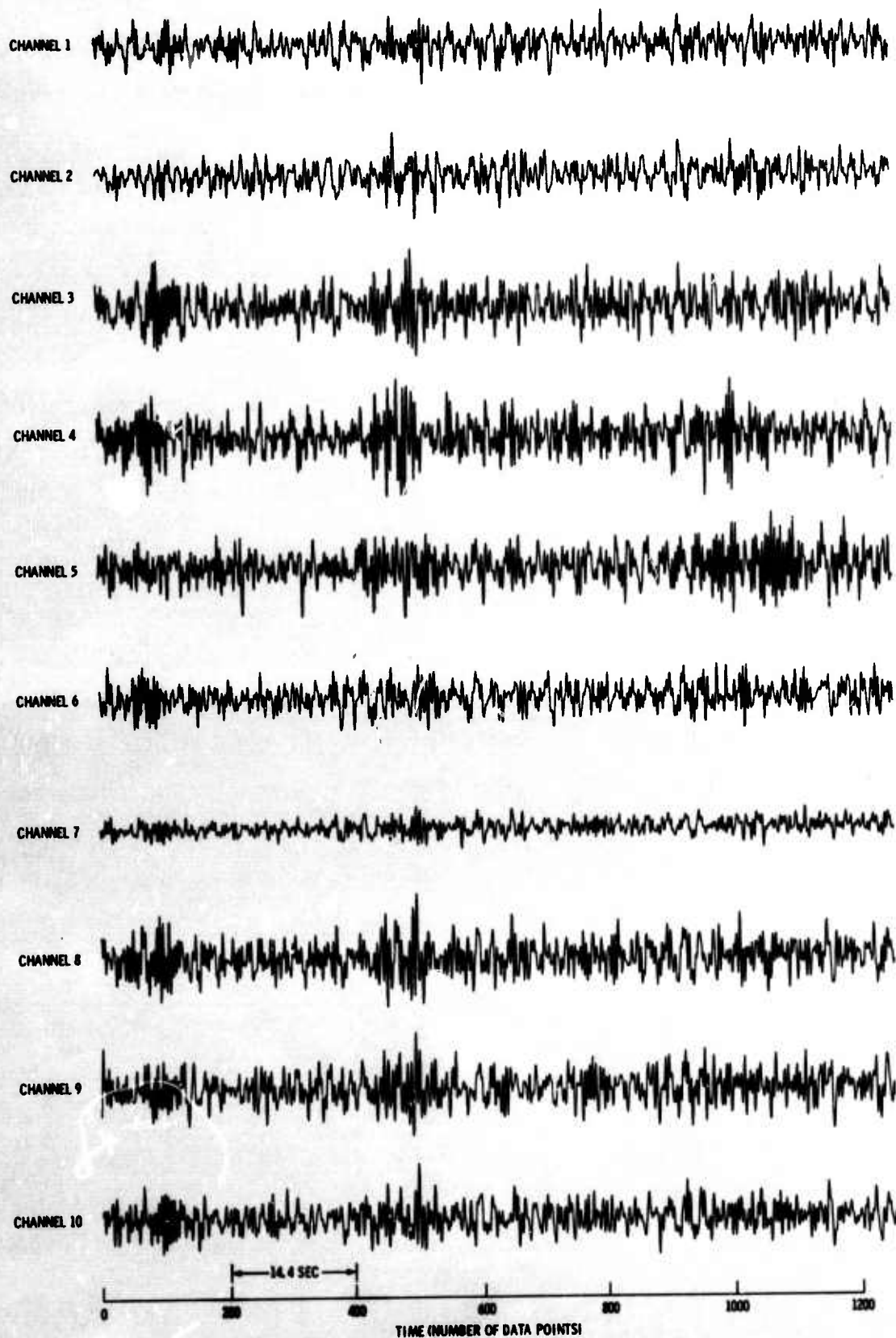


Figure II-15. Original UBO Noise Northeast Data

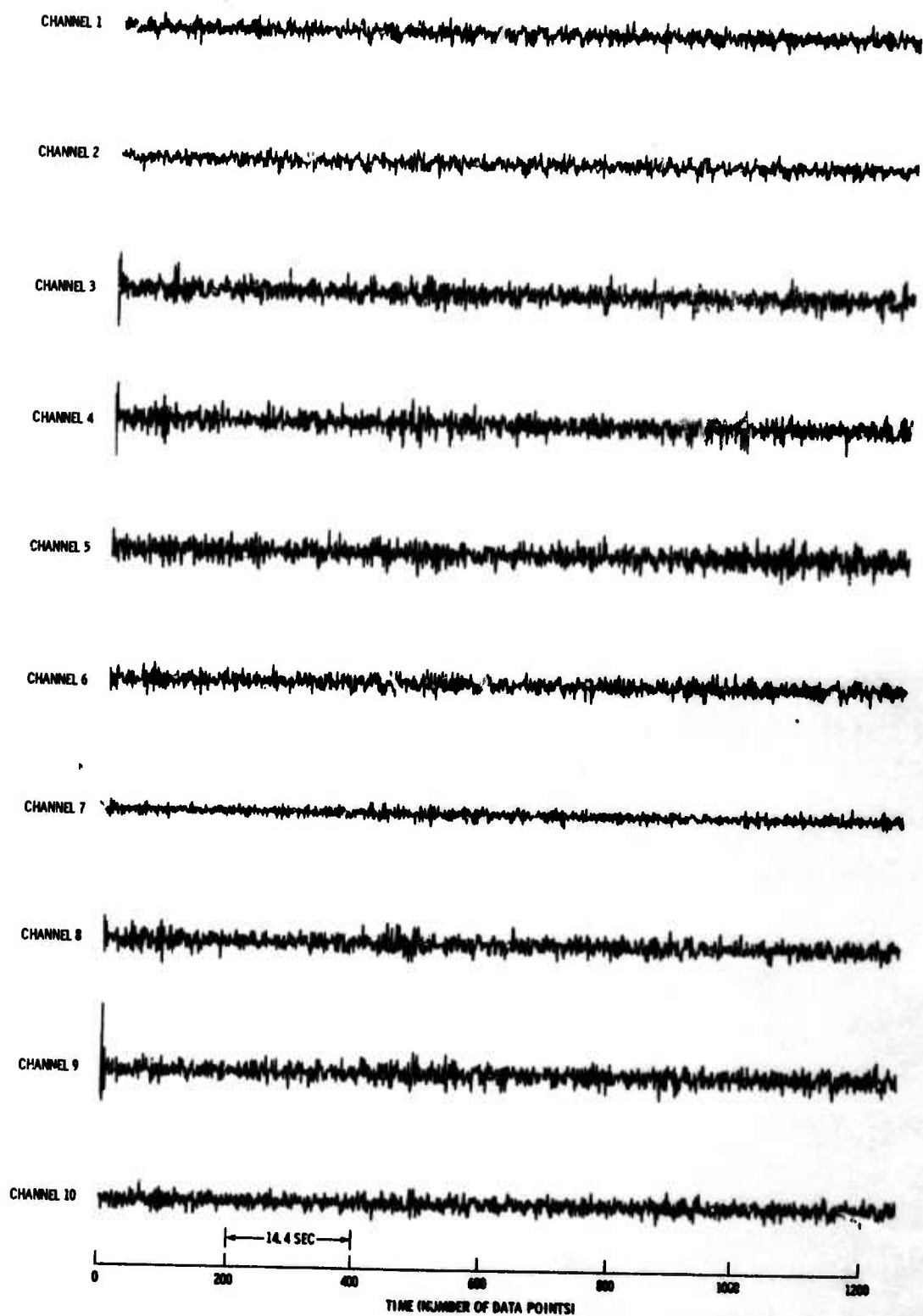


Figure II-16. Whitened UBO Noise Northeast Data



Adaptive 27-point filters were designed identically for unwhitened and whitened data. One run was made for each data type, giving nine passes through the data. As in previous cases, each filter coefficient was set to 0 at the beginning of the first pass and then, at the beginning of each subsequent pass, was set to its value at the end of each preceding pass. Values of k_g for both the unwhitened and whitened cases were 0.0015 (learning), 0.0015, 0.0010, 0.0005, 0.00025, 0.000125, 0.00005, 0.0020, and 0.0025. Mean-square-error as a function of k_g and Wiener mean-square-error for unwhitened and whitened data are shown in Figure II-17.

Adaptive and Wiener error traces for unwhitened data are shown in Figure II-18 and for whitened data in Figure II-19. Figures II-20 and II-21 are power spectra of channel 10 and the Wiener and adaptive error traces.

Again, the whitened data give a linear mean-square-error vs k_g with greater slope than the previous two sets of UBO data. Wiener mean-square-error is approached with decreasing k_g for both data sets. Larger-amplitude wave bursts caused the divergence of the adaptive procedure for the unwhitened data in previous tests (Figure II-15).

D. LASA SUBARRAY B1

The sample of LASA data shown in Figure II-22 was filtered by two different procedures. In the first procedure, where the six seismometers of the inner ring plus the center seismometer were used, 25-point filters were applied to all seven channels to predict one point ahead on the center seismometer (channel 1). Wiener and adaptive results of this processing of unwhitened data were included in a TI special report.¹ The seven channels used in this procedure have since been whitened with a 9-point deconvolution filter designed from the autocorrelation of channel 1 and the whitened data (Figure II-23) filtered adaptively. The whitened data were not Wiener-filtered.

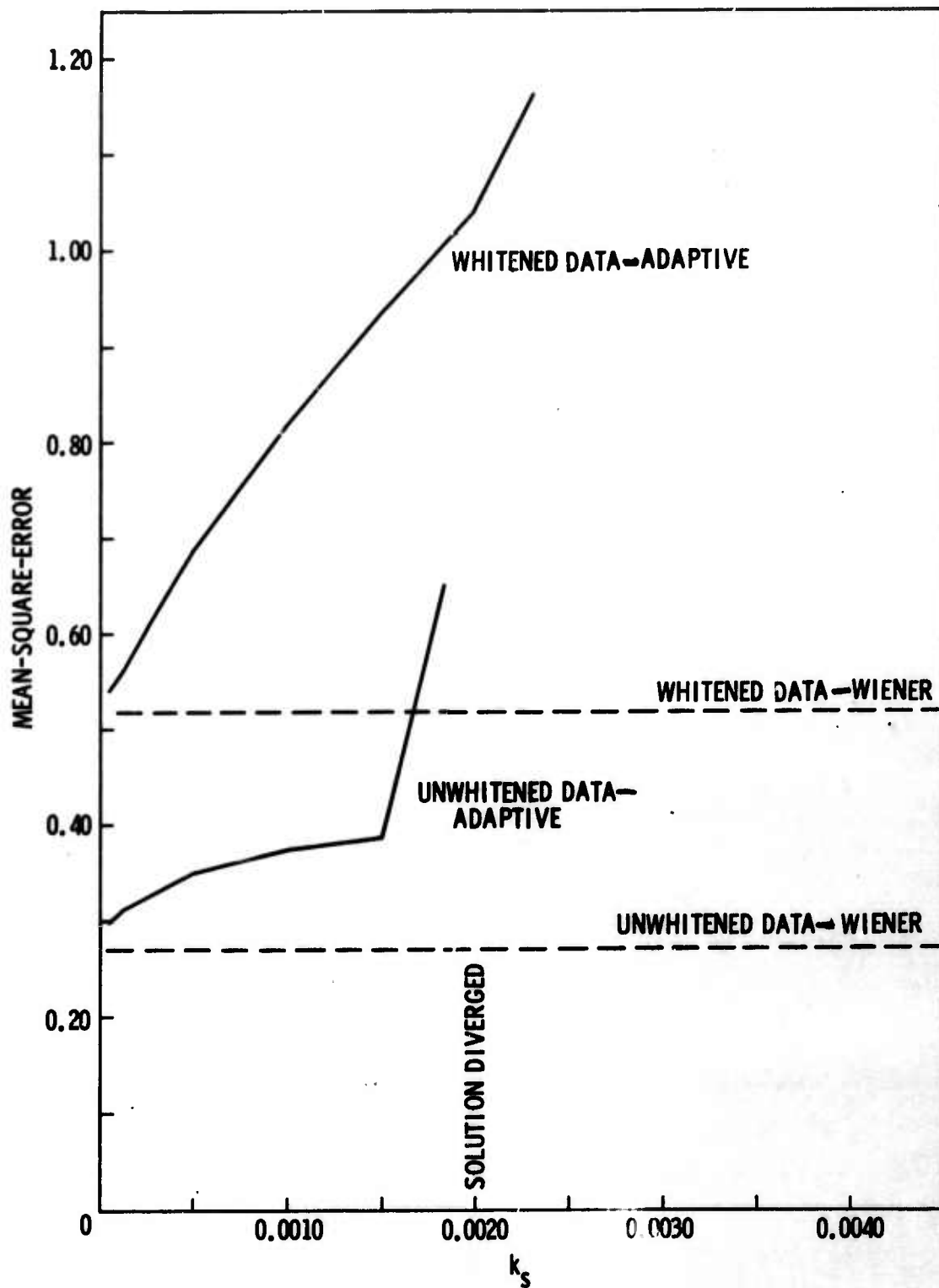


Figure II-17. Mean-Square-Error Vs k_s for UBO Noise Northeast

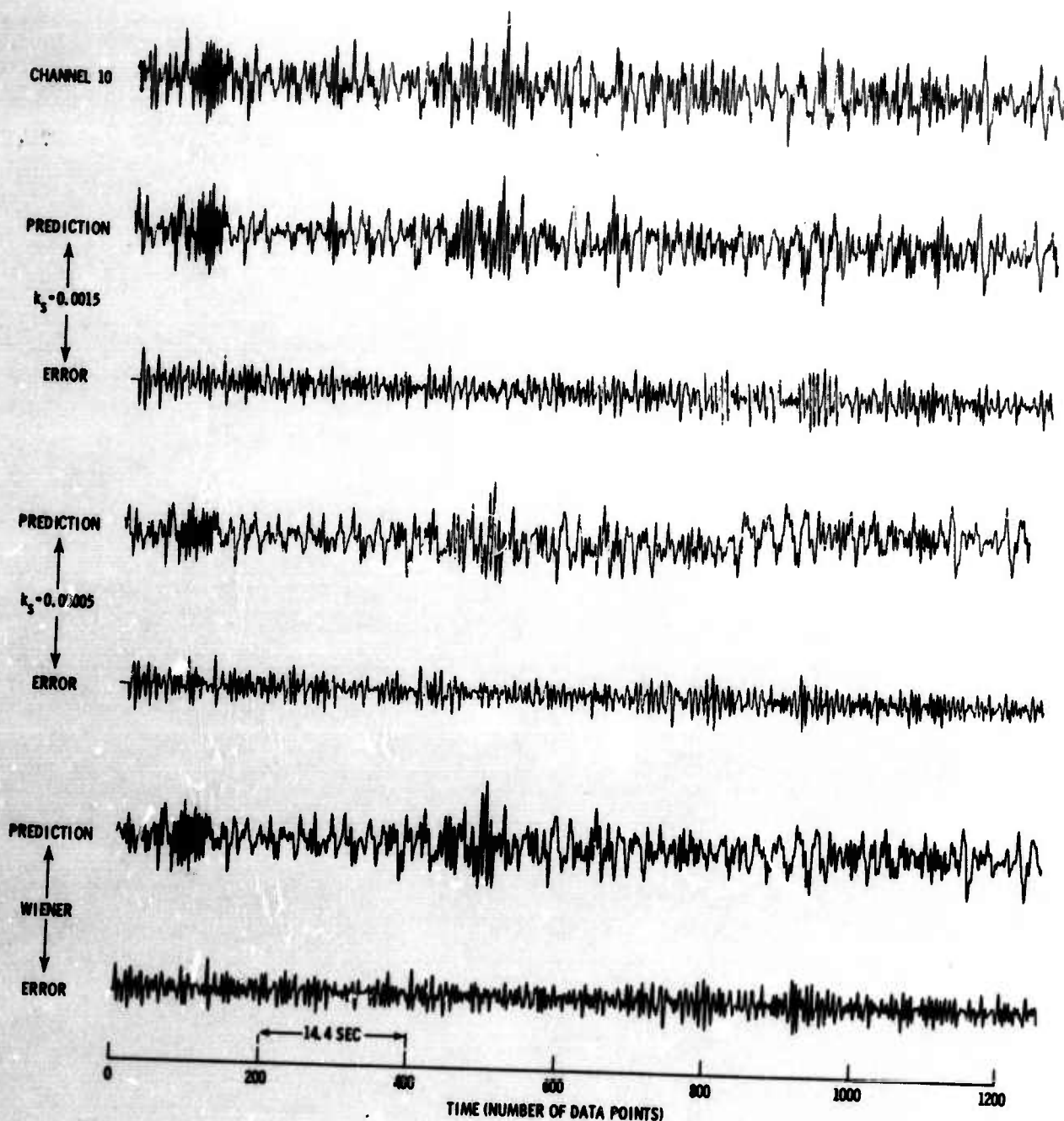


Figure II-18. Wiener and Adaptive Outputs for UBO Noise Northeast

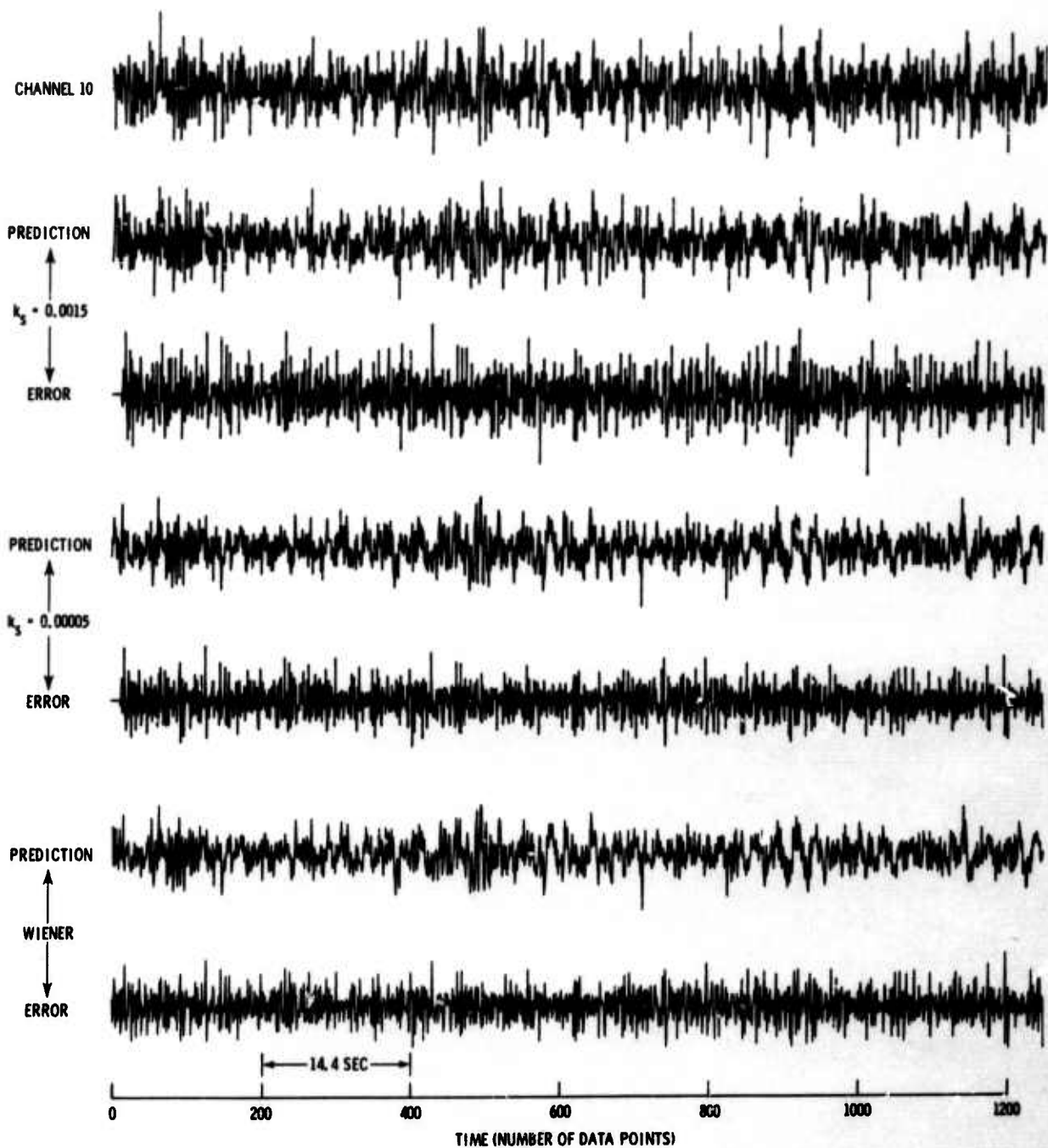


Figure II-19. Wiener and Adaptive Outputs for Whitened UBO Noise Northeast

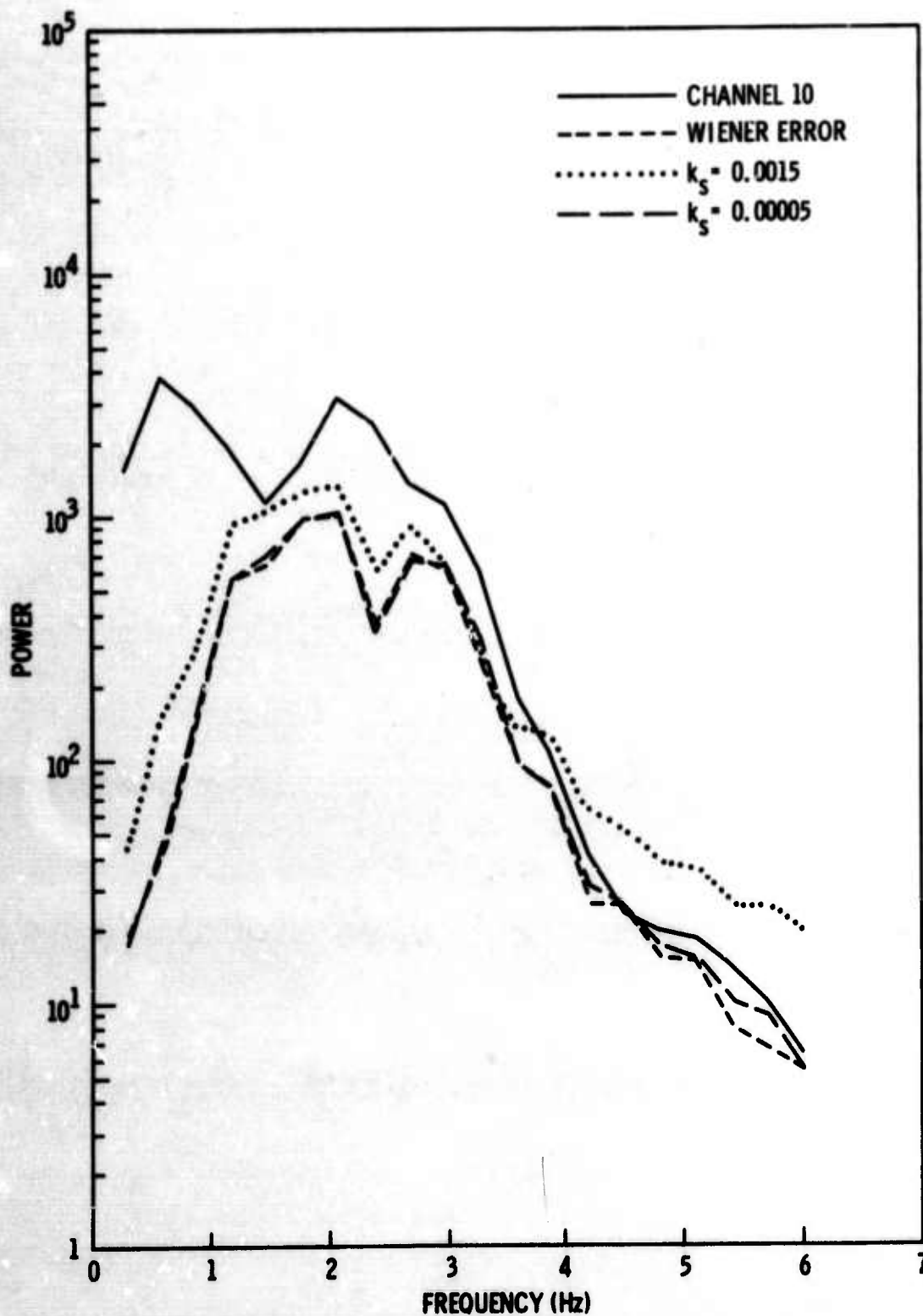


Figure II-20. Power Spectra of Channel 10, Wiener Errors, and Adaptive Errors for UBO Noise Northeast

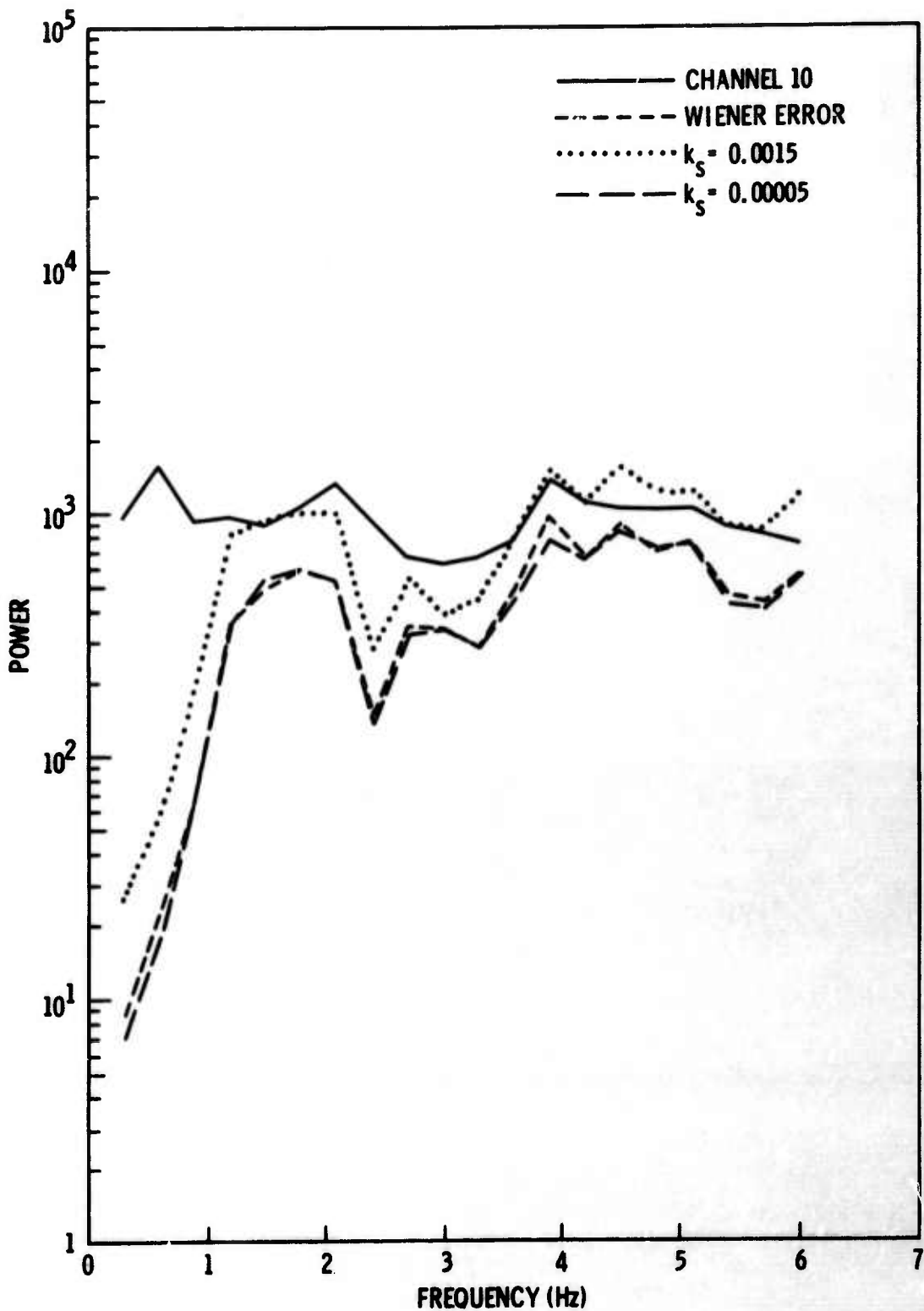


Figure II-21. Power Spectra of Channel 10, Wiener Errors, and Adaptive Errors for Whitened UBO Noise Northeast

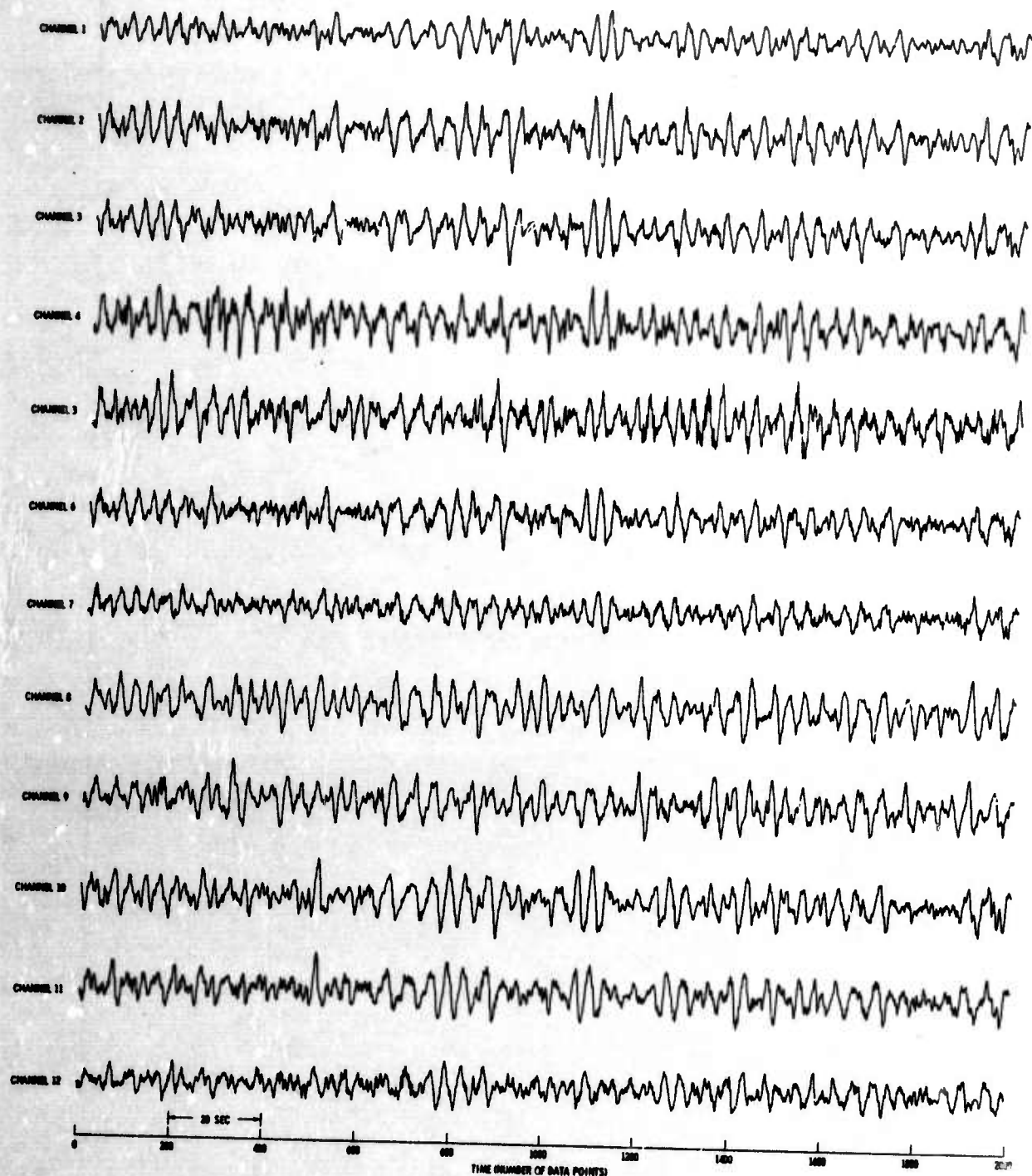


Figure II-22. Prefiltered and Resampled LASA Subarray B1
Center Seismometer and First Ring

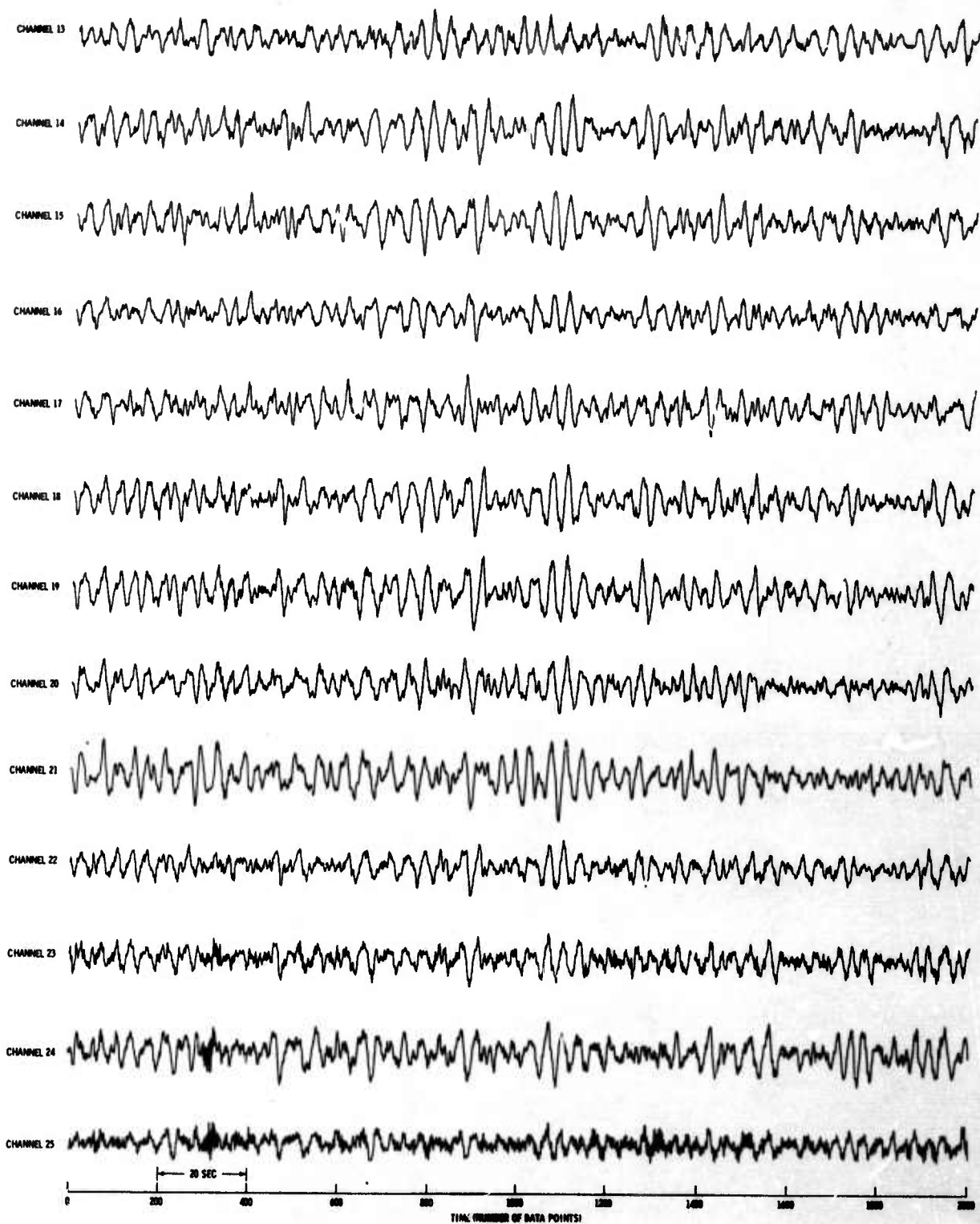


Figure II-22. (Contd)

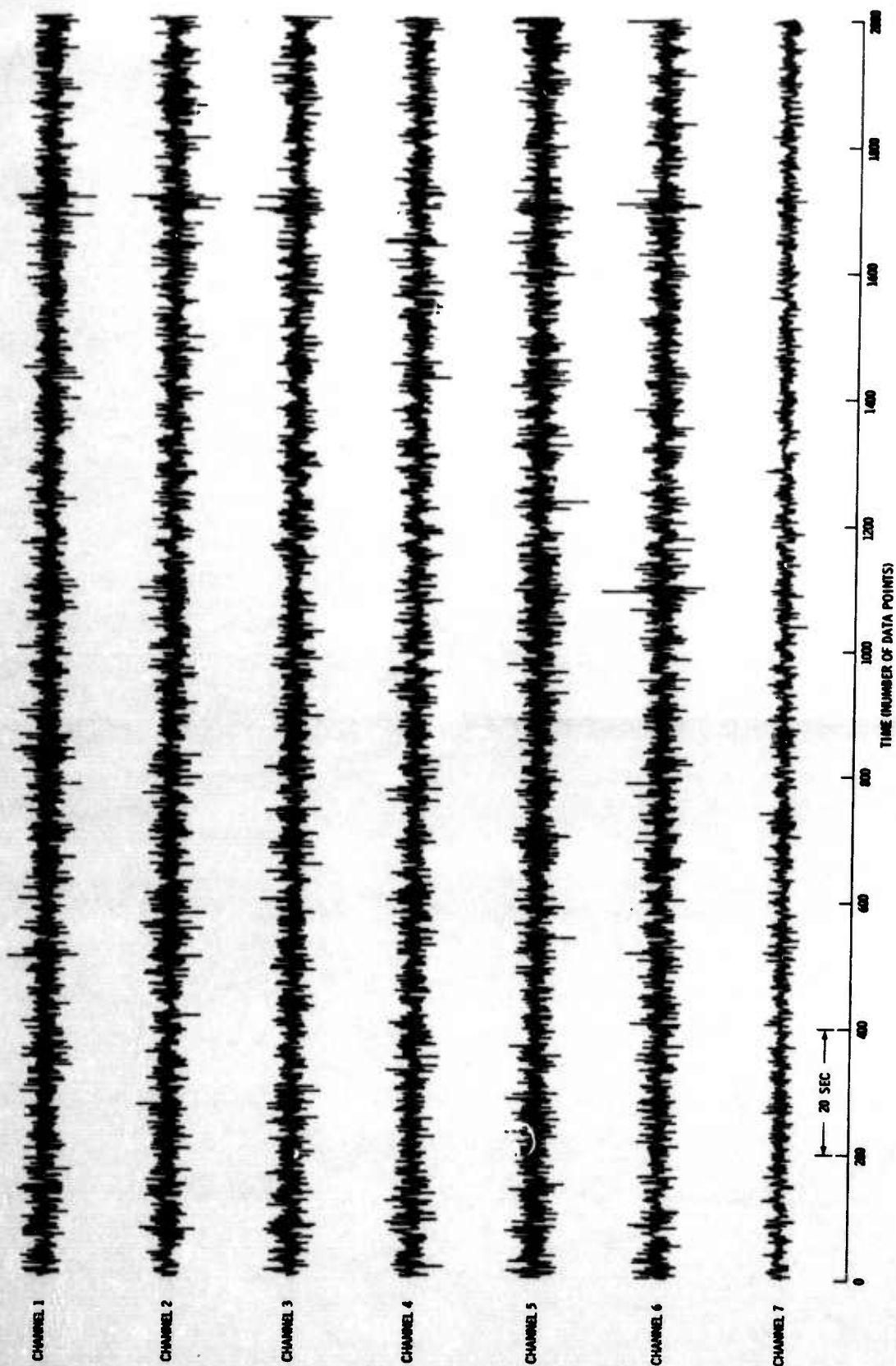


Figure II-23. Prefiltered, Resampled, and Whitened LASA Subarray B1 Center Seismometer and First Ring



Adaptive processing of the whitened data consisted of eight passes, with filter coefficients initially set at 0. Initial filter coefficients for subsequent passes equaled their values at the end of the previous pass. Values of k_g were 0.001 (learning), 0.001, 0.0005, 0.00025, 0.000125, 0.0000625, 0.002, and 0.0025. Plots of mean-square-error vs k_g for adaptively processed unwhitened and whitened data are given in Figure II-24 along with the normalized Wiener mean-square-error of 0.031 for the unwhitened data.

Prediction and prediction-error traces for the 7-channel data are given in Figures II-25 and II-26, and spectra of these traces are plotted in Figures II-27 and II-28.

The second processing procedure for these data used a 25-point filter on all 25 channels to predict the center seismometer (channel 1) one point ahead. Adaptive filtering was performed on the unwhitened data only. In this case, no data whitening or Wiener filtering was attempted.

The adaptive run consisted of nine passes through the data, with the filter coefficients set to 0 at the beginning of the first pass and set equal to their values at the end of the previous pass to begin subsequent passes. Values of k_g for these passes were 0.00025 (learning), 0.00025, 0.00015, 0.00005, 0.000025, 0.000005, 0.000375, 0.0005, and 0.00075.

Mean-square-error of prediction as a function of k_g for this case is shown in Figure II-29, with the prediction and prediction-error traces in Figure II-30 and the corresponding power spectra in Figure II-31.

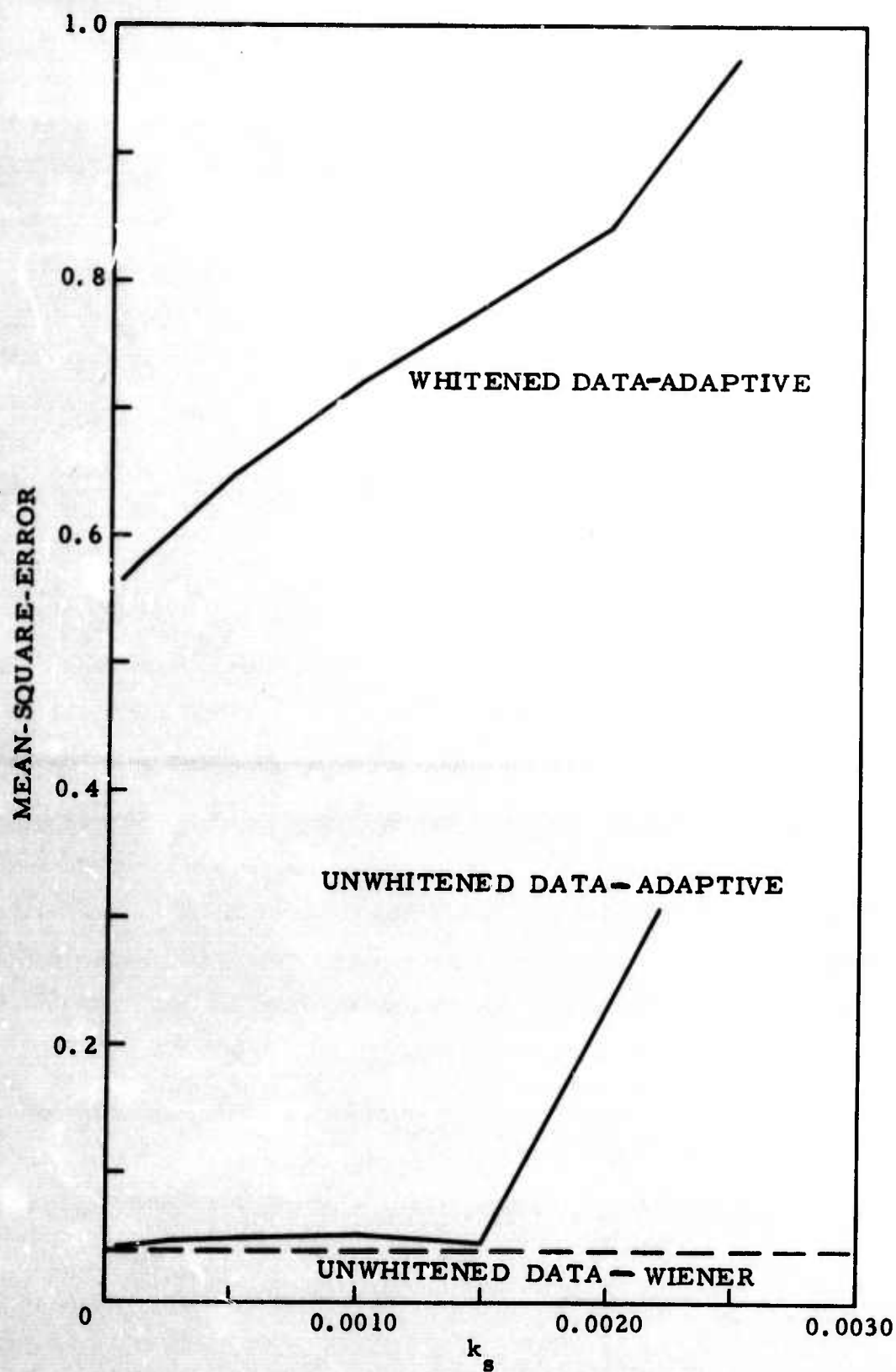


Figure II-24. Mean-Square-Error Vs k_s for Prefiltered and Resampled LASA Subarray B1 Center Seismometer and First Ring

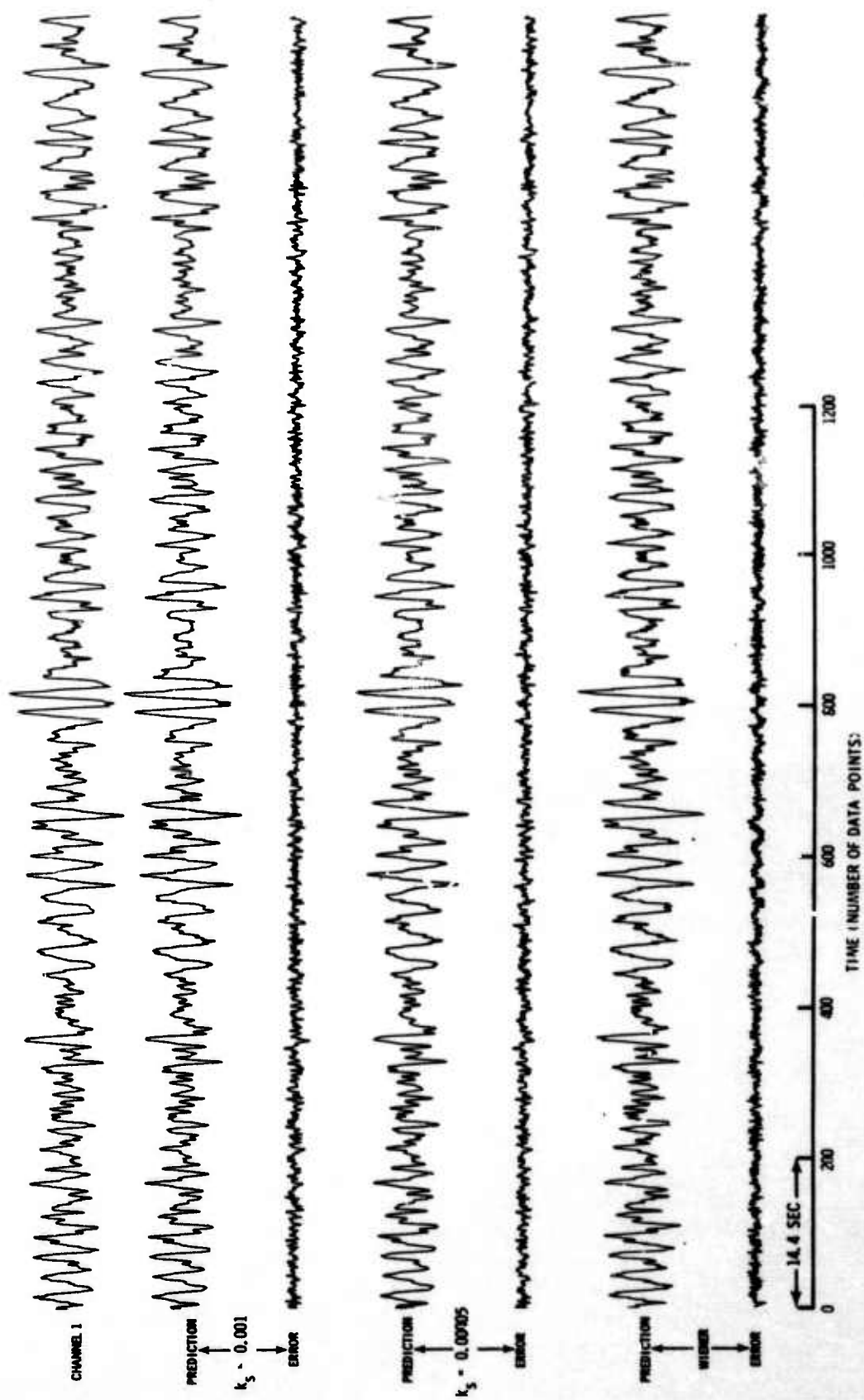


Figure II-25. Wiener and Adaptive Outputs for Prefiltered and Resampled LASA Subarray B1 Center Seismometer and First Ring

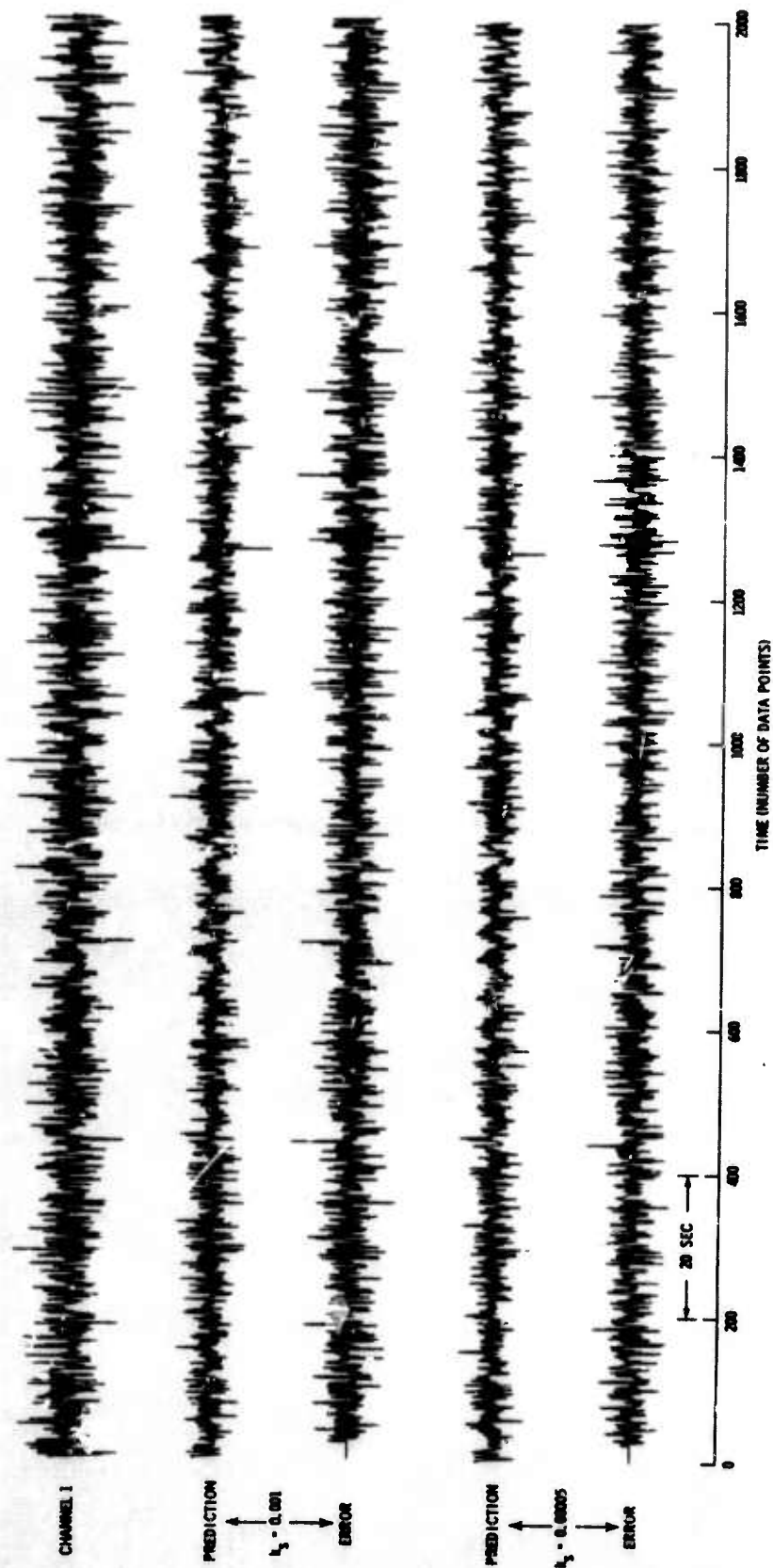


Figure II-26. Wiener and Adaptive Outputs for Prefiltered, Resampled, and Whitenened LA3A Subarray B1 Center Seismometer and First Ring

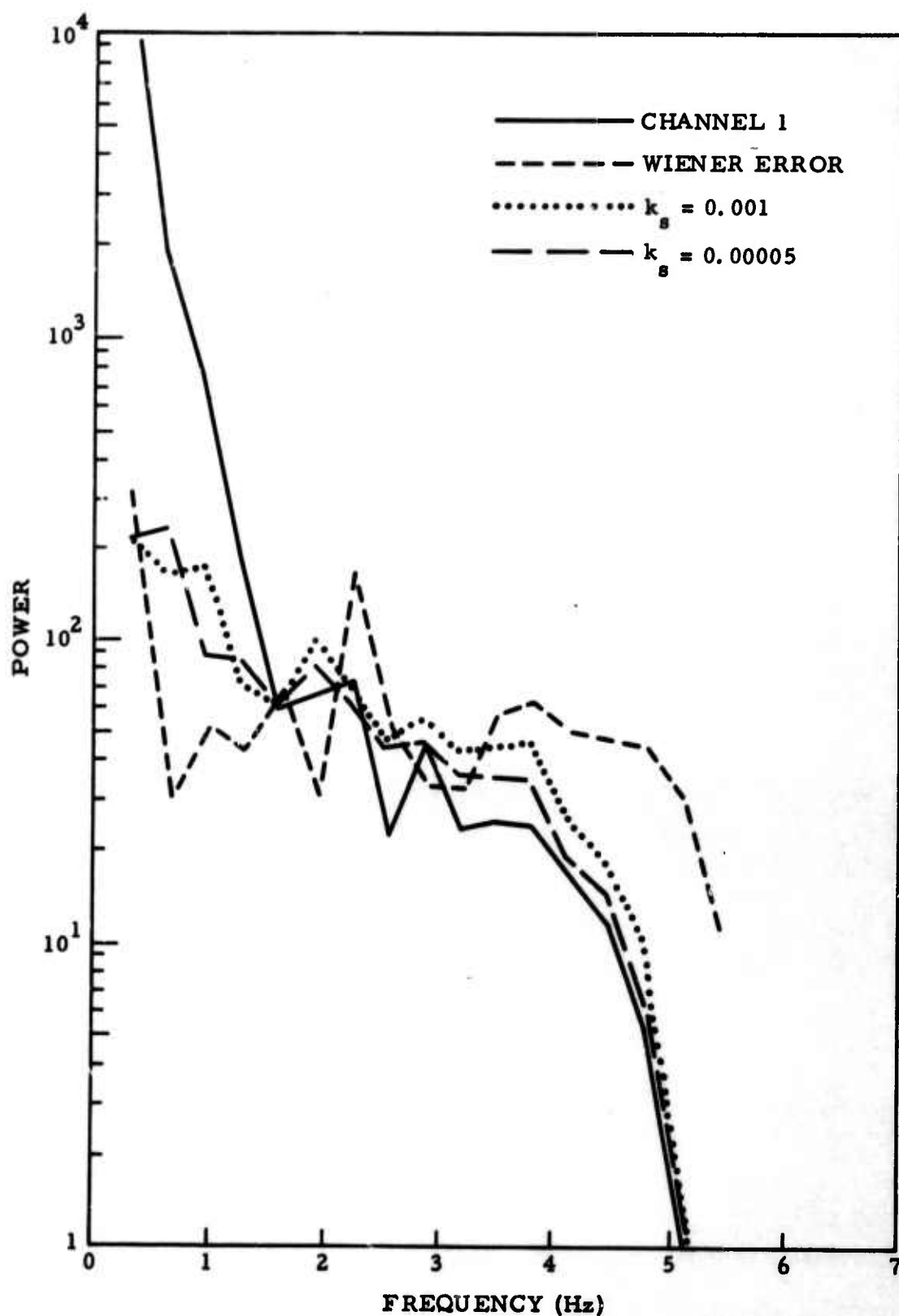


Figure II-27. Power Spectra of Channel 10, Wiener Errors, and Adaptive Errors for Prefiltered and Resampled LASA Subarray B1 Center Seismometer and First Ring

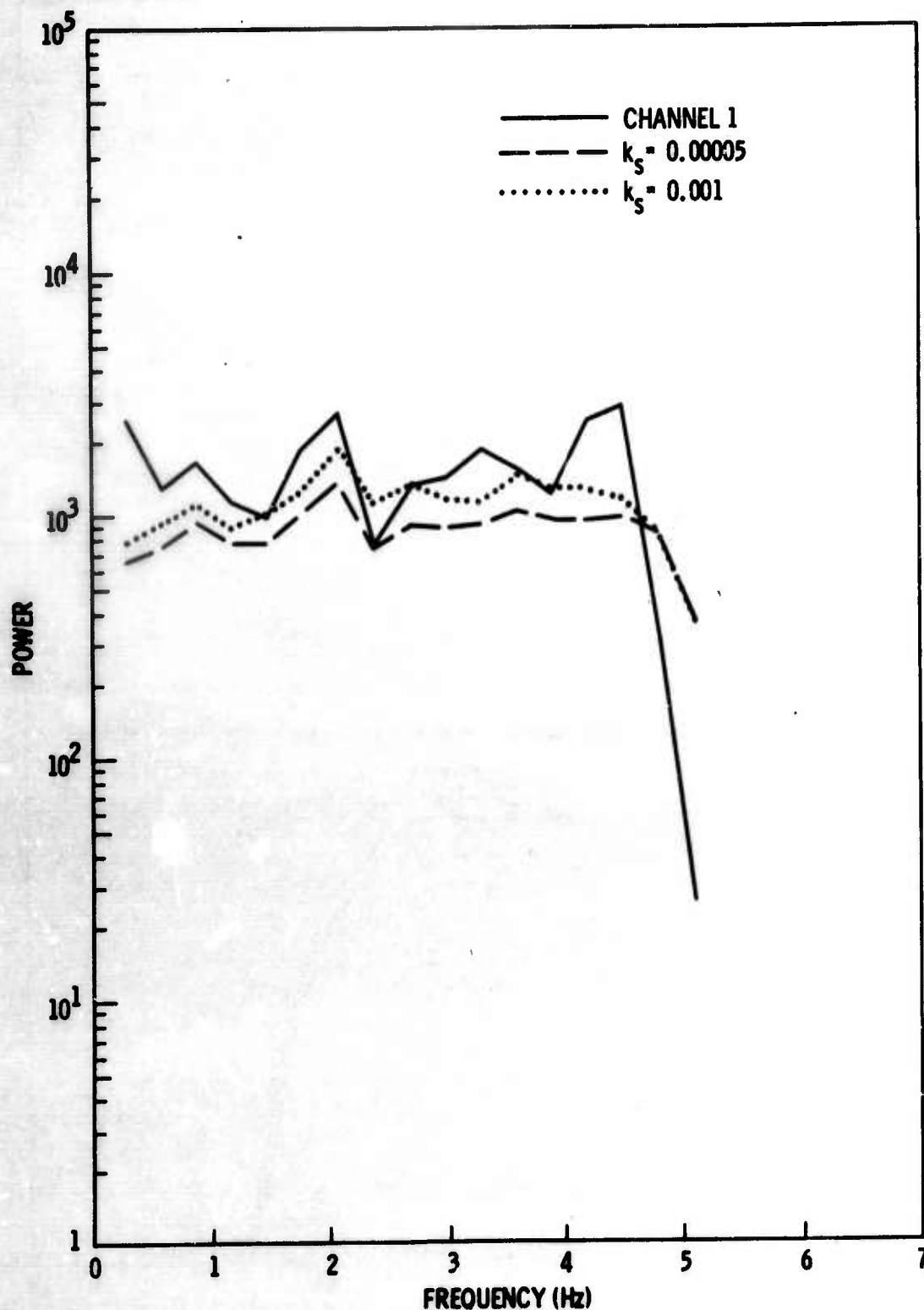


Figure II-28. Power Spectra of Channel 10, Wiener Errors, and Adaptive Errors for Prefiltered, Resampled, and Whited LASA Subarray B1 Center Seismometer and First Ring

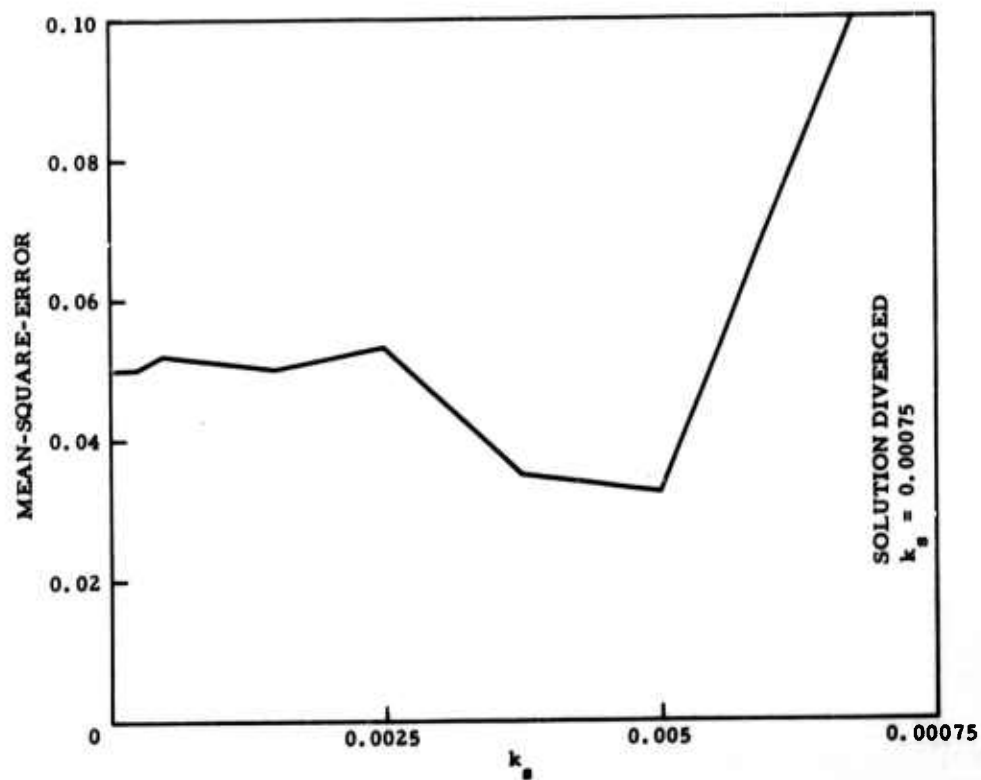


Figure II-29. Mean-Square-Error Vs k_s for
LASA Subarray B1, 25 Channels

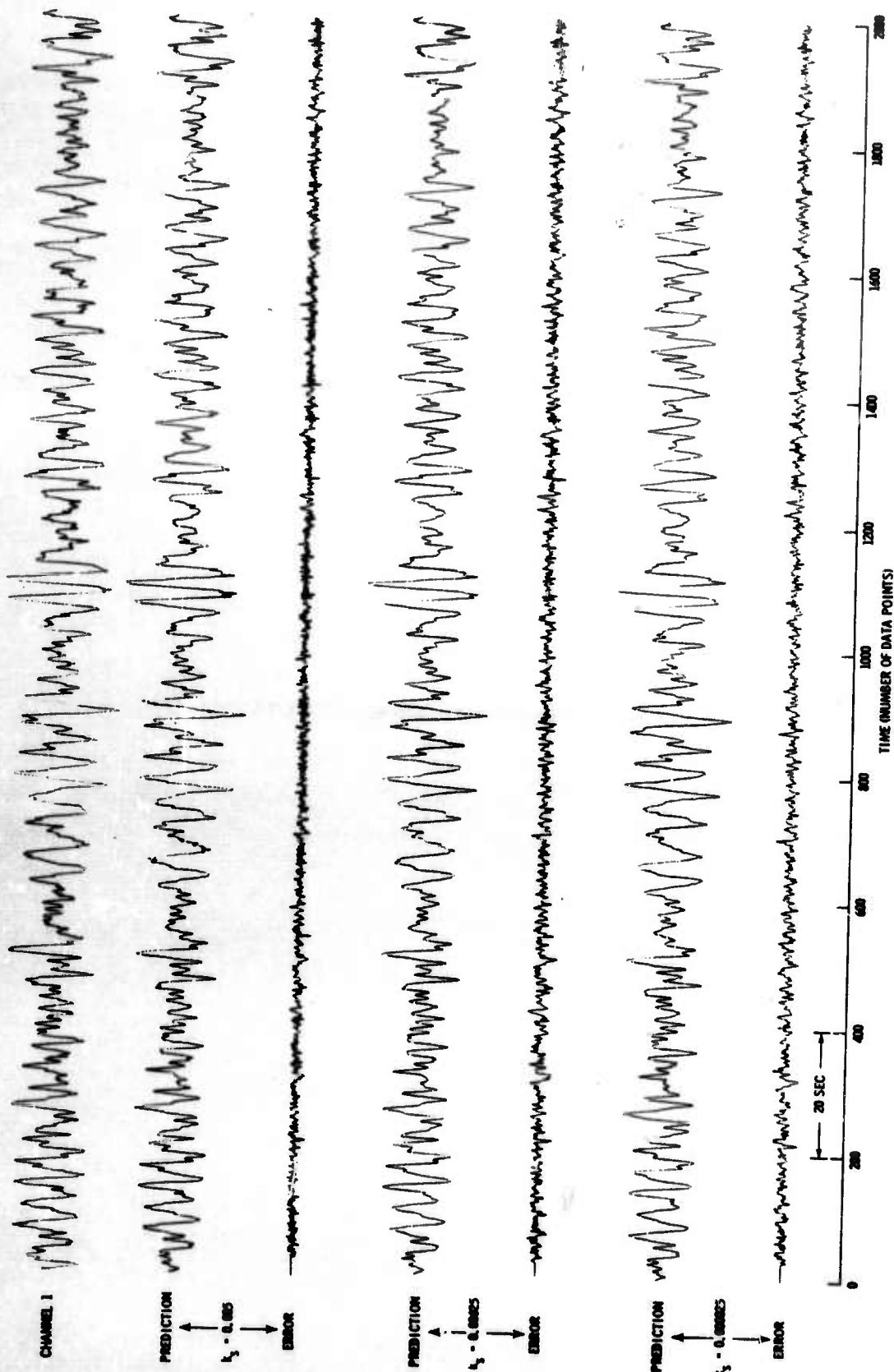


Figure II-30. Error Traces for LASA Subarray B1, 25 Channels

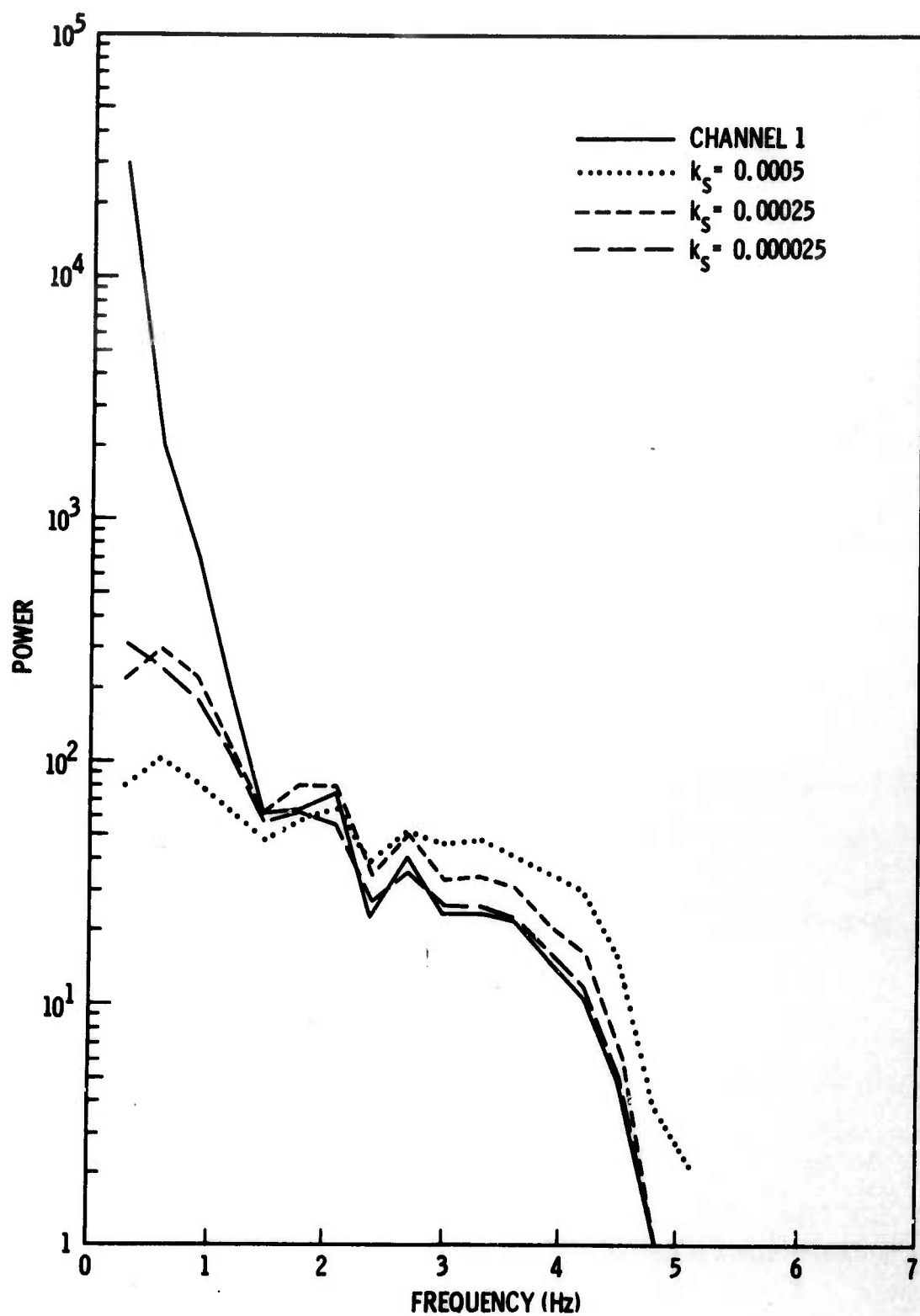


Figure II-31. Power Spectra of Adaptive Error Traces for LASA Subarray B1, 25 Channels



E. ARRAY DATA

Special Report No. 1 discusses the processing of 13 channels of array data (Figure II-32) using 37-point Wiener and adaptive filters designed to predict channel 1 from channels 2 through 13, the output point being at the center. These data were resampled to a 72-msec sample period and prewhitened. Power spectra of the unwhitened and partially whitened data showed the whitening effect of the prewhitening filter to be very small except at frequencies below 1 Hz. At frequencies above 1 Hz, the prewhitening filter left the data virtually unchanged. The partially whitened data, therefore, were whitened again with a 9-point deconvolution filter designed from the autocorrelation of channel 1 (Figure II-33).

With filter coefficients initially set at 0, one adaptive filtering run consisting of six passes was made on the whitened data, the k_g values being 0.0005 (learning), 0.0005, 0.00025, 0.000125, 0.00005, and 0.00075. The whitened data were not Wiener-filtered because 37 points and 13 channels exceeded the dimensions of the existing filter-design program on the IBM 7044. Figure II-34 plots mean-square-error as a function of k_g for the whitened data and presents previous adaptive and Wiener results for the partially whitened data.

The prediction and prediction-error traces for partially whitened and whitened data are given in Figures II-35 and II-36, respectively. Their power spectra are given in Figures II-37 and II-38.

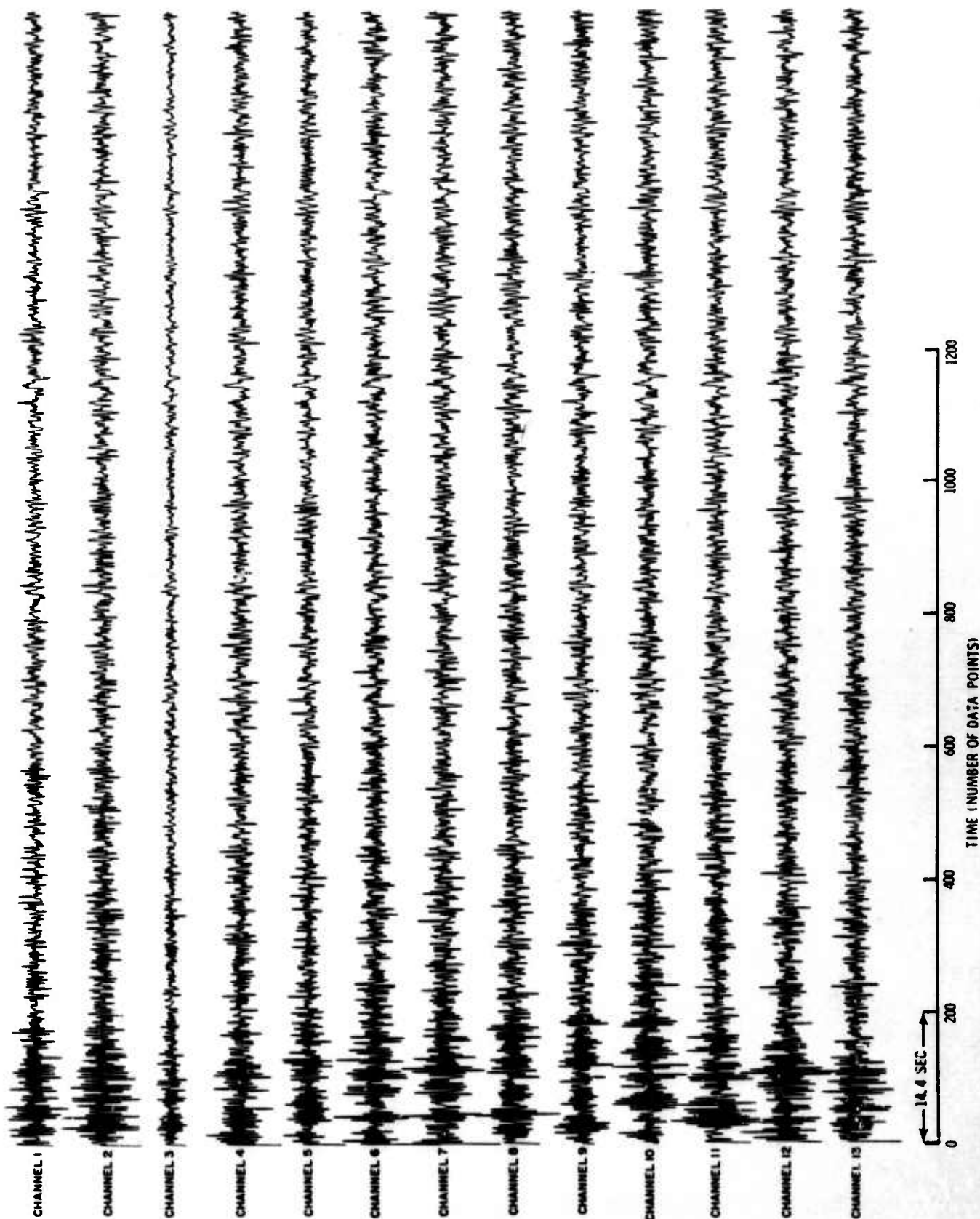


Figure II-32. Prefiltered and Resampled Array Data

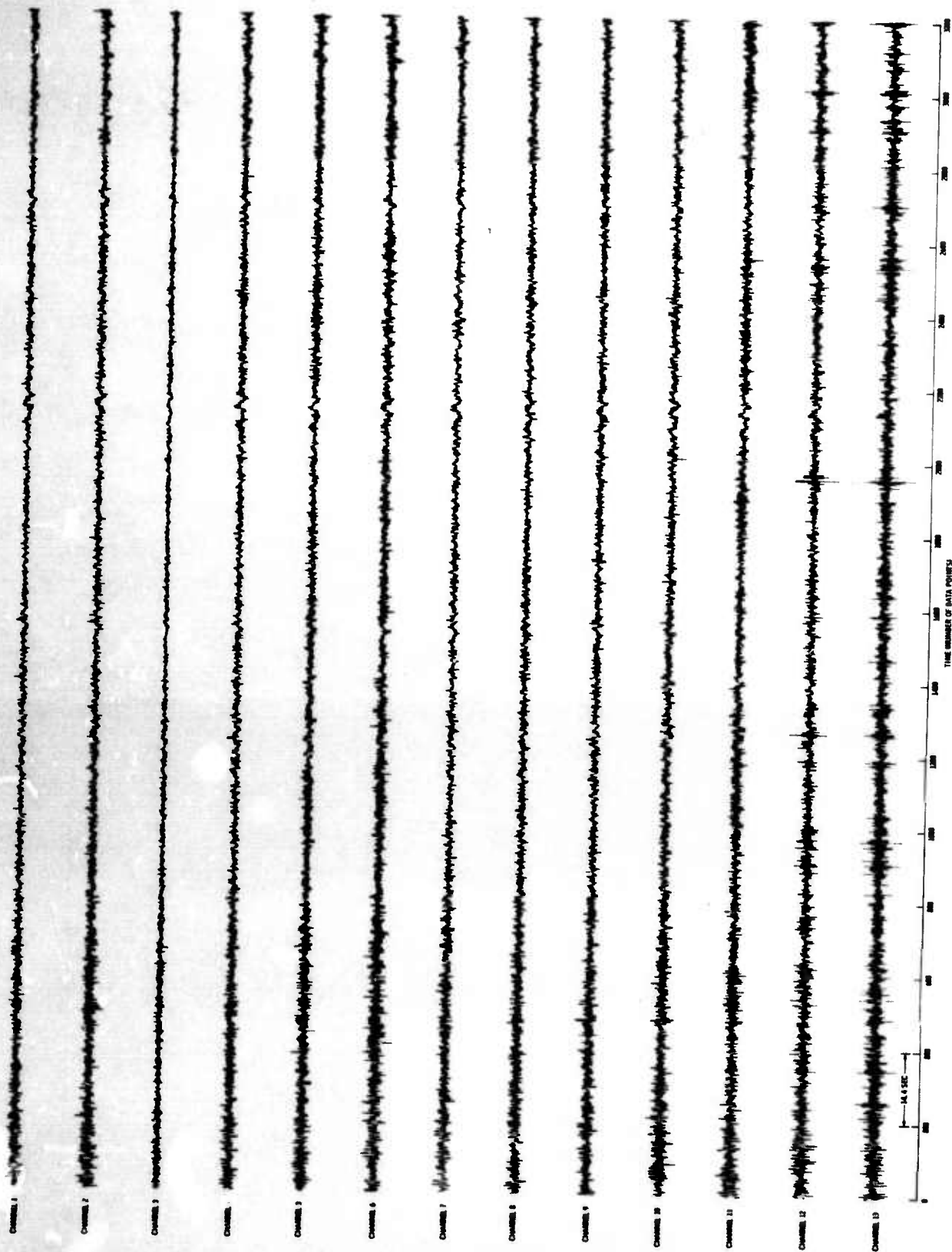


Figure II-33. Prefiltered, Resampled, and Whitened Array Data

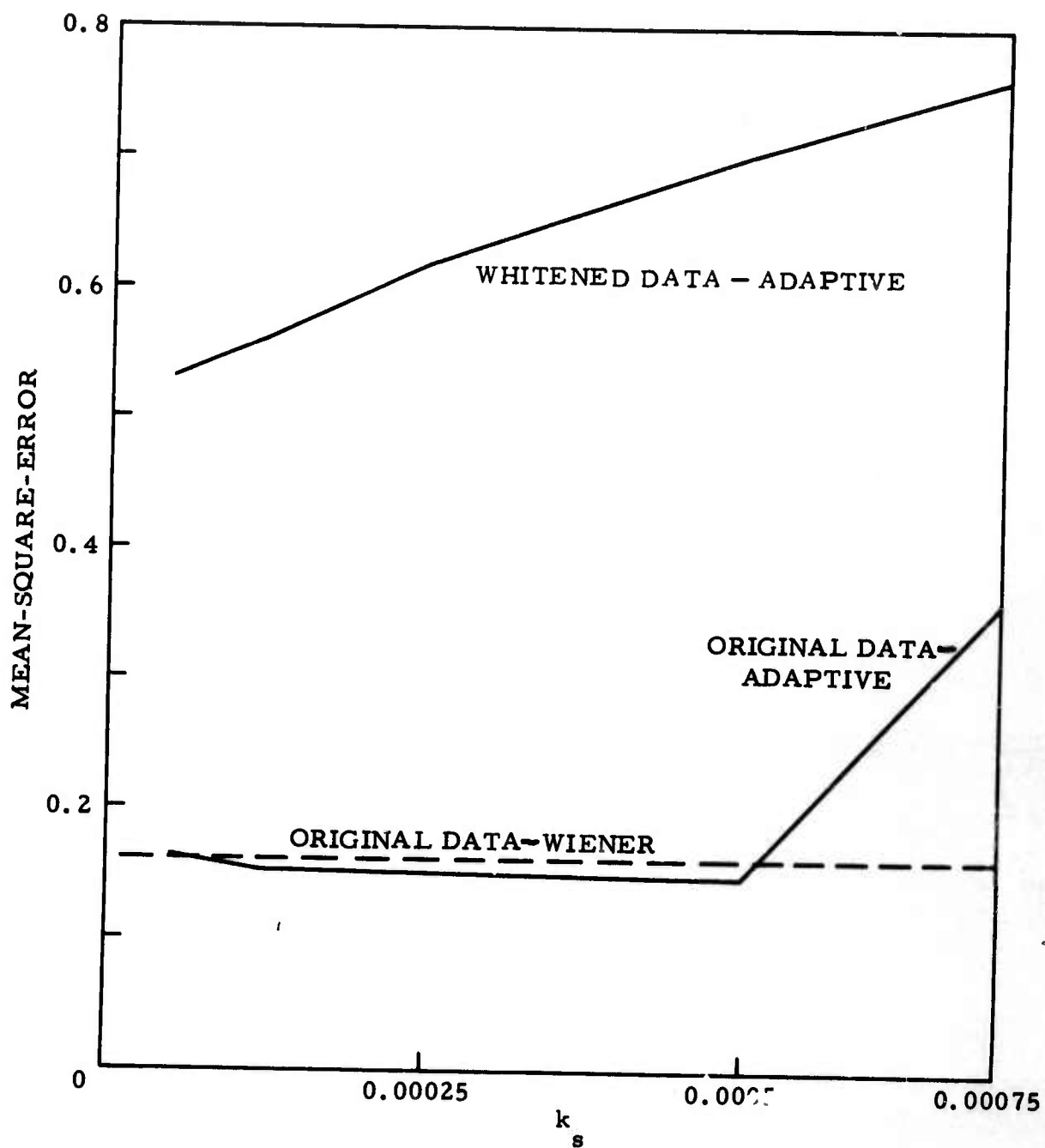


Figure II-34. Mean-Square-Error Vs k_s for Array Data

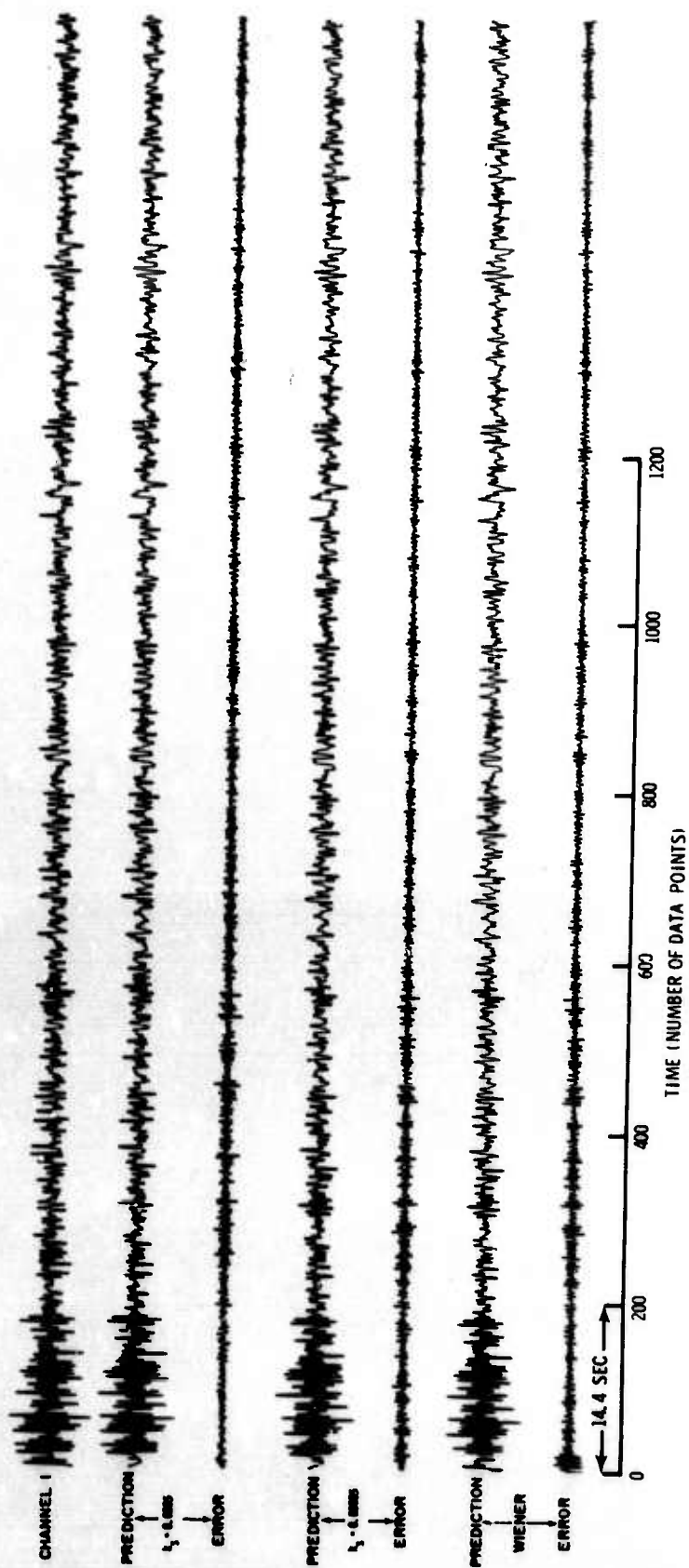


Figure II-35. Wiener and Adaptive Filter Outputs for Array Data

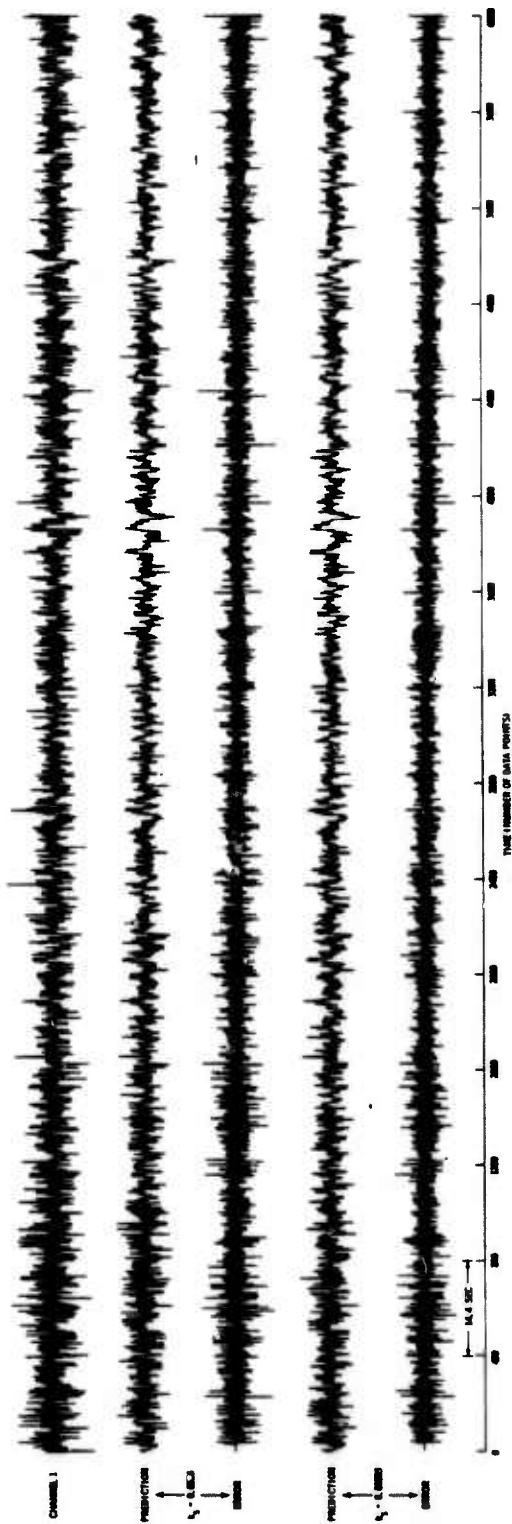


Figure II-36. Adaptive Filter Outputs for Whiten Array Data

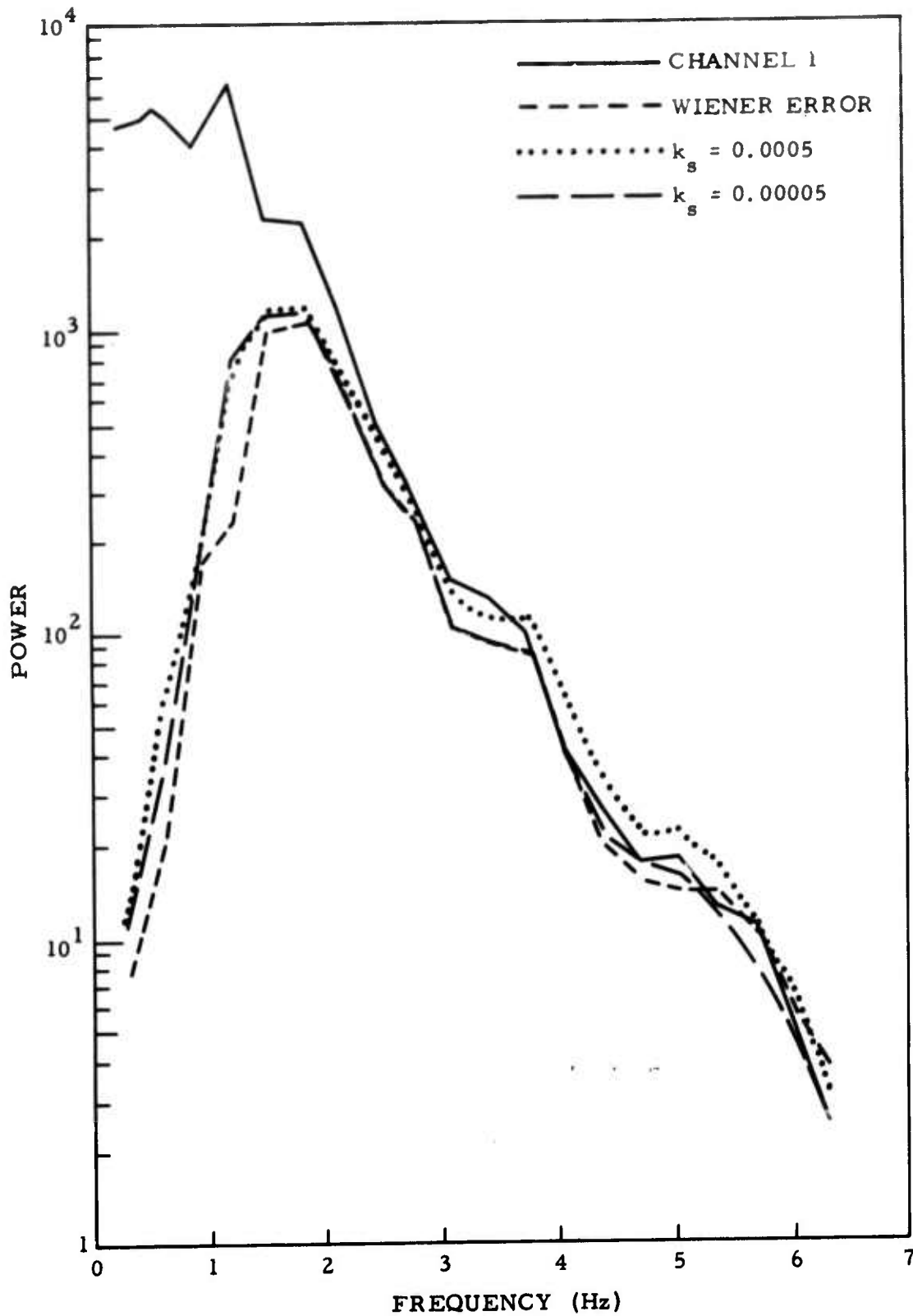


Figure II-37. Power Spectra of Channel 1, Wiener Error, and $k_s = 0.0005, 0.00005$ for Array Data

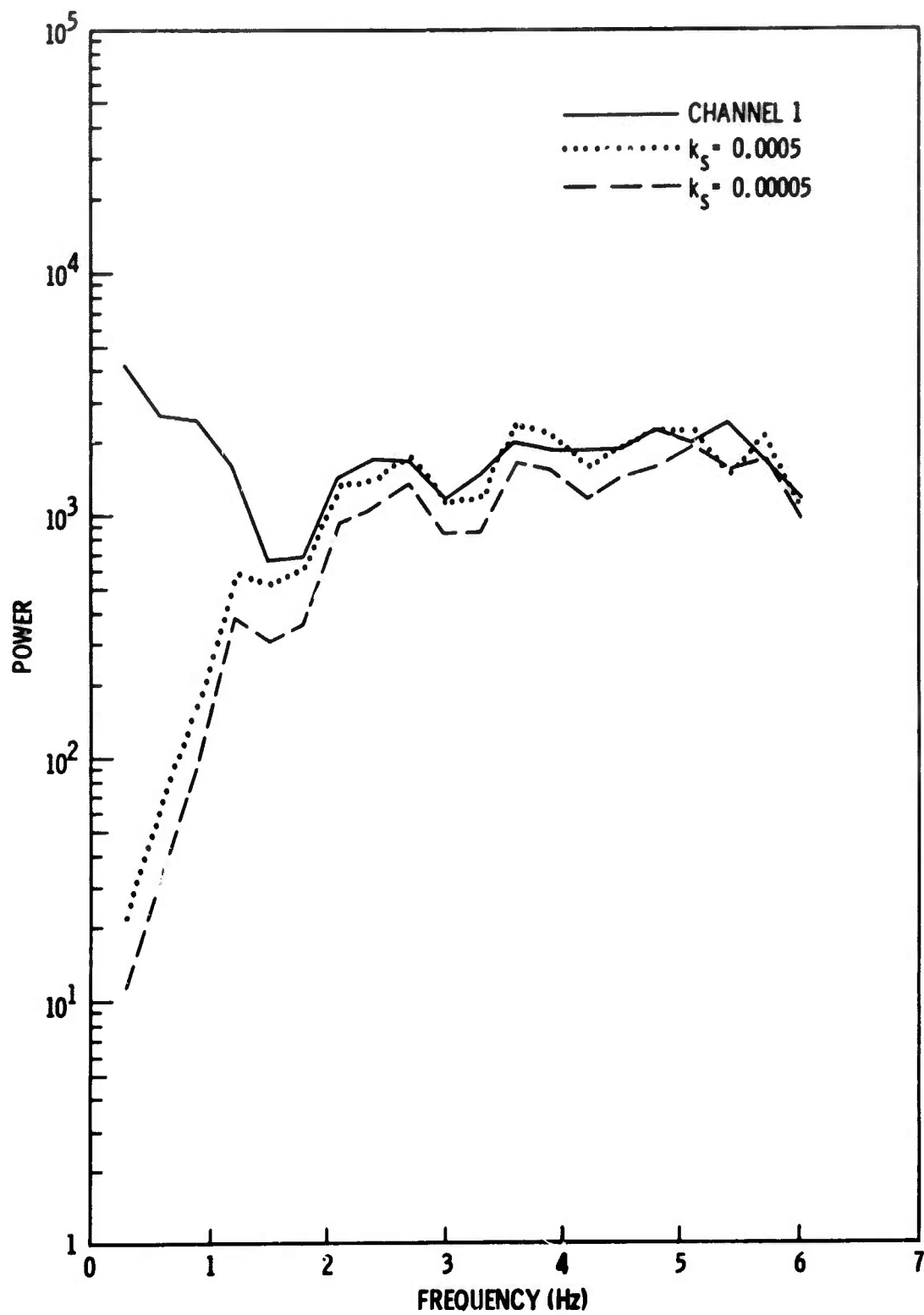


Figure II-38. Power Spectra of Channel 1 and $k_s = 0.0005$, 0.00005 for Whitened Array Data

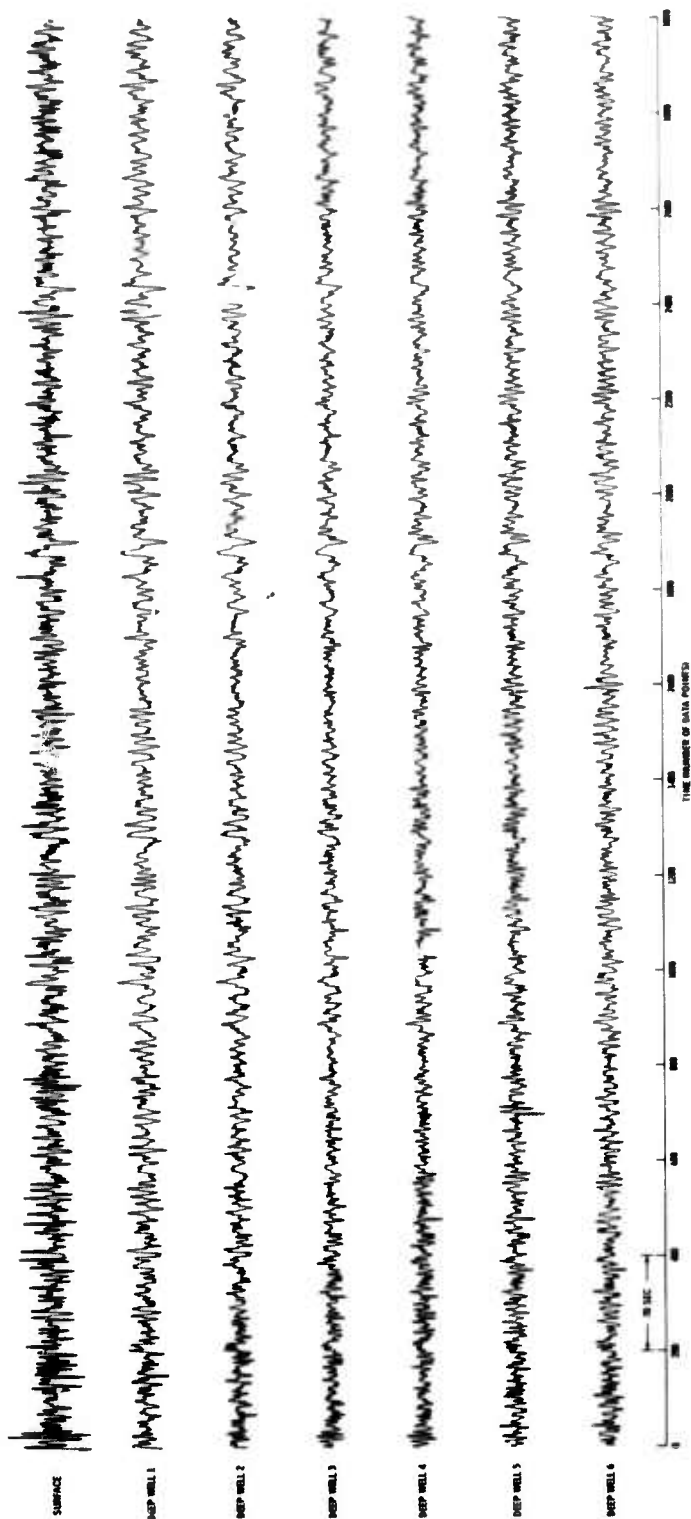


Figure II-39. Vertical Array A Data



F. VERTICAL ARRAY A

This sample consists of short-period vertical-component data from six deep-well seismometers and one surface seismometer at the top of the well (Figure II-39). The two prediction problems considered here are to use the six deep-well channels to predict the surface and to predict the top deep-well channel from the other five deep-well channels. Sample period of these data is 72 msec, and the data have been slightly prewhitened. Both adaptive and Wiener filtering were performed using 37-point filters with output points at the center. No whitening, except for the very slight prewhitening already mentioned, was attempted on these data.

To predict the surface seismometer, eight adaptive passes were made, with k_g values of 0.0015 (learning), 0.0015, 0.0010, 0.0005, 0.00025, 0.000125, 0.0000625, and 0.0020. Filter coefficients again were 0 for the first pass and the values at the end of the previous pass for subsequent passes. Figure II-40 plots k_g vs mean-square-error for this problem and also shows a Wiener mean-square-error of 0.089. Wiener and adaptive filter outputs and their power spectra are shown in Figures II-41 and II-42, respectively.

The second problem, i. e., predicting the top deep-well channel from the other deep wells, was run in the same manner as the first problem except nine rather than eight adaptive passes were used. The first eight values of k_g were the same as those in the first problem, and the ninth value was 0.0025. Results are presented in Figures II-43 through II-45.

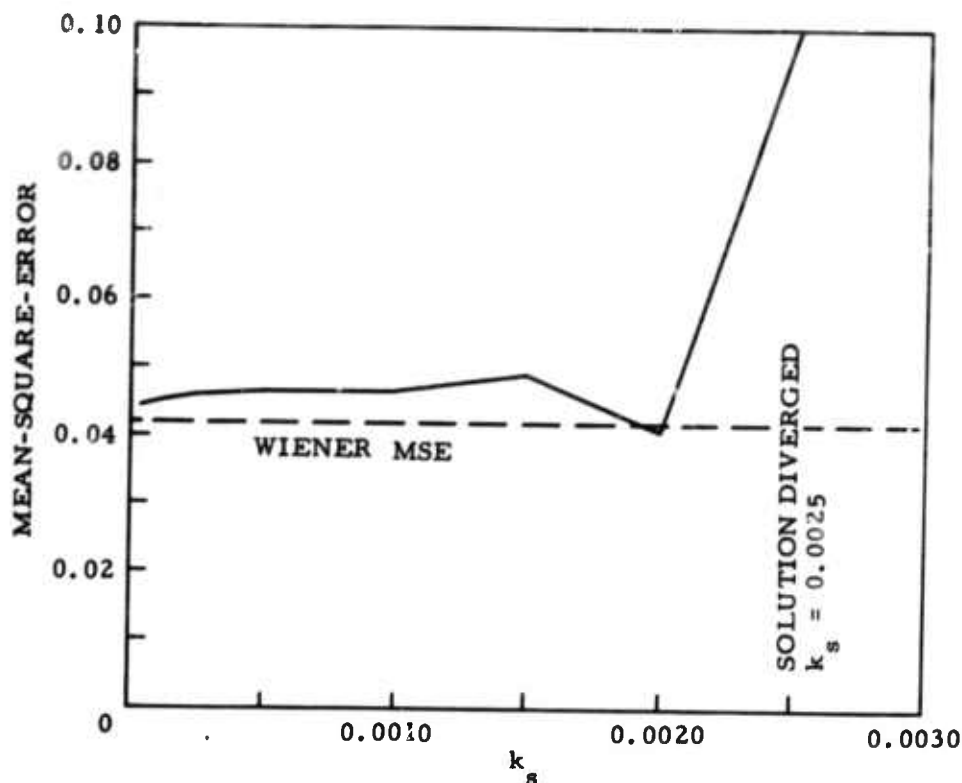


Figure II-40. Mean-Square-Error Vs k_s for Vertical Array A Predicting Surface Seismometer

G. VERTICAL ARRAY B

These data were recorded at the same array as the previous sample. These data (Figure II-46) were processed in the same manner as sample A and, with one exception, all statements about sample A and its processing apply to sample B. The exception is that the adaptive run for the second prediction problem consisted of eight passes rather than nine, with the 0.0025 k_s value omitted.

Results of processing data sample B are presented in Figures II-47 through II-52.

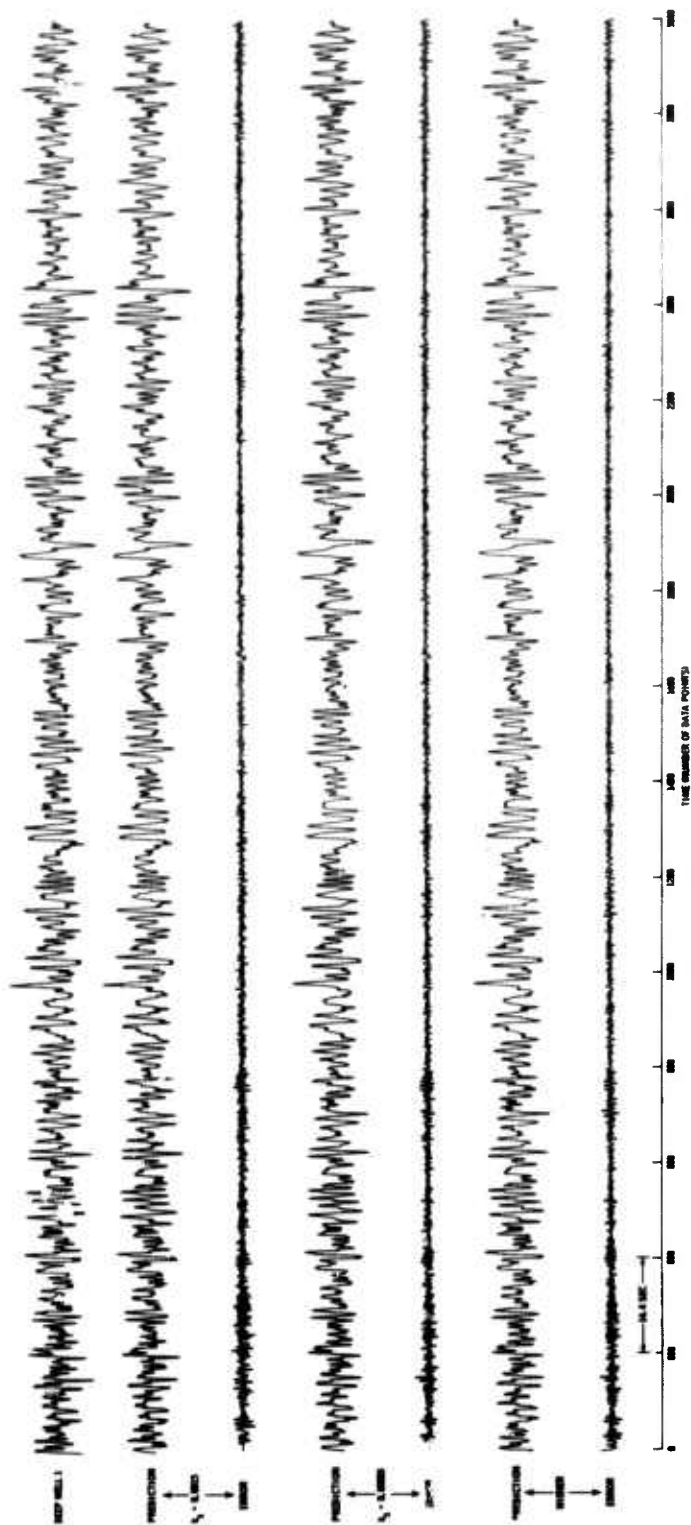


Figure II-41. Error Outputs for Vertical Array A Predicting Surface Seismometer

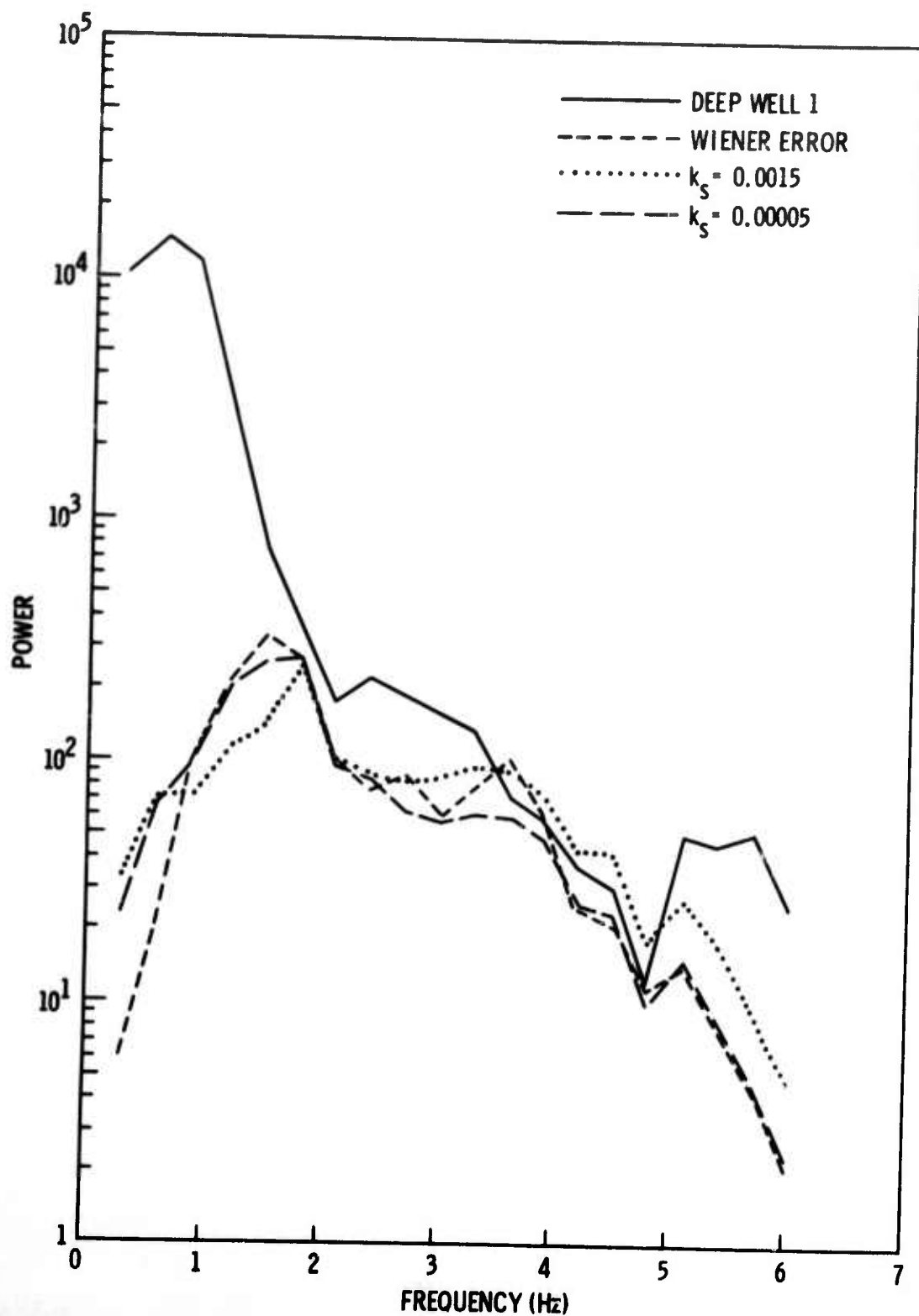


Figure II-42. Power Spectra for Vertical Array A Predicting Surface Seismometer

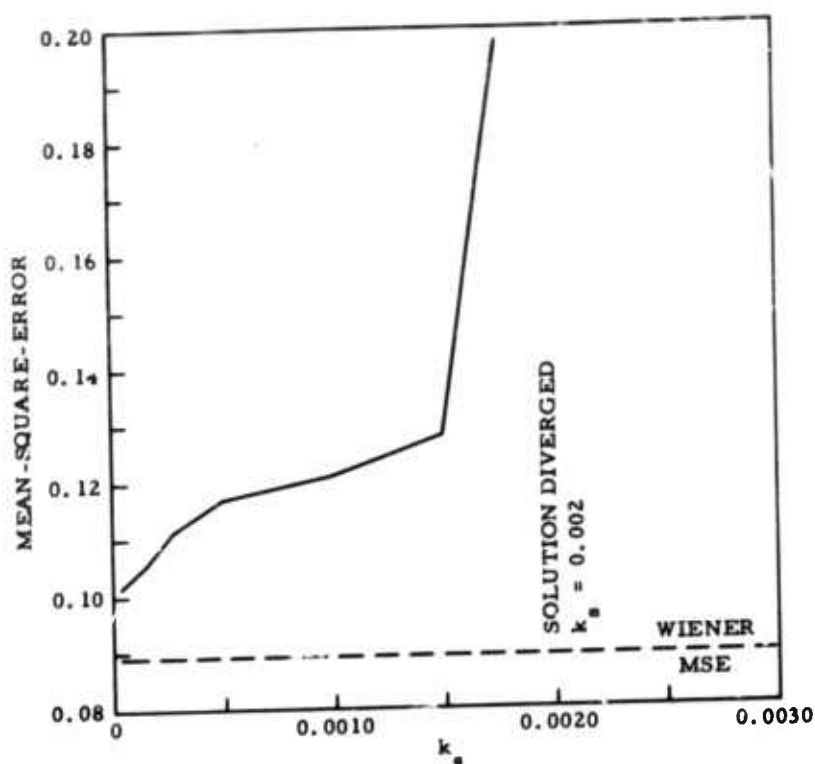


Figure II-43. Mean-Square-Error Vs k_g for Vertical Array A Predicting Top Deep-Well Seismometer

H. LASA SUBARRAY B1, RING-STACKED

The 25 short-period, vertical seismometers of LASA subarray B1 were stacked by rings to give the eight data channels shown in Figure II-53. Channel 1 is the output of the center seismometer; channel 2 is the summation of the six instruments in the first ring; and channels 3 through 8 are summations of the three instruments in each ring, starting with the second ring and moving toward the larger rings. These data were resampled to a 100-msec sample period and normalized as usual by the filtering program to unit variance.

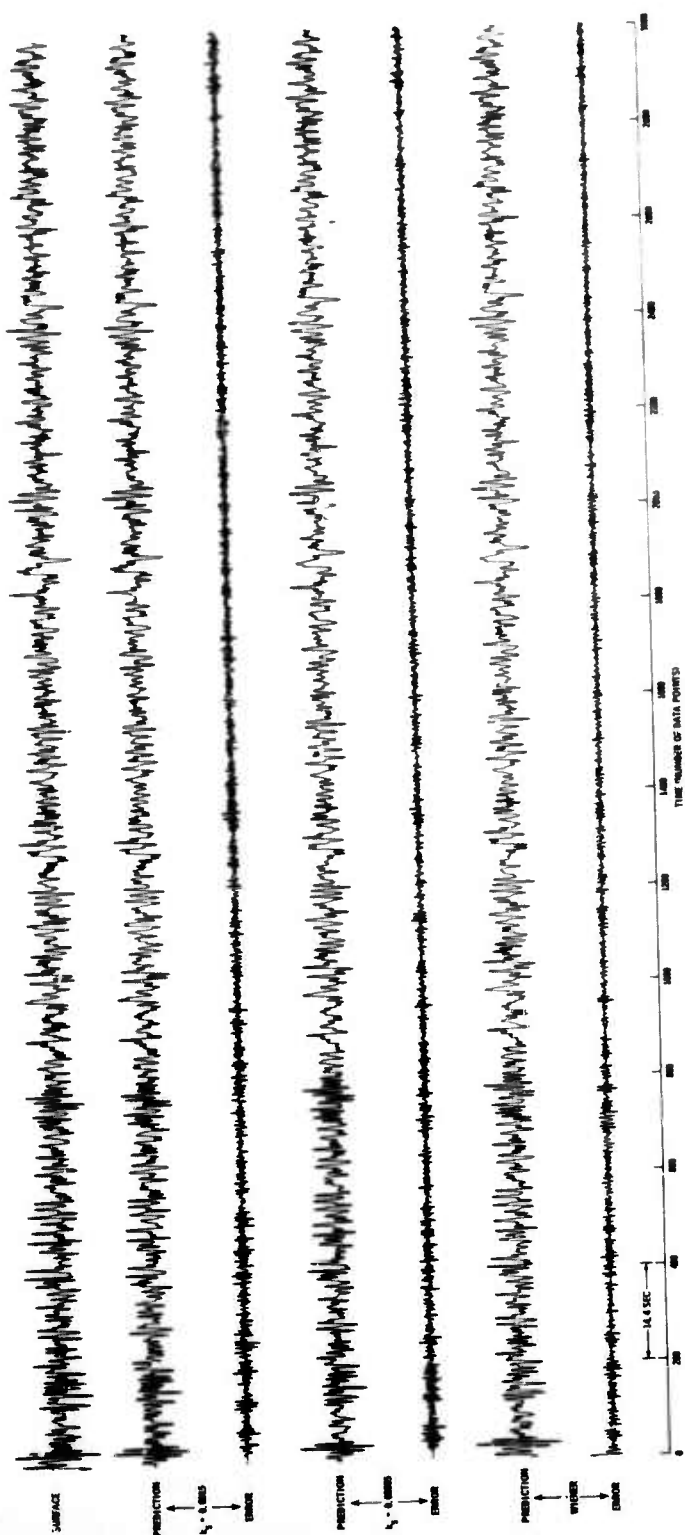


Figure II-44. Error Outputs for Vertical Array A Predicting Top Deep-Well Seismometer

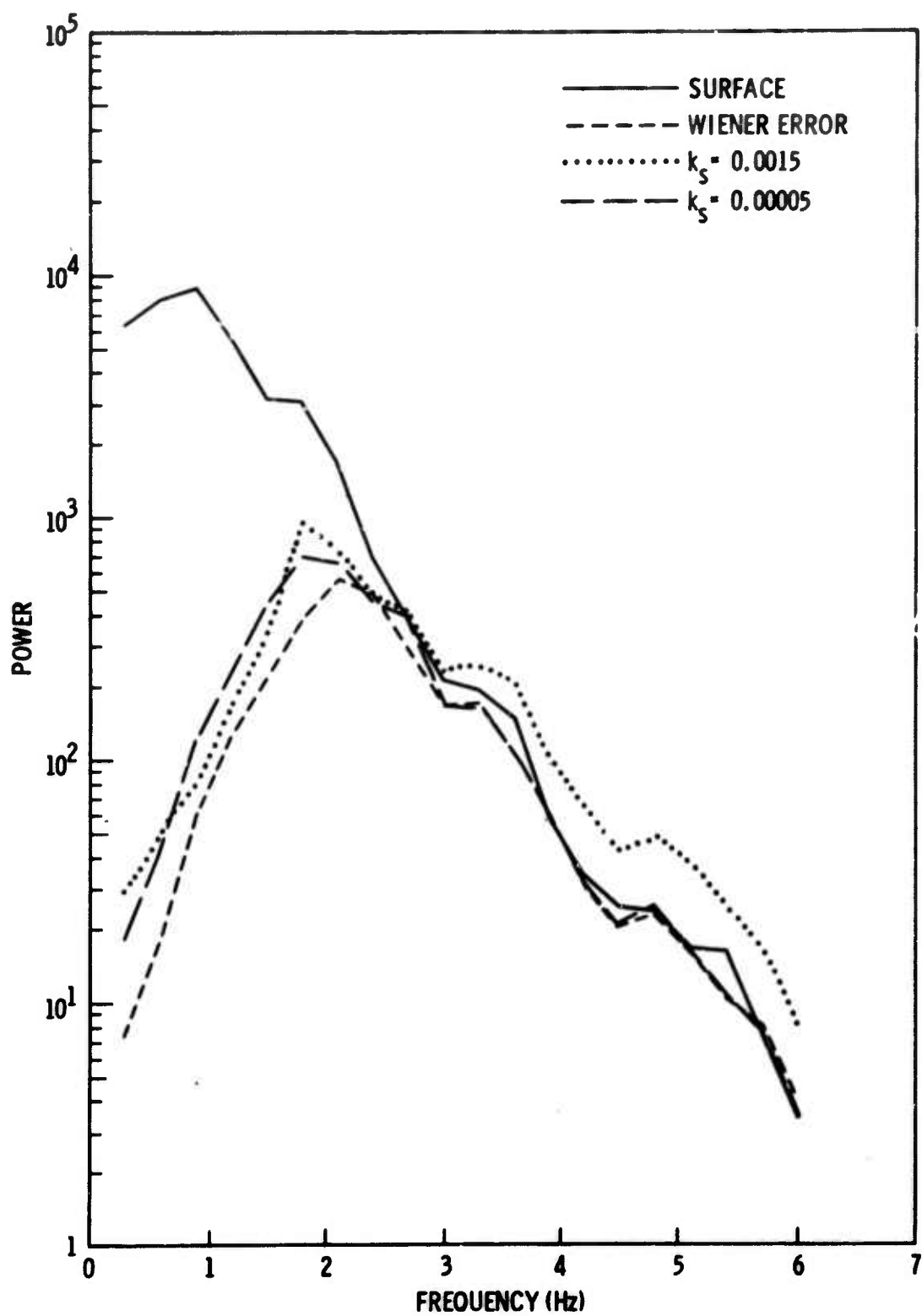


Figure II-45. Power Spectra for Vertical Array A
Predicting Top Deep-Well Seismometer

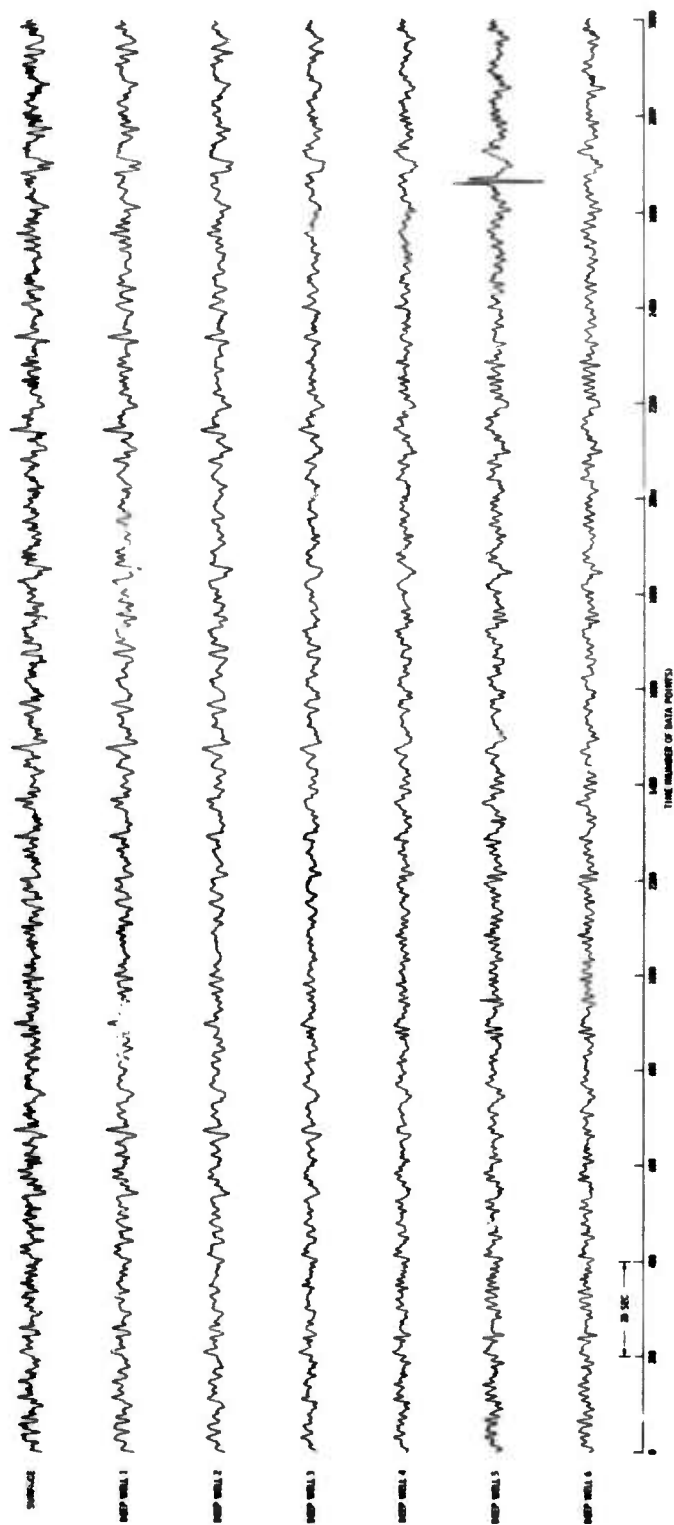


Figure II-46. Vertical Array B Data

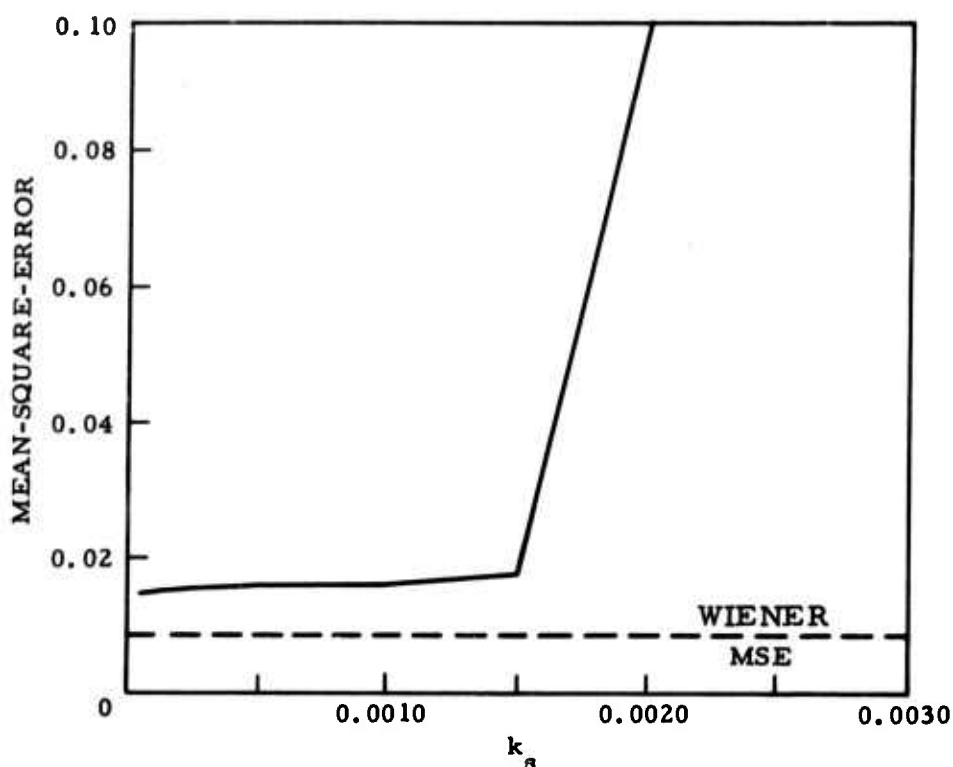


Figure II-47. Mean-Square-Error Vs k_s for Vertical Array B Predicting Surface Seismometer

Wiener prediction-error filtering was accomplished previously on these data using a 35-point filter, with output at the center point, to predict the center seismometer from the seven ring-stacked channels. The Wiener processing was duplicated adaptively with eight passes through the data. Filter coefficients were set initially at 0 for the first pass and at the last values of the previous passes to begin the remaining passes. Values of k_s were 0.0015 (learning), 0.0015, 0.0010, 0.0005, 0.00025, 0.000125, 0.0000625, and 0.0020. Figure II-54 plots mean-square-error of prediction as a function of k_s , and Figure II-55 shows the adaptive predictions and prediction-error traces.

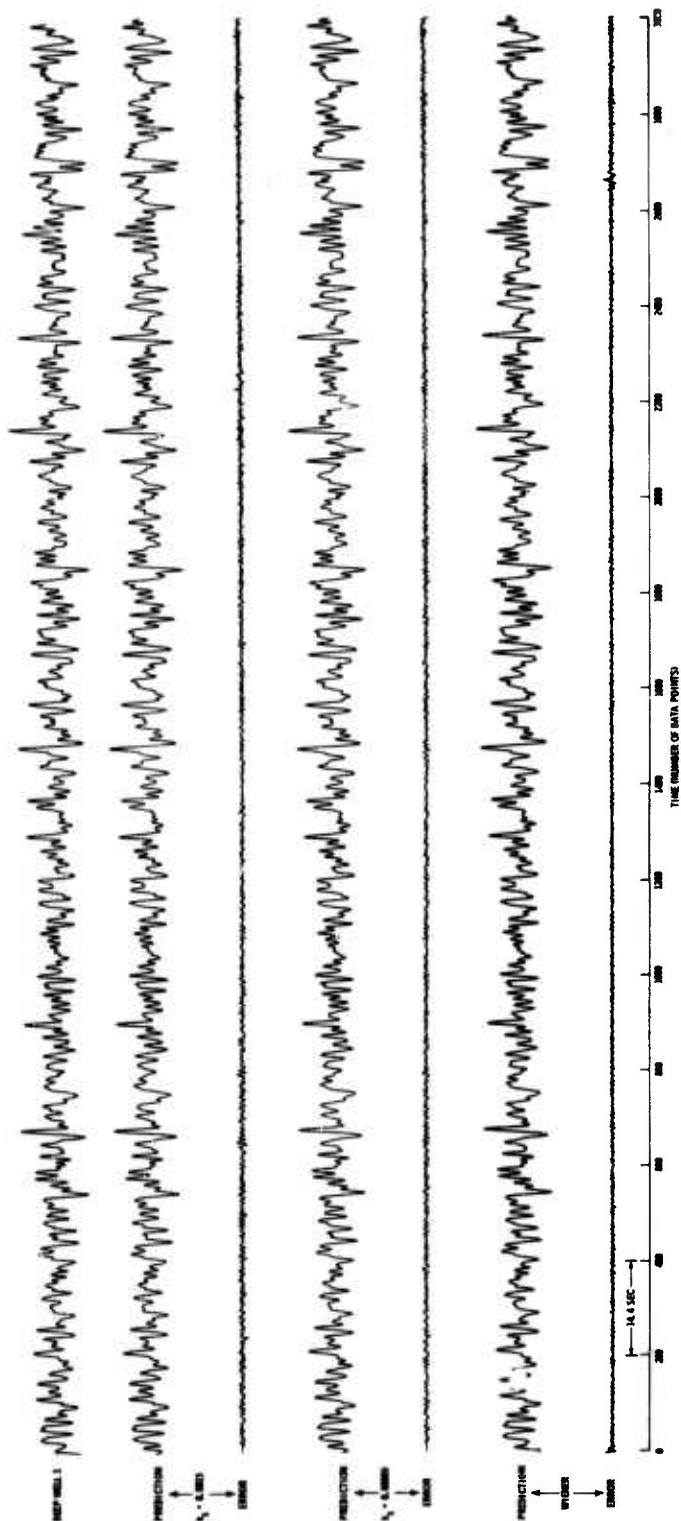


Figure II-48. Error Outputs for Vertical Array B Predicting Surface Seismometer

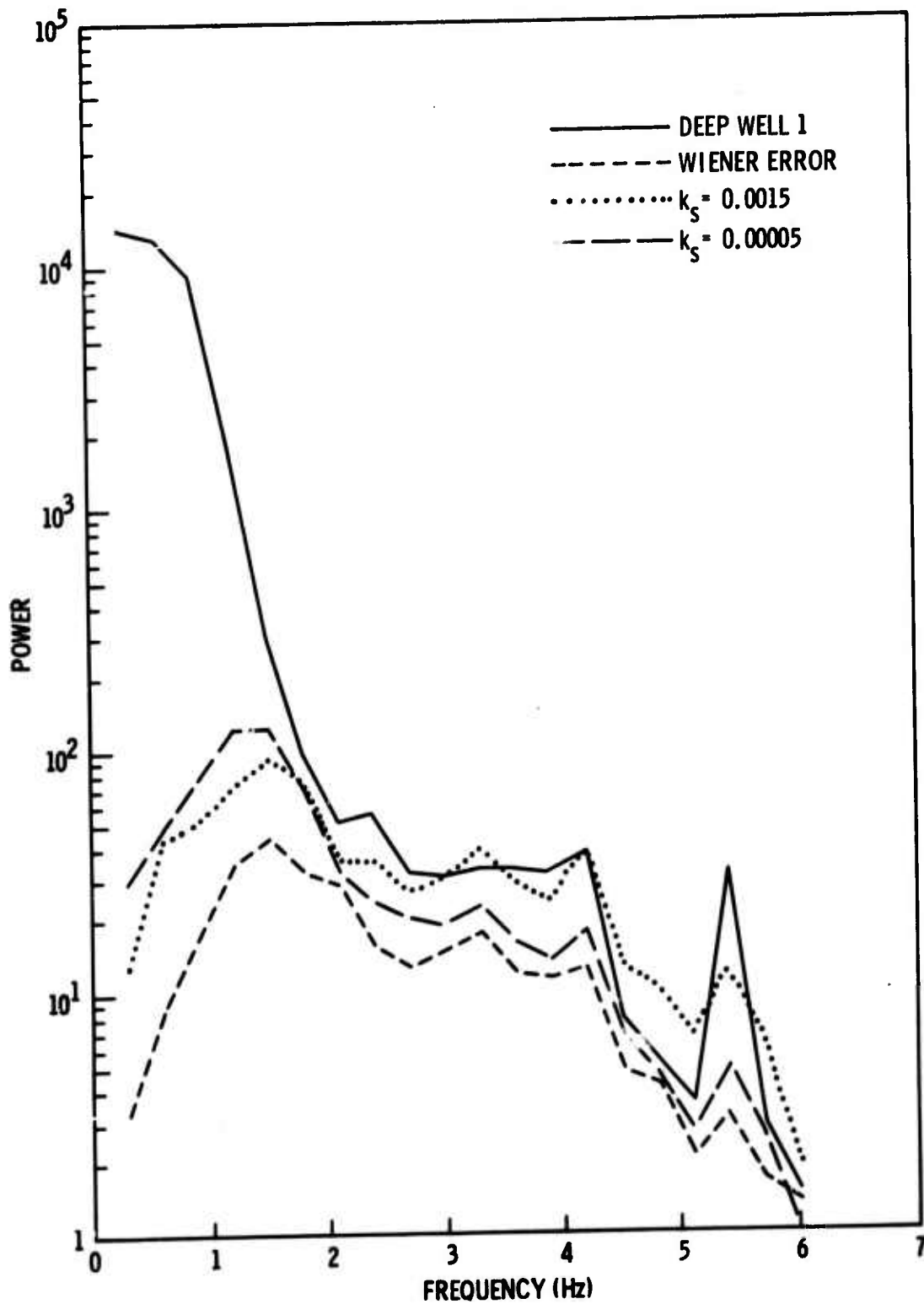


Figure II-49. Power Spectra for Vertical Array B Predicting Surface Seismometer

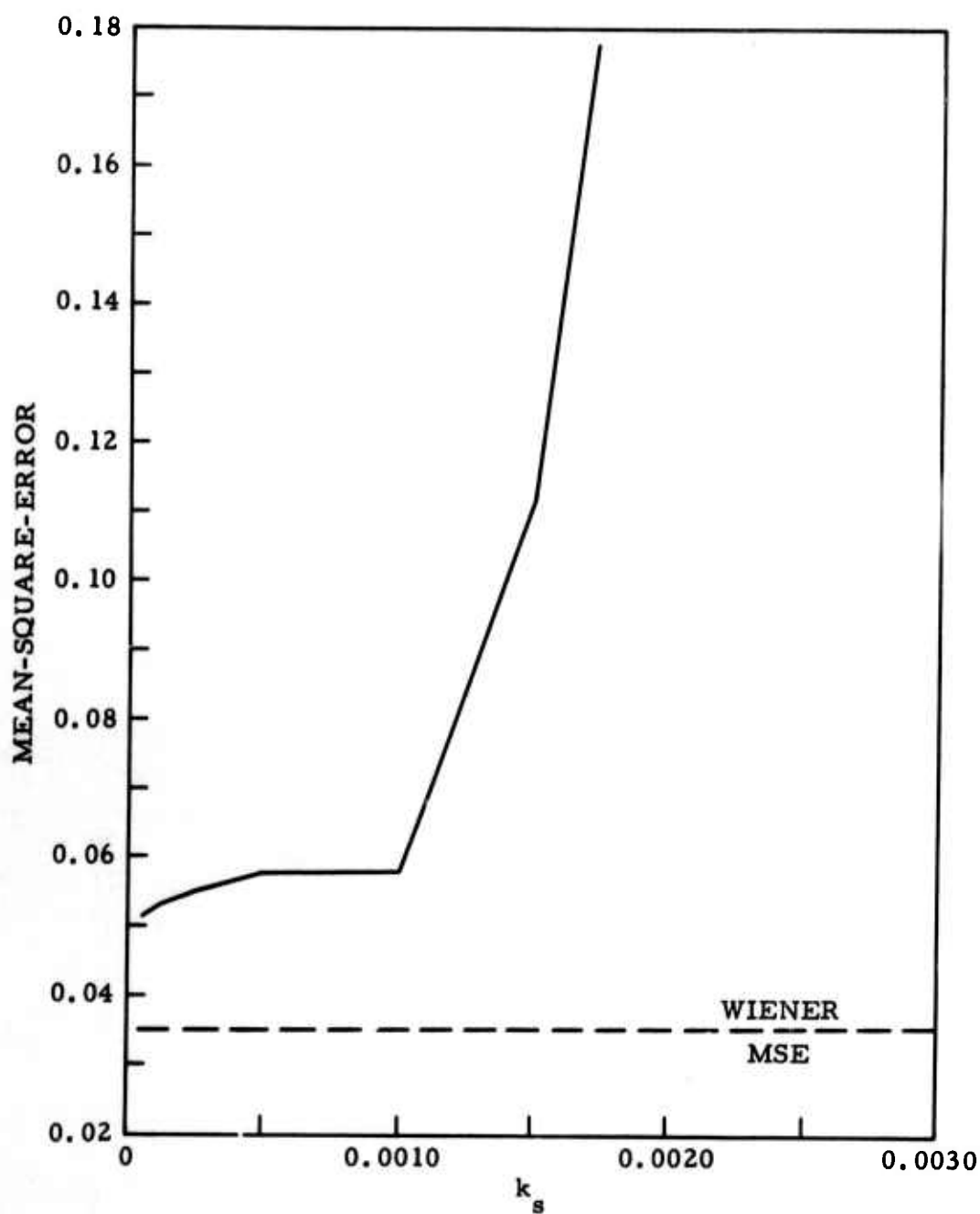


Figure II-50. Mean-Square-Error Vs k_s for Vertical Array B
Predicting Top Deep-Well Seismometer

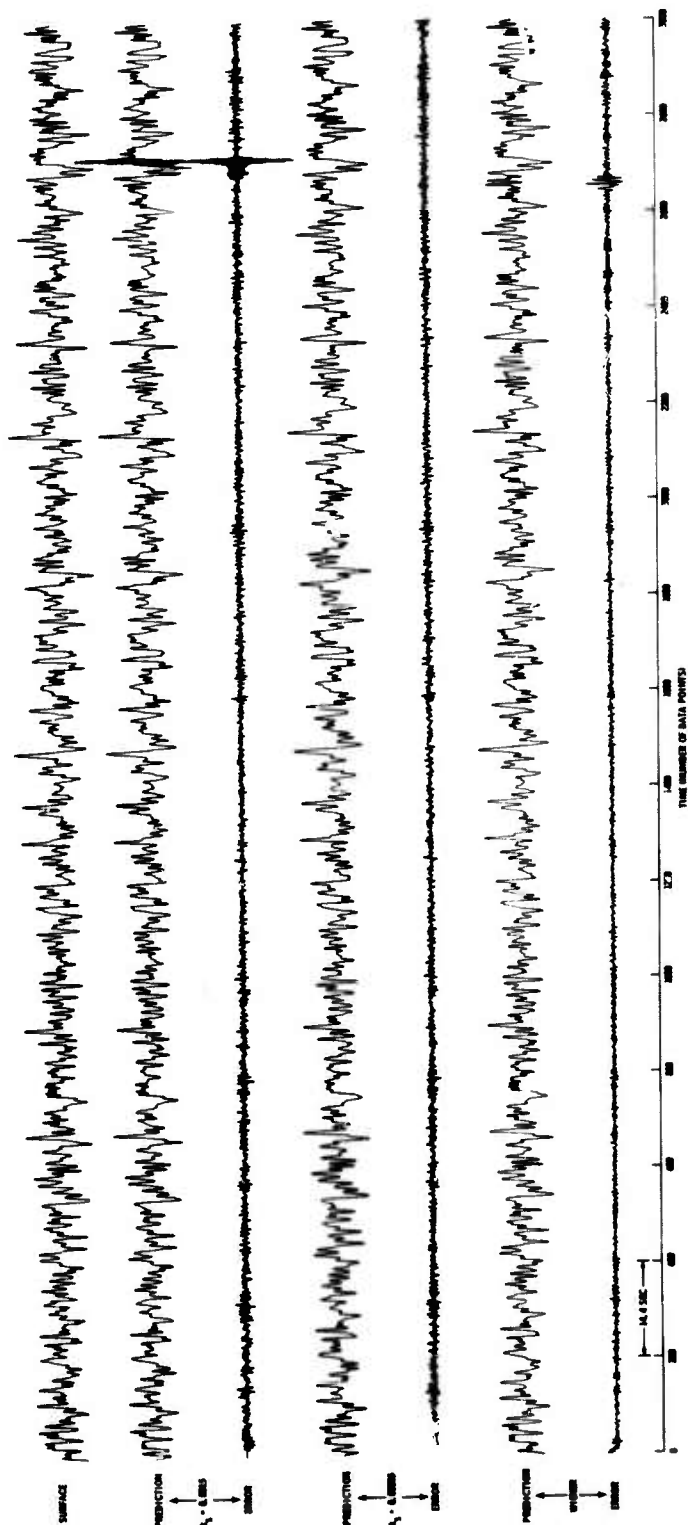


Figure II-51. Error Outputs for Vertical Array B Predicting Top Deep-Well Seismometer

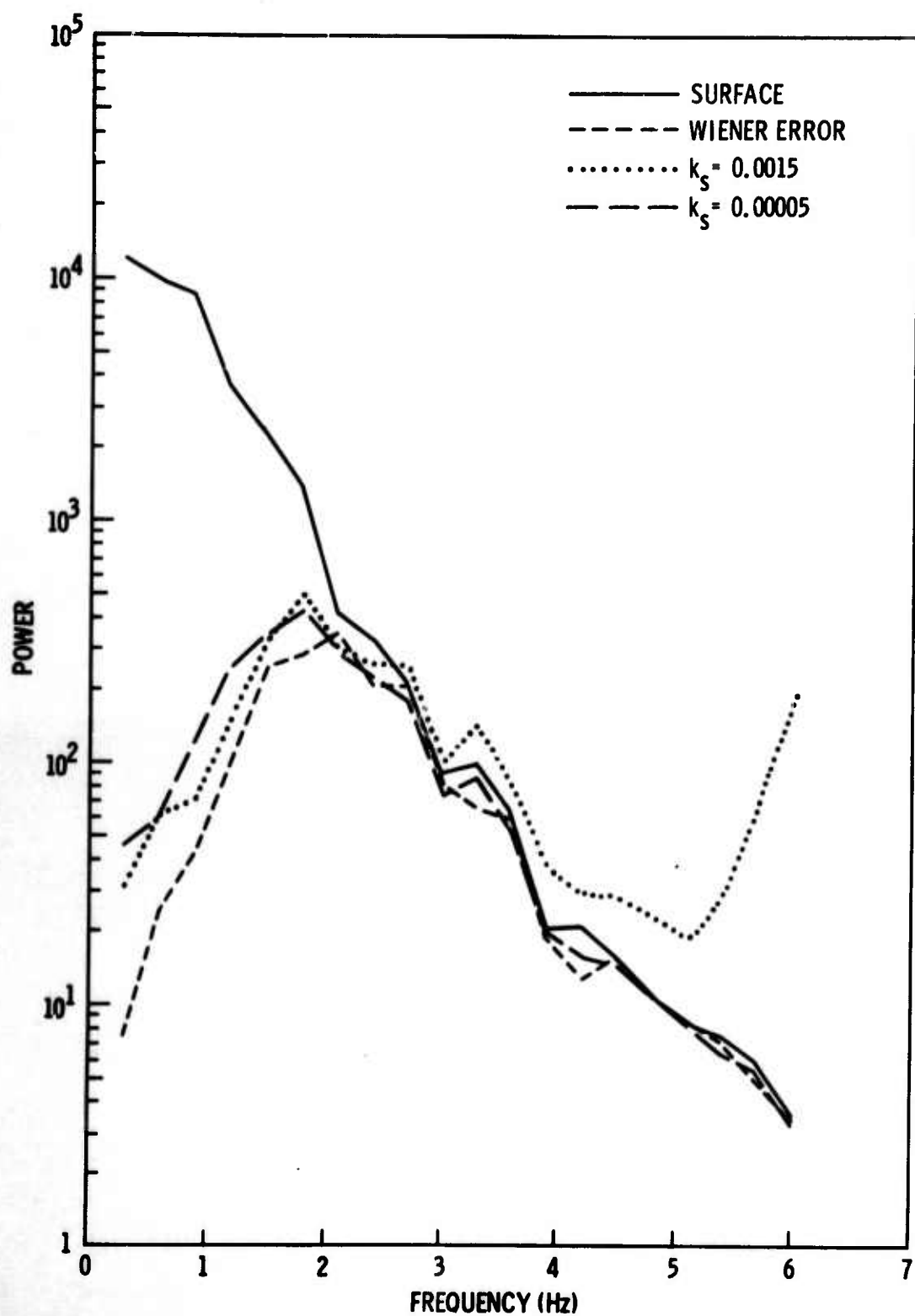


Figure II-52. Power Spectra for Vertical Array B
Predicting Top Deep-Well Seismometer



CENTER SEISMOGRAPH

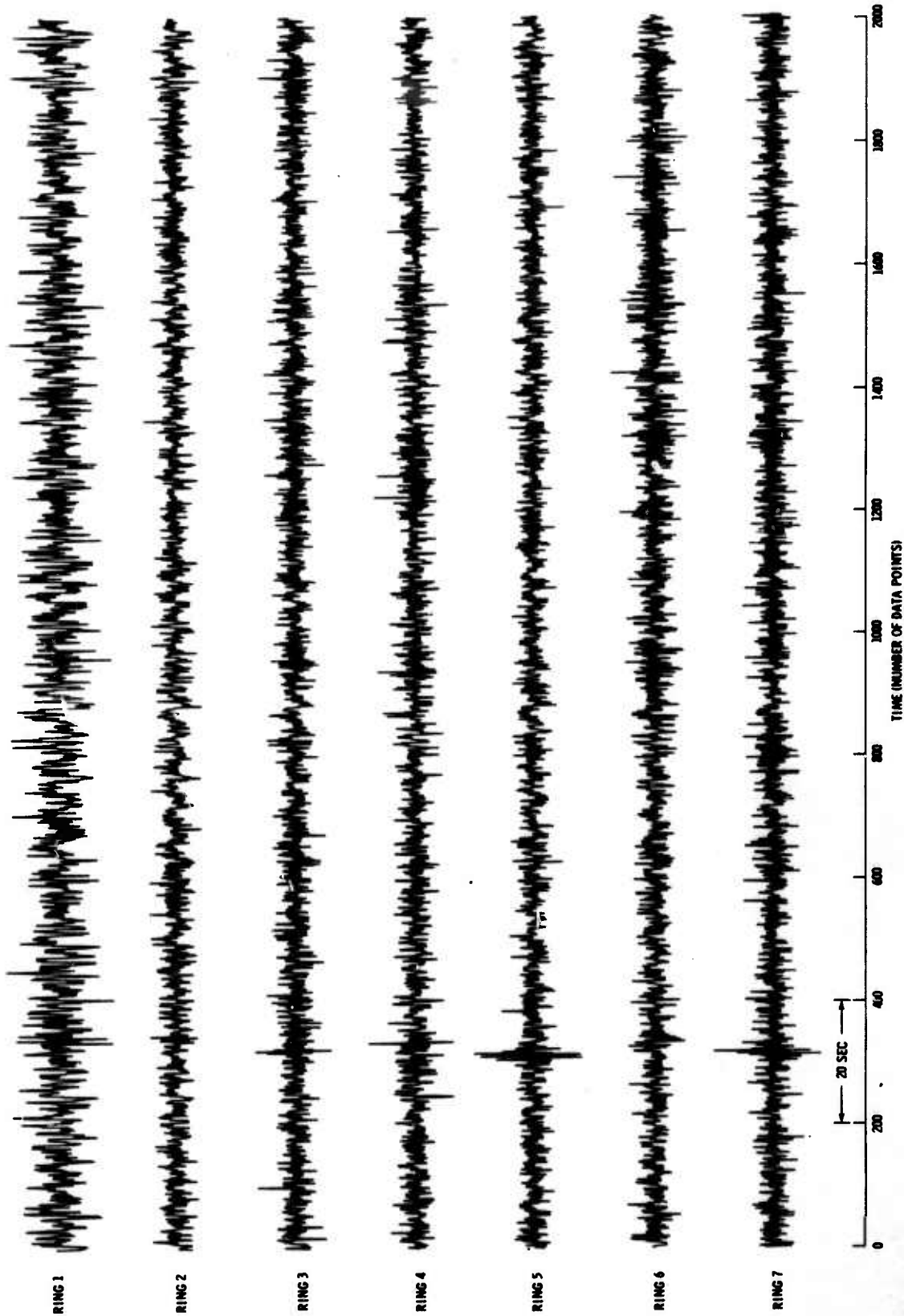


Figure II-53. LASA Subarray B1 Ring-Stacked Data

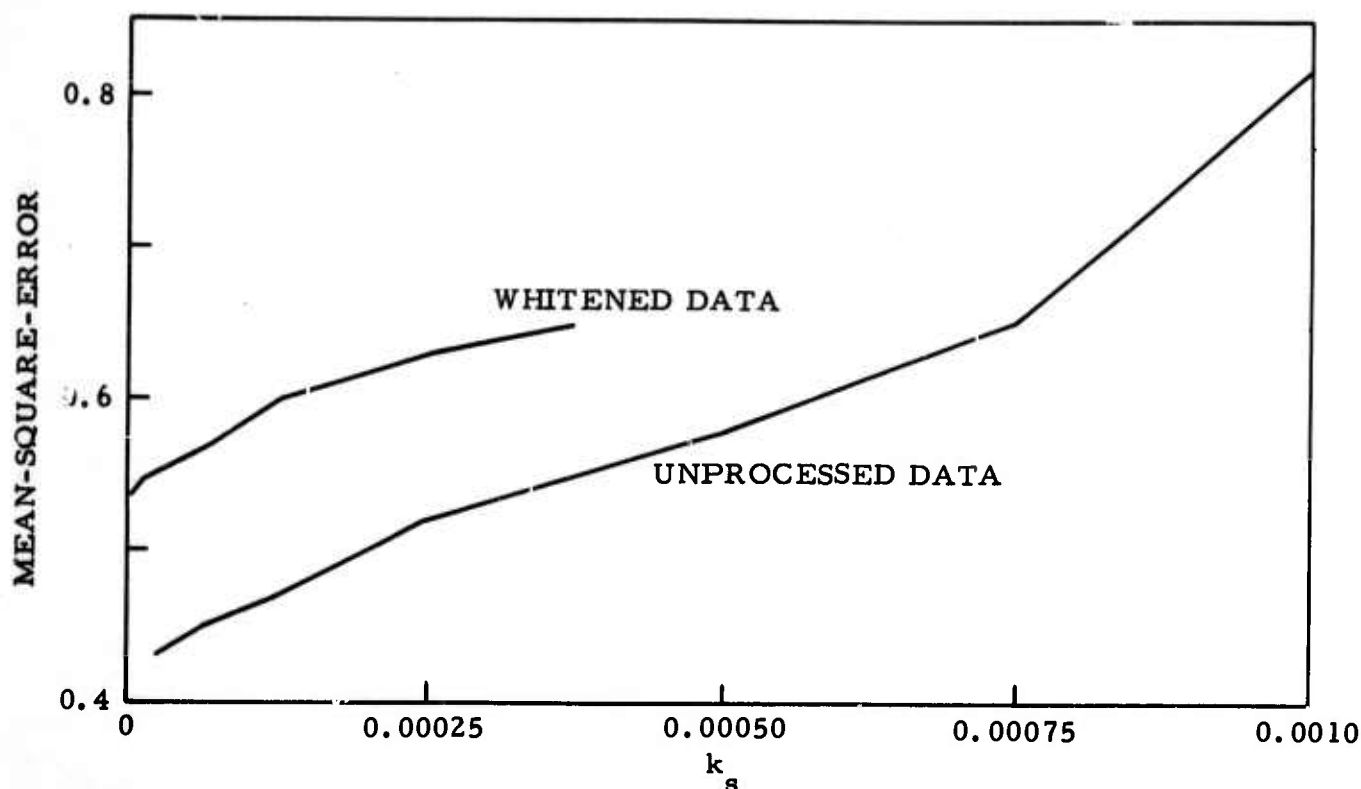


Figure II-54. Mean-Square-Error Vs k_s for
LASA Subarray B1, Ring-Stacked

The ratio of prediction-error power to center seismometer power as a function of frequency is given in Figure II-56 for the Wiener, large k_s , and small k_s error traces.

A 9-point deconvolution filter designed from channel 1 was applied to all channels to whiten the data (Figure II-57). Seven adaptive passes were made on the whitened data, with k_s values of 0.0005 (learning), 0.0005, 0.00025, 0.000125, 0.00005, 0.000025, and 0.00075. Filter coefficients for each pass were initialized as they were for the unwhitened data. No Wiener filtering was attempted on the whitened data. Mean-square-error vs k_s for the whitened data is included in Figure II-55. Adaptive filter prediction and error traces for the whitened data are given in Figure II-58.

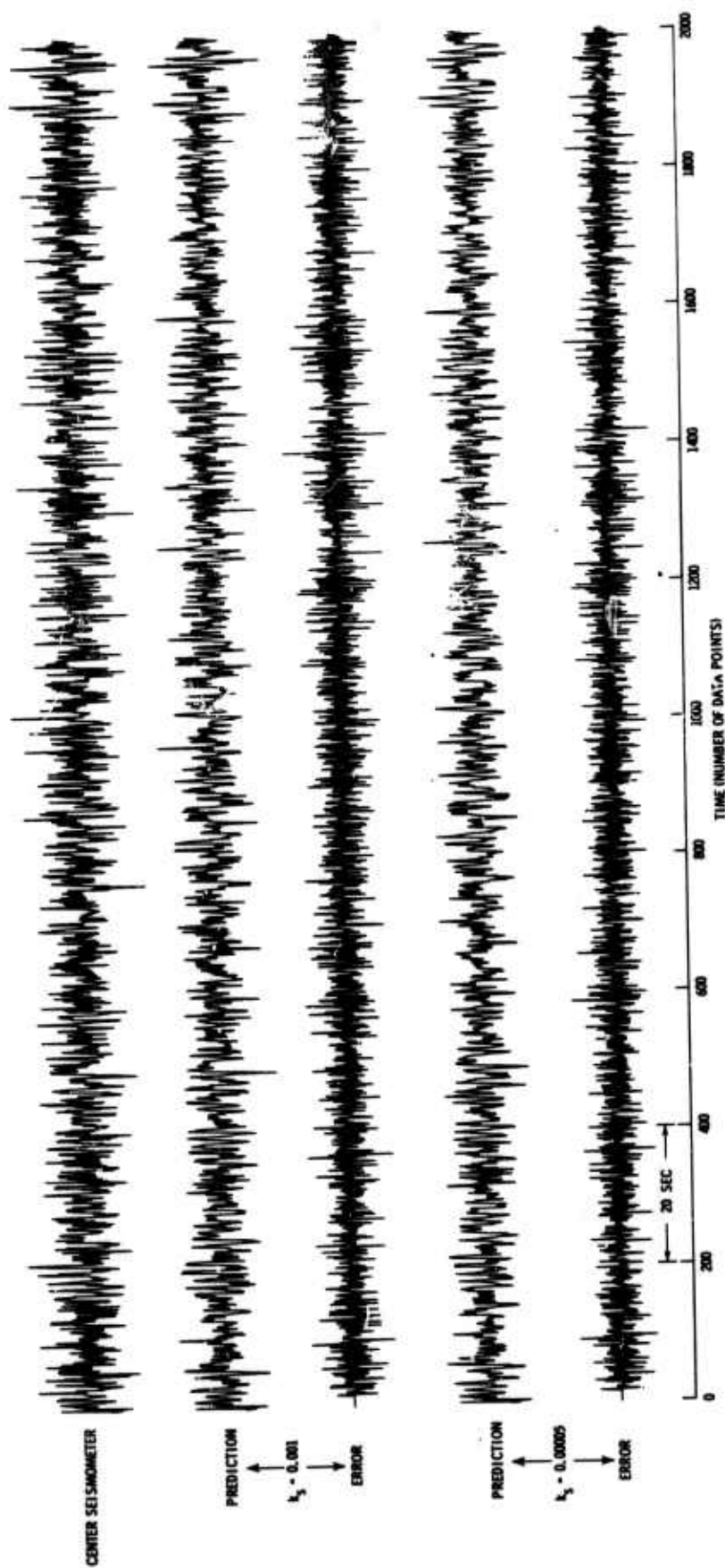


Figure II-55. Adaptive Prediction Error for LASA Subarray B1, Ring-Stacked

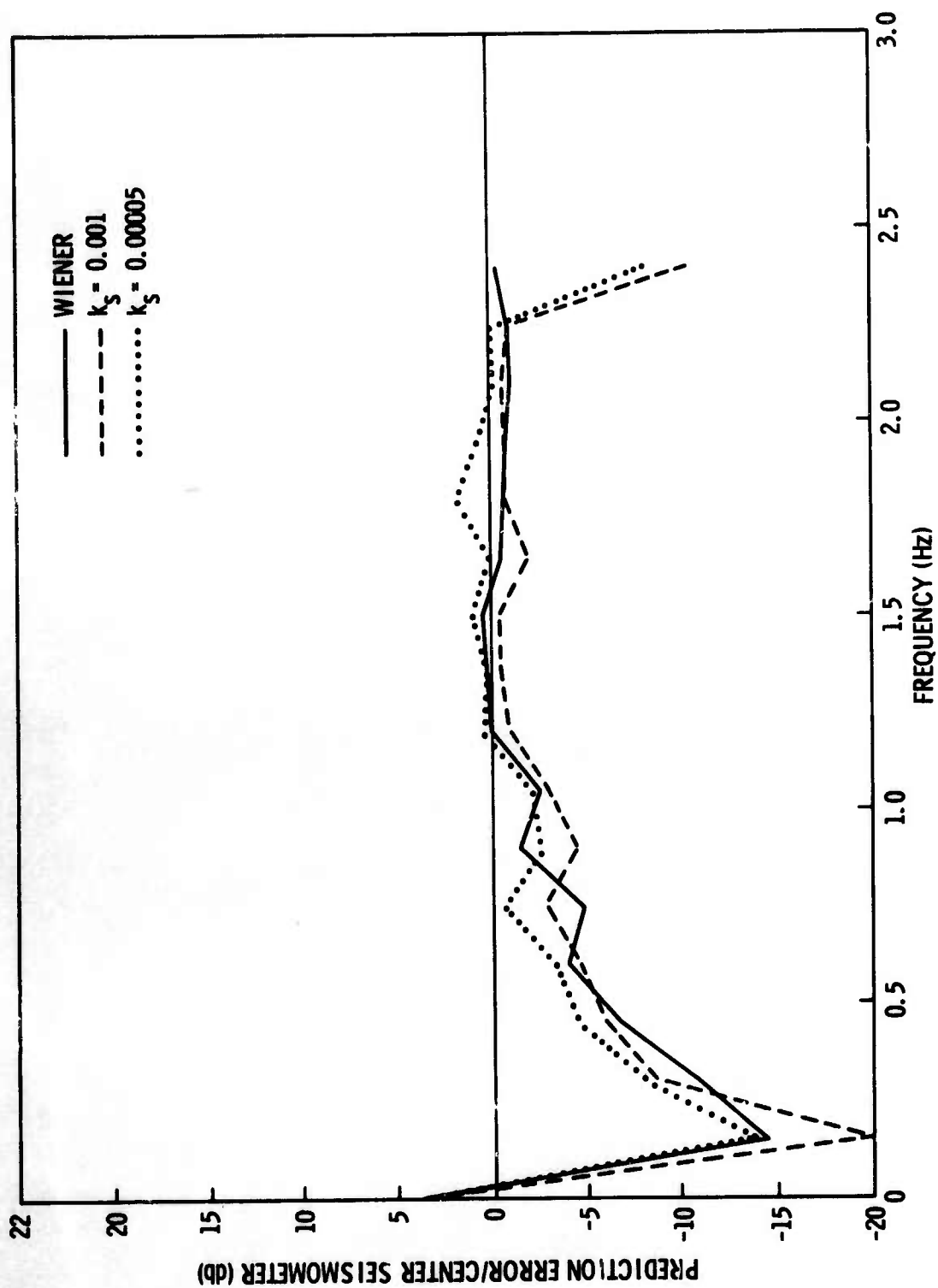


Figure II-56. Error to Center-Seismometer Power Ratio of Wiener and Adaptive Filtering for LASA Subarray B1, Ring-Stacked

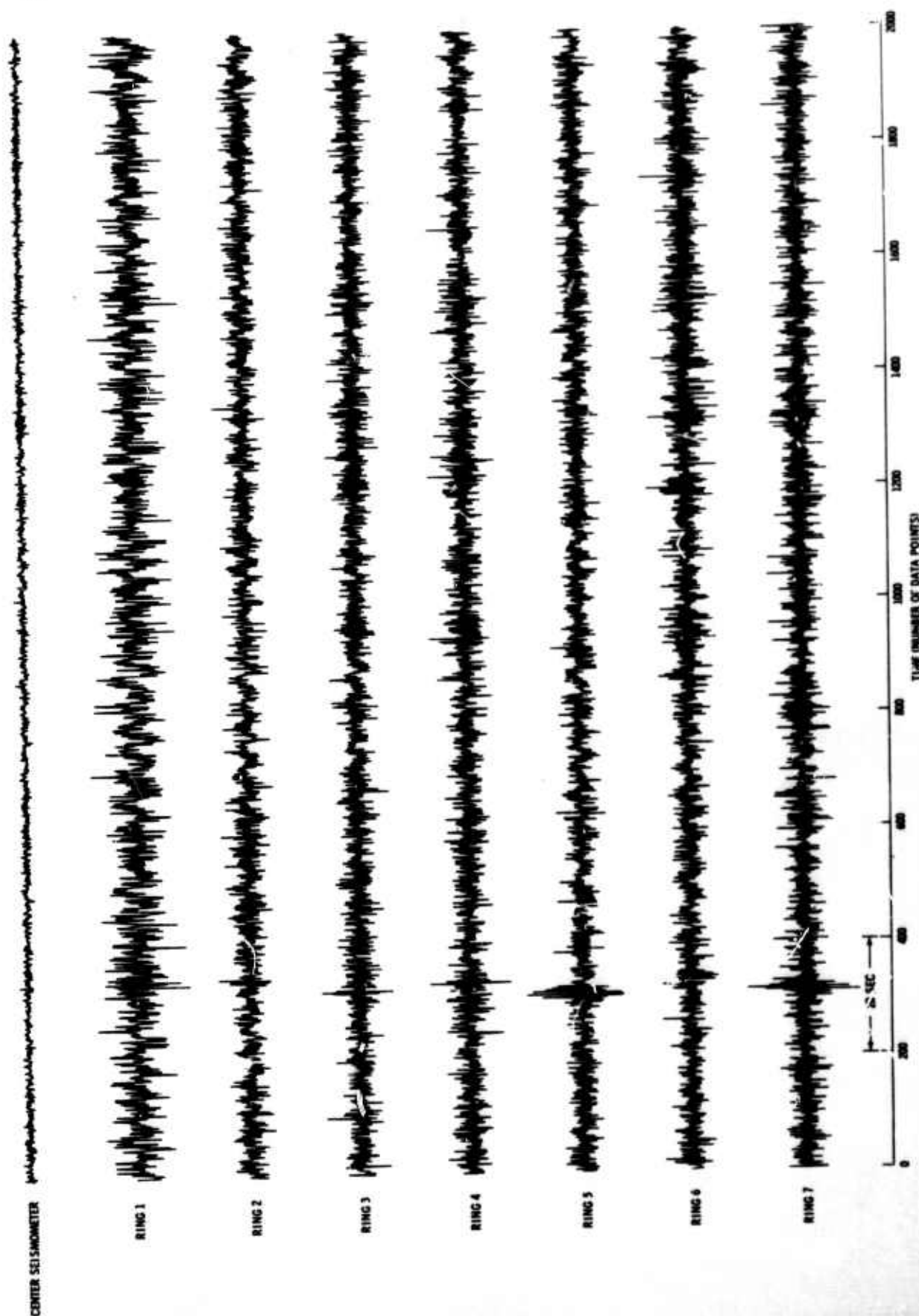


Figure II-57. LASA Subarray B1 Whitenened Ring-Stacked Data

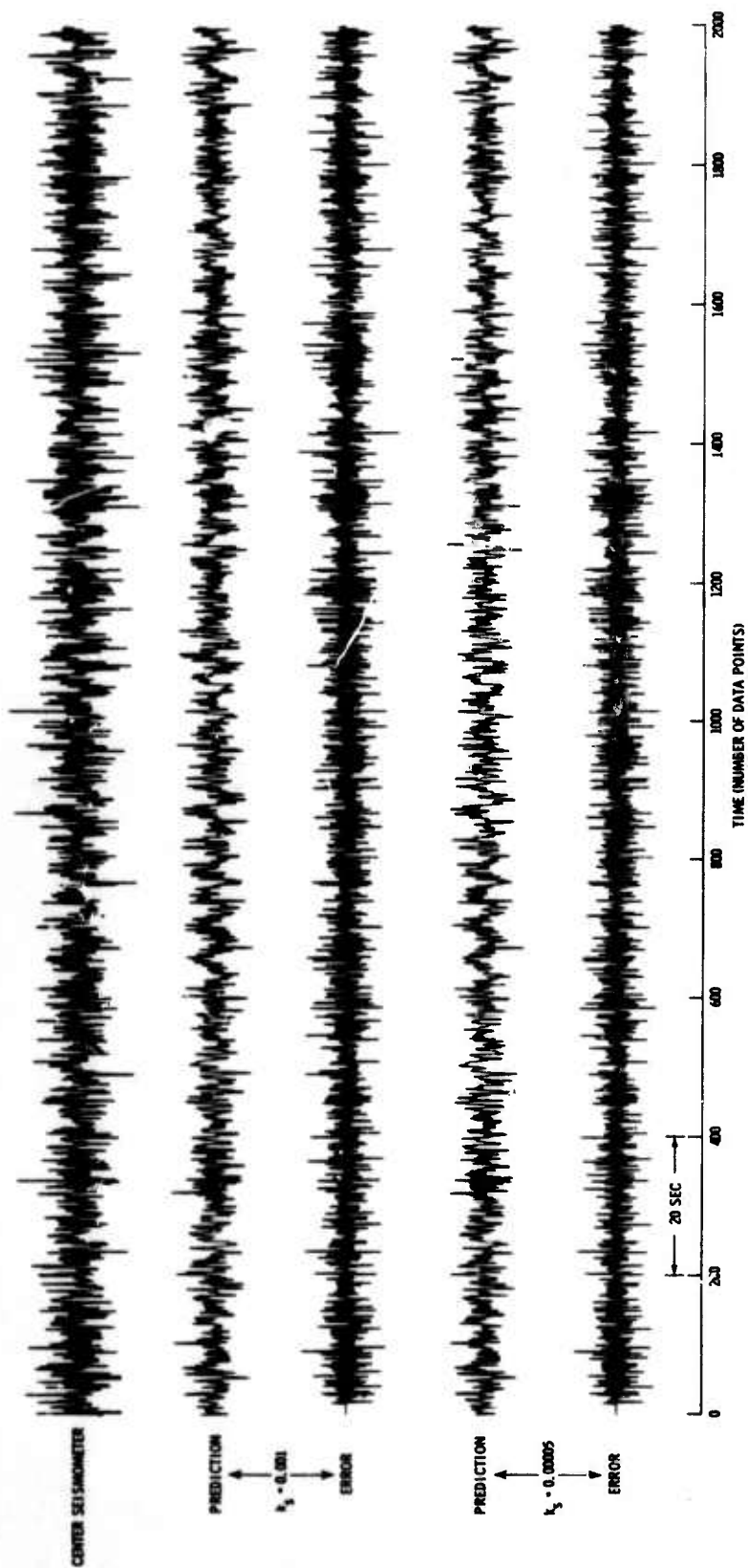


Figure II-58. Adaptive Prediction Error for LASA Subarray B1 Whitenened Ring-Stacked Data



I. LASA LONG-PERIOD 3339

A 10-channel set of LASA data consisting of the long-period north and east horizontal channels from subarrays A0, B1, B2, B3, and B4 was used to predict the long-period vertical channel of subarray A0. The sampling period of these data (Figure II-59) was 1 sec and the foldover frequency, therefore, 0.5 Hz. Prediction was accomplished adaptively and with Wiener filters designed from correlation-function estimates computed from this noise sample. Filter length in both cases was 11 points, with the output point at the center of the filter. The normalized mean-square-error of prediction of the Wiener filter applied to the design data was 0.42. Adaptive mean-square-error as a function of k_s is given in Figure II-60. Seven adaptive passes were made, with k_s values of 0.0025 (learning), 0.0025, 0.00125, 0.000625, 0.0003125, 0.00015625, and 0.000078125. Initial filter coefficients at the beginning of each pass were set to their values at the end of the previous pass except for the first pass, where initial coefficients were 0.

Outputs of the Wiener and adaptive filters are shown in Figure II-61. Also included in this figure are the outputs of two adaptive runs where k_s was varied with time. In the first case, the value of k_s used on the n^{th} filter update, $k_s(n)$, was equal to 0.25 divided by the sum of squares of all data points used to make the n^{th} prediction. In the second case, $k_s(n)$ was computed by dividing 0.25 by an estimated sum of squares. The n^{th} estimate was $(1 - \alpha)$ times the $(n - 1)^{\text{th}}$ estimate plus α times the sum of squares of the new data points. Under this system, the data at $n\Delta t$ are weighted in the estimate by α , the data at $(n - 1)\Delta t$ by α^2 , at $(n - 2)\Delta t$ by α^3 , etc. Varying α , therefore, varies the sensitivity of $k_s(n)$ to sudden changes in input power. In both cases, the mean-square-error of prediction for time-varying k_s was 0.28, which equaled the best value obtained with a fixed k_s .



SEMI-ANNUAL SUMMARY

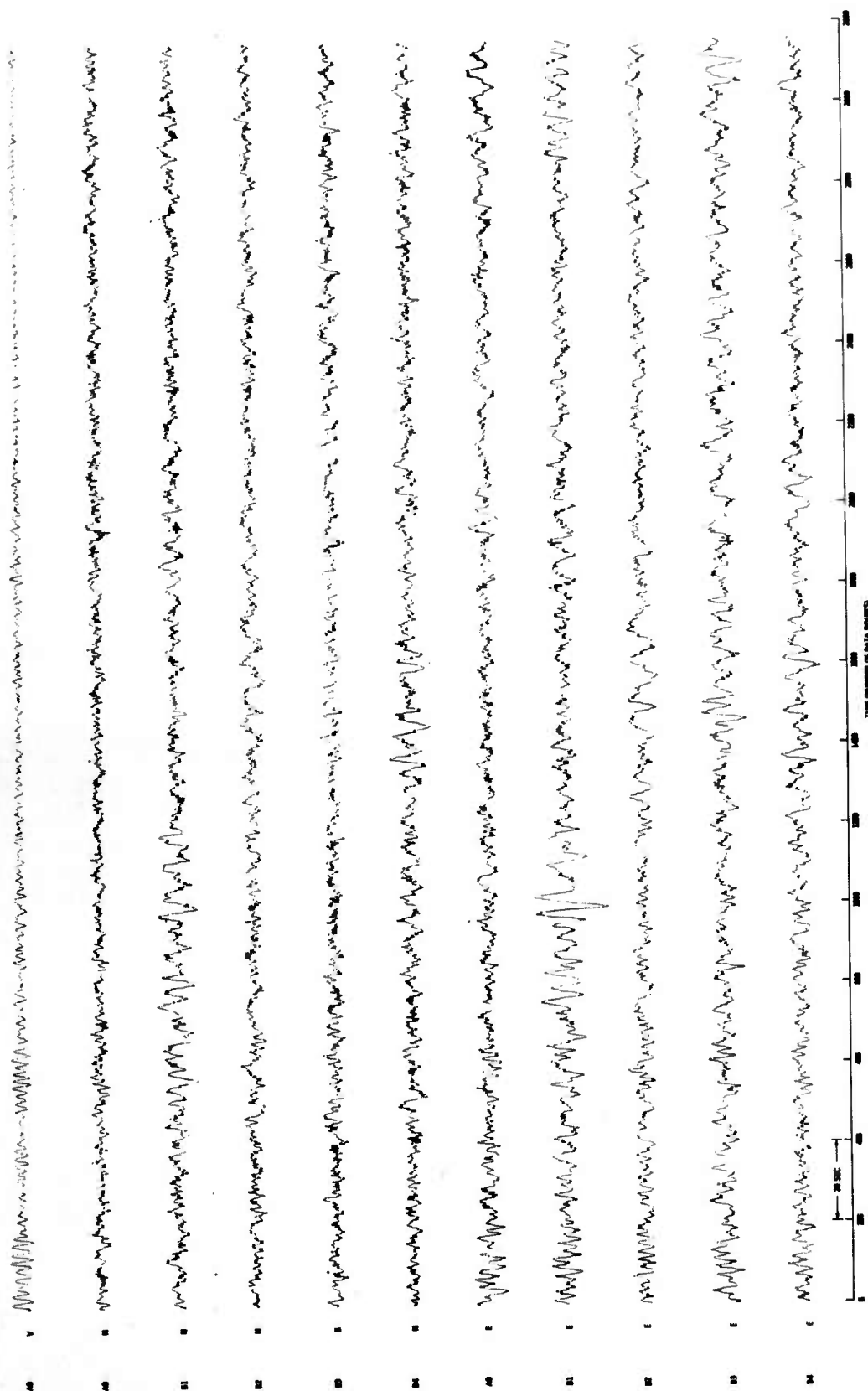


Figure II-59. LASA Long-Period 3339 Data

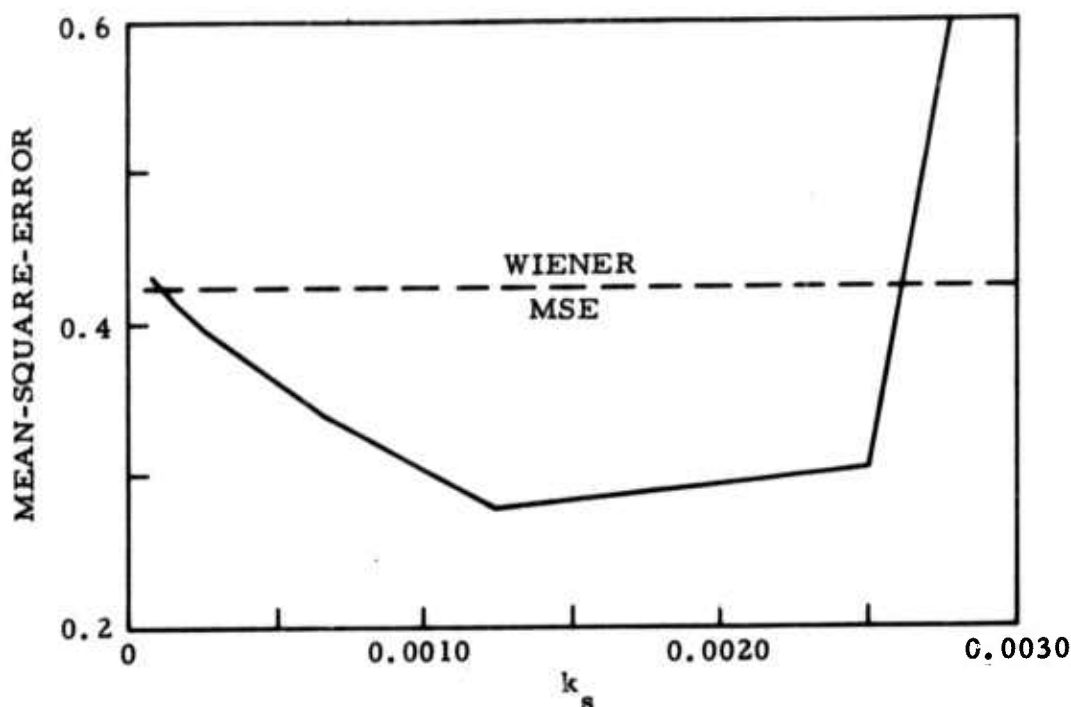


Figure II-60. Mean-Square-Error Vs k_s for LASA Long-Period 3339

Power spectra of the A0 vertical channel and the prediction-error traces for large- k_s and small- k_s adaptive passes are shown in Figure II-62. The adaptive algorithm became temporarily unstable for $k_s = 0.0025$, resulting in the large high-frequency content seen in this case.

J. LASA LONG-PERIOD 1196

The second sample of long-period LASA data consisted of the same instrument outputs as the previous sample except that the B2-north instrument was omitted. Adaptive and Wiener 15-point filters were designed to predict the vertical trace of subarray A0 from the nine horizontal channels. Figure II-63 shows these data which were recorded with a 1-sec sample period.

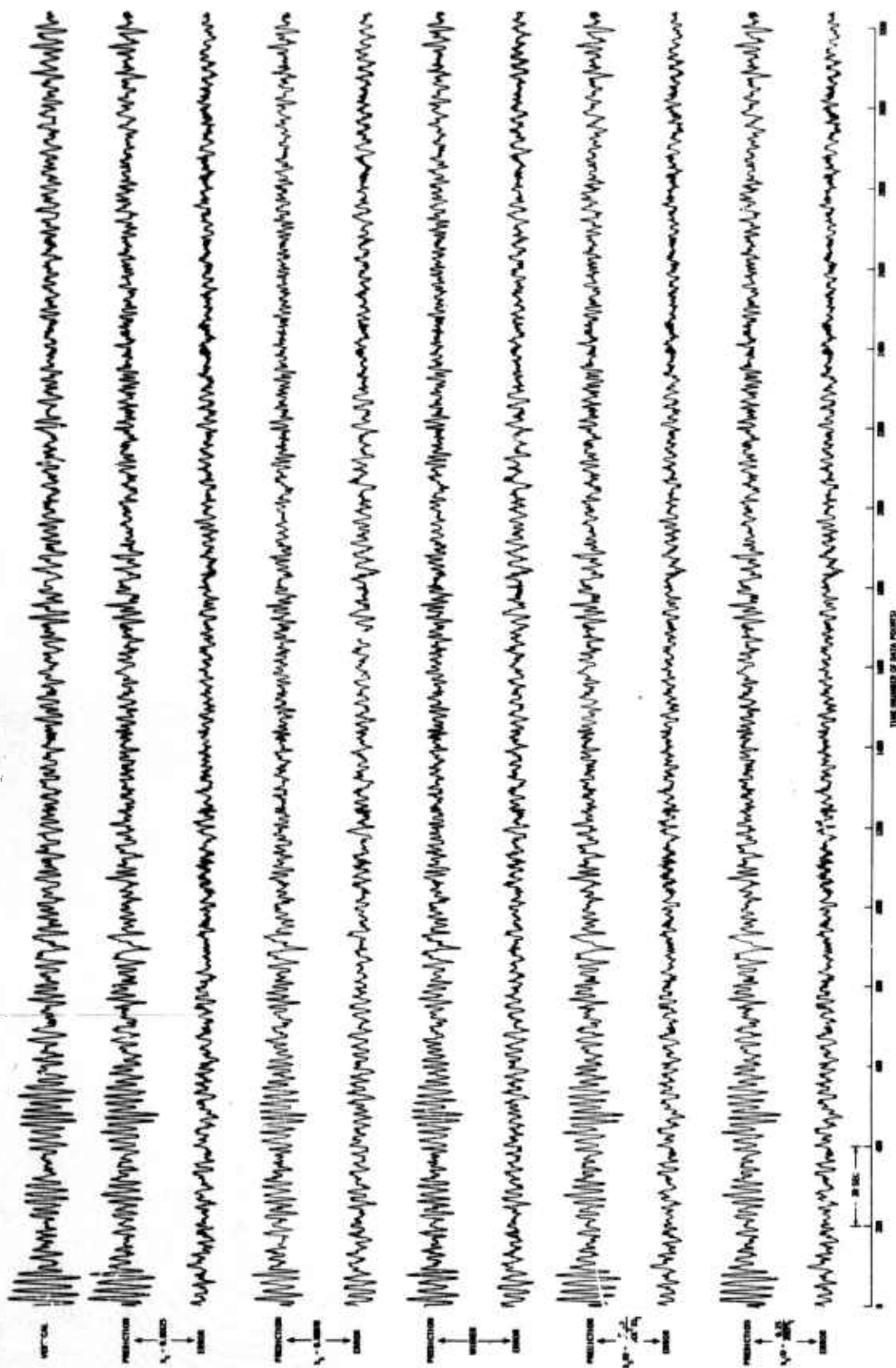


Figure II-61. Error Traces for LASA Long-Period 3339

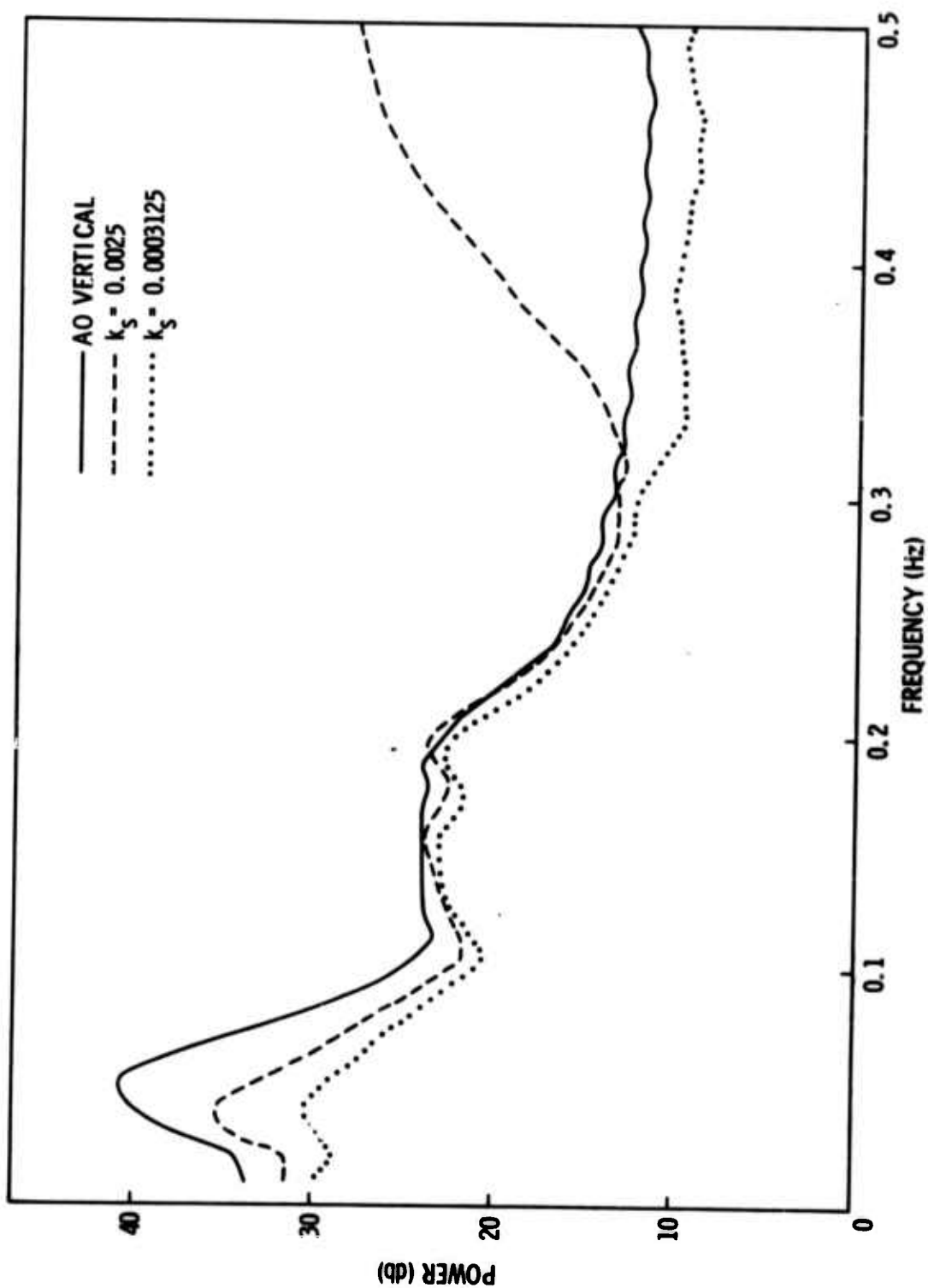


Figure II-62. Power Spectra for LASA Long-Period 3339

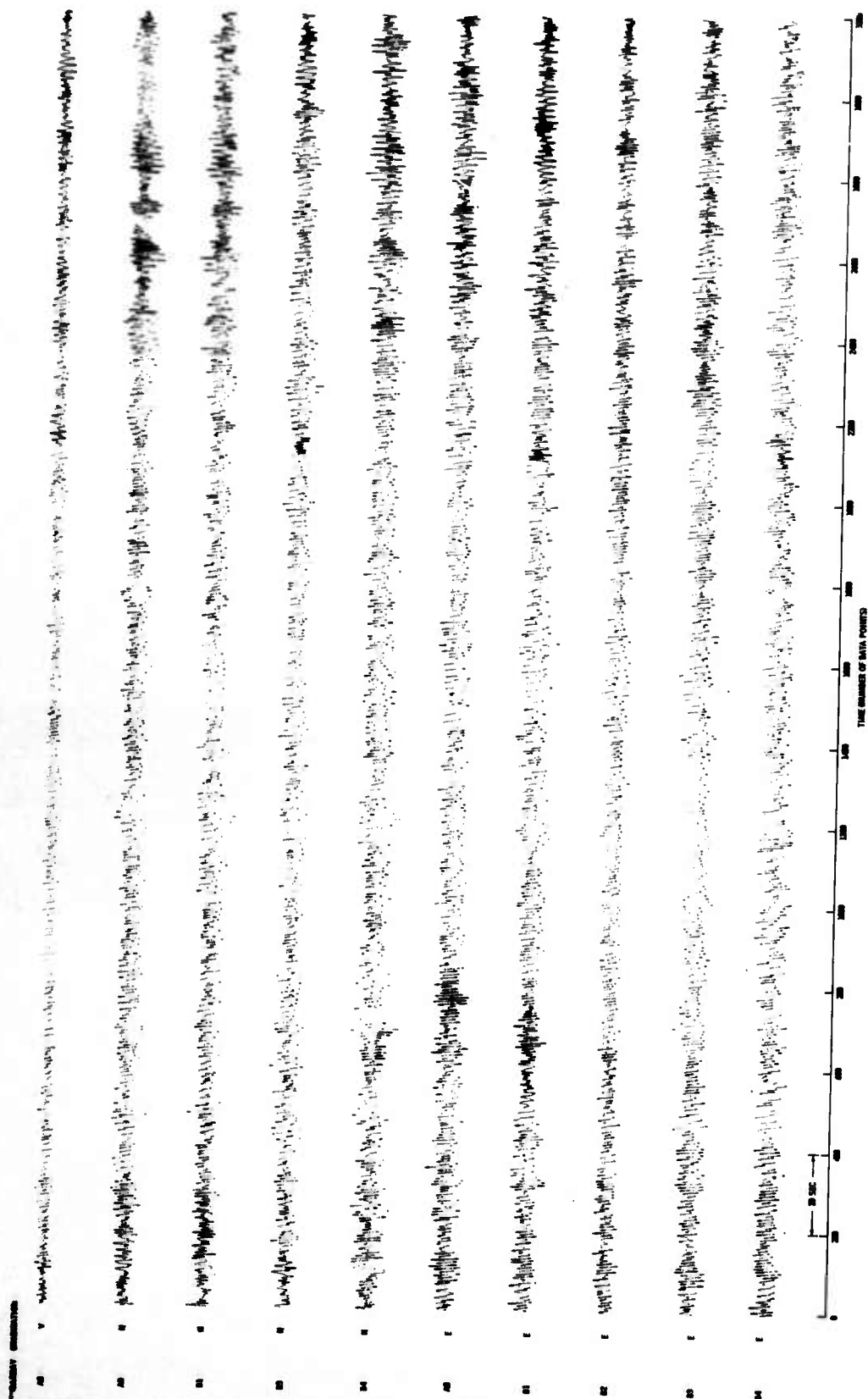


Figure II-63. LASA Long-Period 1196 Data



The normalized mean-square-error of the Wiener prediction filter was 0.18 when applied to the design data. Figure II-64 shows mean-square-error vs k_s for the adaptive filtering. Six adaptive passes were made, with k_s values of 0.0025 (learning), 0.0025, 0.00125, 0.000625, 0.0003125, and 0.00015625. Filter coefficients equaled 0 at the beginning of pass 1 and were set to their values at the end of the previous pass to begin all other passes.

Outputs of adaptive and Wiener filters are shown in Figure II-65. Power spectra of the A0 vertical channel and error traces for four values of k_s are given in Figure II-66.

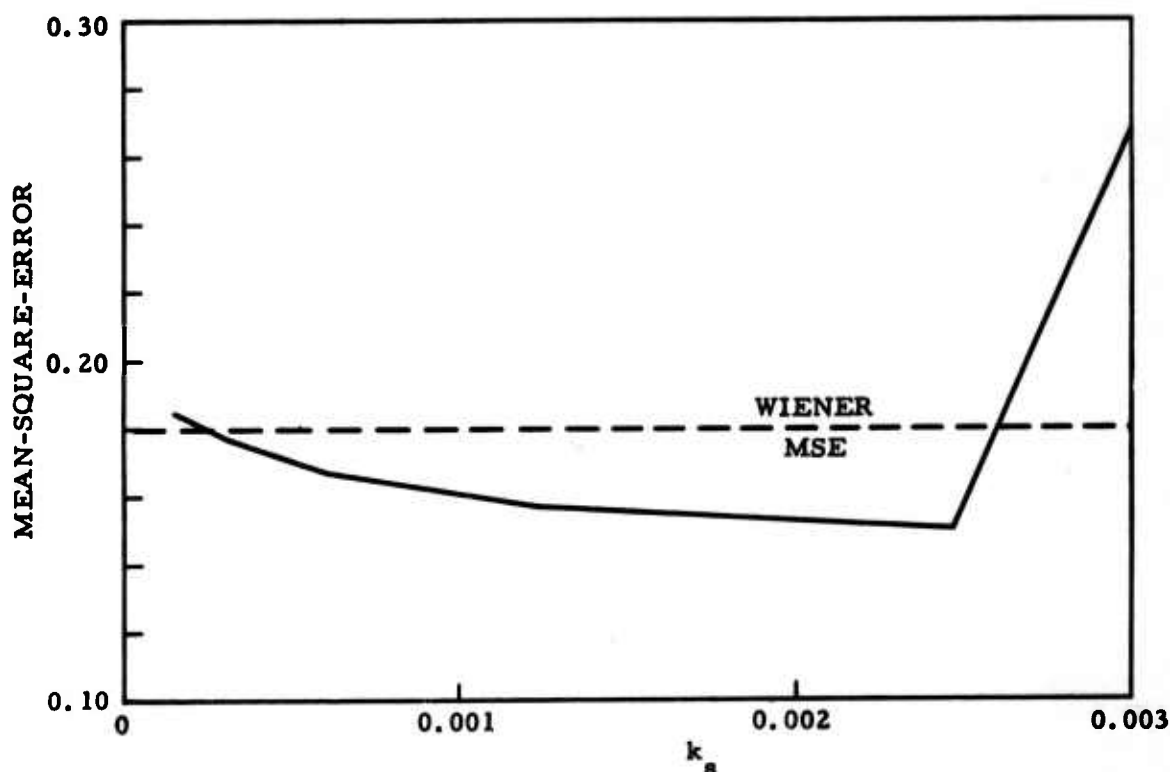


Figure II-64. Mean-Square-Error Vs k_s for LASA Long-Period 1196

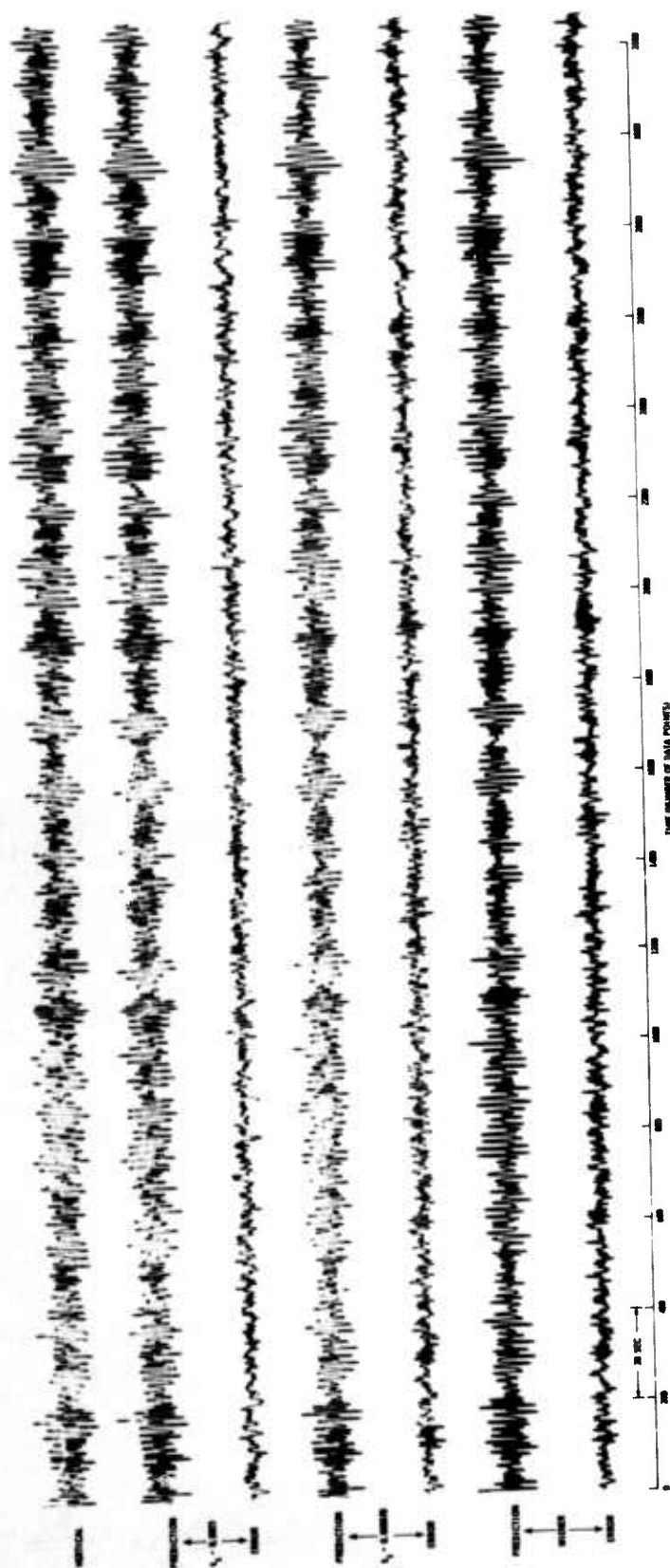


Figure II-65. Wiener and Adaptive Error Outputs for LASA Long-Period 1196

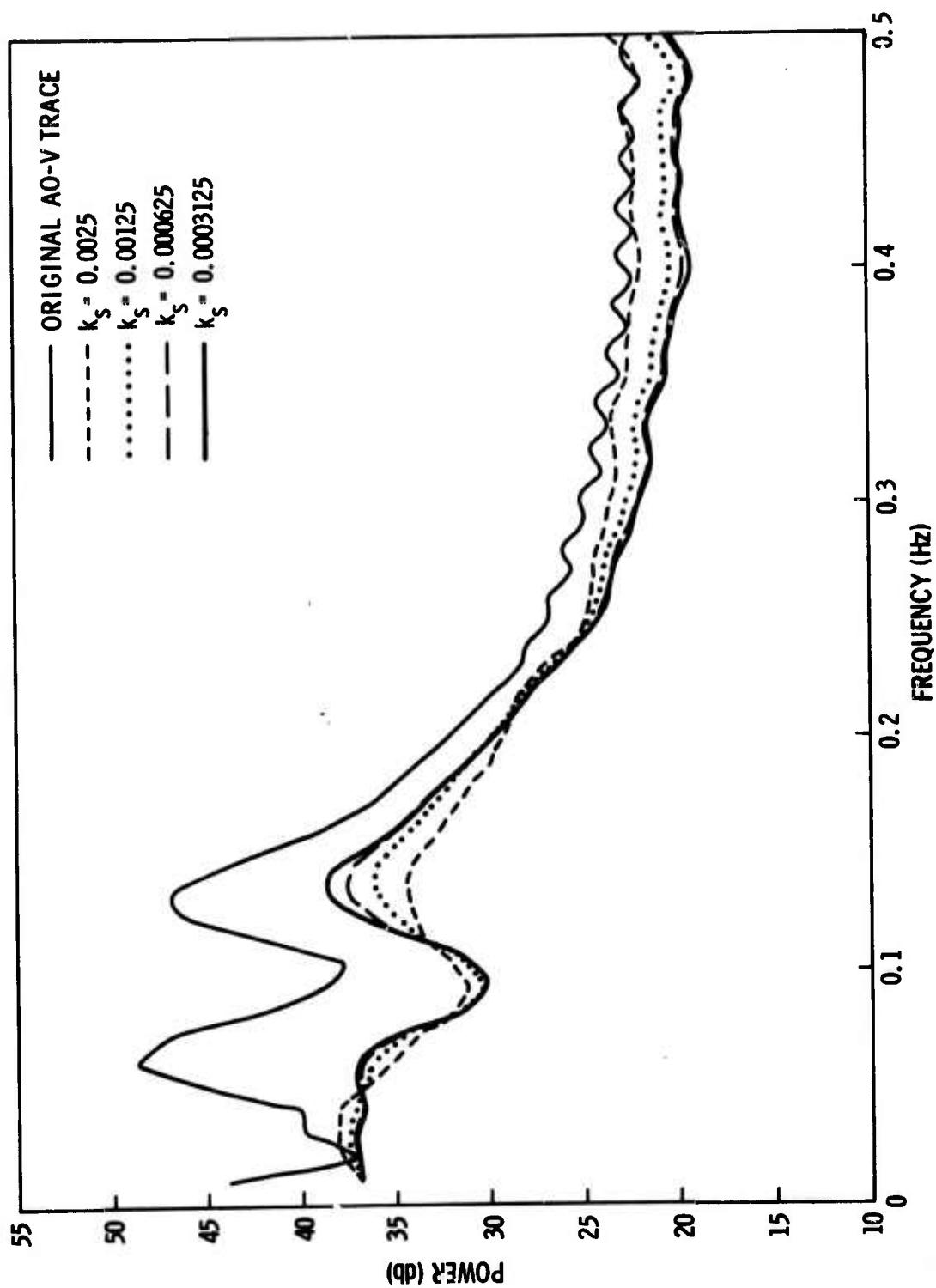


Figure II-66. Power Spectra for LASA Long-Period 1196

BLANK PAGE



SECTION III

MAXIMUM-LIKELIHOOD FILTERING

A maximum-likelihood filter (MLF) is one which minimizes output power under the constraint that the sum of the filter coefficients across channels is 0 for all but the 0-lag point, whose sum is 1. Under these constraints, the filter will pass infinite velocity signal-undistorted. In Special Report No. 1, two adaptive MLF algorithms were derived.¹ The first, referred to as the reduced-gradient algorithm, involves predicting one of the data channels from the difference traces resulting from subtracting each channel from the channel to be predicted. In the other method, the full-gradient algorithm, the mean across channels is predicted from difference traces obtained by subtracting each data channel from the mean across channels. In both cases, the prediction error has been shown to be theoretically equivalent to the conventional maximum-likelihood output.

In this report, results of the adaptive maximum-likelihood processing of three data samples are given. The first sample is the Aleutian Islands event recorded at LASA that was processed for Special Report No. 1.¹ In that report, a quantitative comparison between adaptive results obtained by TI and conventional maximum-likelihood results obtained by SDL was not possible because the passband of the bandpass filters applied to the data prior to MLF was not the same. Applying the SDL recursive bandpass filter prior to MLF during this study provides a direct comparison between the conventional and adaptive methods possible.



The second data sample consisted of 19 channels of CPO noise data to which a theoretical signal was added at 12 km/sec and at infinite velocity. Signal-to-noise ratios of 1 and 10 were tried for each velocity. Reduced-gradient MLF, full-gradient MLF, summation, and Wiener infinite-velocity signal extraction were performed on these data.

The final adaptive MLF problem was to adapt five samples of 16-channel array data over all five samples in an attempt to duplicate the results obtained with a Wiener infinite-velocity signal-extraction filter designed from stacked correlations of these five data samples.

A. LASA SUBARRAY C1, ALEUTIAN ISLANDS EVENT

Special Report No. 1 indicates that adaptive MLF results generally were similar to the SDL results obtained by conventionally processing these same data. However, the use of different bandpass filters prior to MLF made quantitative comparison of the two methods impossible. Therefore, it was thought advisable to repeat the adaptive processing on bandpass-filtered data with the same recursive filter used by SDL. The data consisted of 19 of the 25 channels of LASA subarray C1, the six seismometers of the inner ring being omitted. The data segment, 2500 points long and sampled at 100-msec intervals, included the signal arrival from an Aleutian Islands event.

A 4-pole recursive bandpass filter (0.5 to 3.0 Hz) supplied by SDL was applied to all channels which were then shifted to line up the signal across channels. The bandpass-filtered and shifted data are shown in Figure III-1. The signal-to-noise ratio on channel 1, defined to be one-half the maximum peak-to-trough amplitude in the signal divided by the rms value of the noise in the fitting interval 0 to 1500, was calculated as 6.75 for the bandpass-filtered data.



The one-sided, 21-point adaptive filters were designed from four passes through the filtering interval. To begin the first pass, coefficients were set to 0 except for those on one end of the filter which equaled $1/19$. The values of k_g for the four passes were 0.00025, 0.00005, 0.000025, and 0.000025. Filter coefficients on passes 2 through 4 were initially equal to their values at the end of the previous pass. Channel 1 and the outputs of the four passes are shown in Figure III-2. The mean-square-errors over the fitting interval were 0.125, 0.081, 0.075, and 0.065. Passes 1, 2, and 3 included only the fitting interval from 0 to 1500 points. On pass 4, the filters were allowed to adapt for 1500 points and then were frozen and applied to the remainder of the sample. Signal-to-noise ratio on the output trace for pass 4 was computed to be 21.1, compared with 23.3 reported by SDL for the conventional maximum-likelihood processing. This is an SNR difference of 1 db. Had more passes been made through the fitting interval, it is believed that the 23.3 figure for SNR could have been more closely approximated.

B. CPO NOISE SAMPLE

A noise sample recorded at the CPO array on 16 October 1964 was maximum-likelihood-filtered using both the full- and reduced-gradient adaptive algorithms. MCF 3, a 25-point Wiener infinite-velocity signal-extraction filter, also was applied to the data. These three methods plus a straight summation are compared for five different cases. In the first case, the noise sample was processed as it was to compare noise rejection of the various methods. For cases 2 through 5, a theoretical signal was added to the noise at infinite velocity and at 12 km/sec, with signal-to-noise ratios of 1 and 10 for each velocity. Signal-to-noise is defined as $1/2$ of the maximum peak-to-trough displacement in the signal divided by the rms value of the noise.

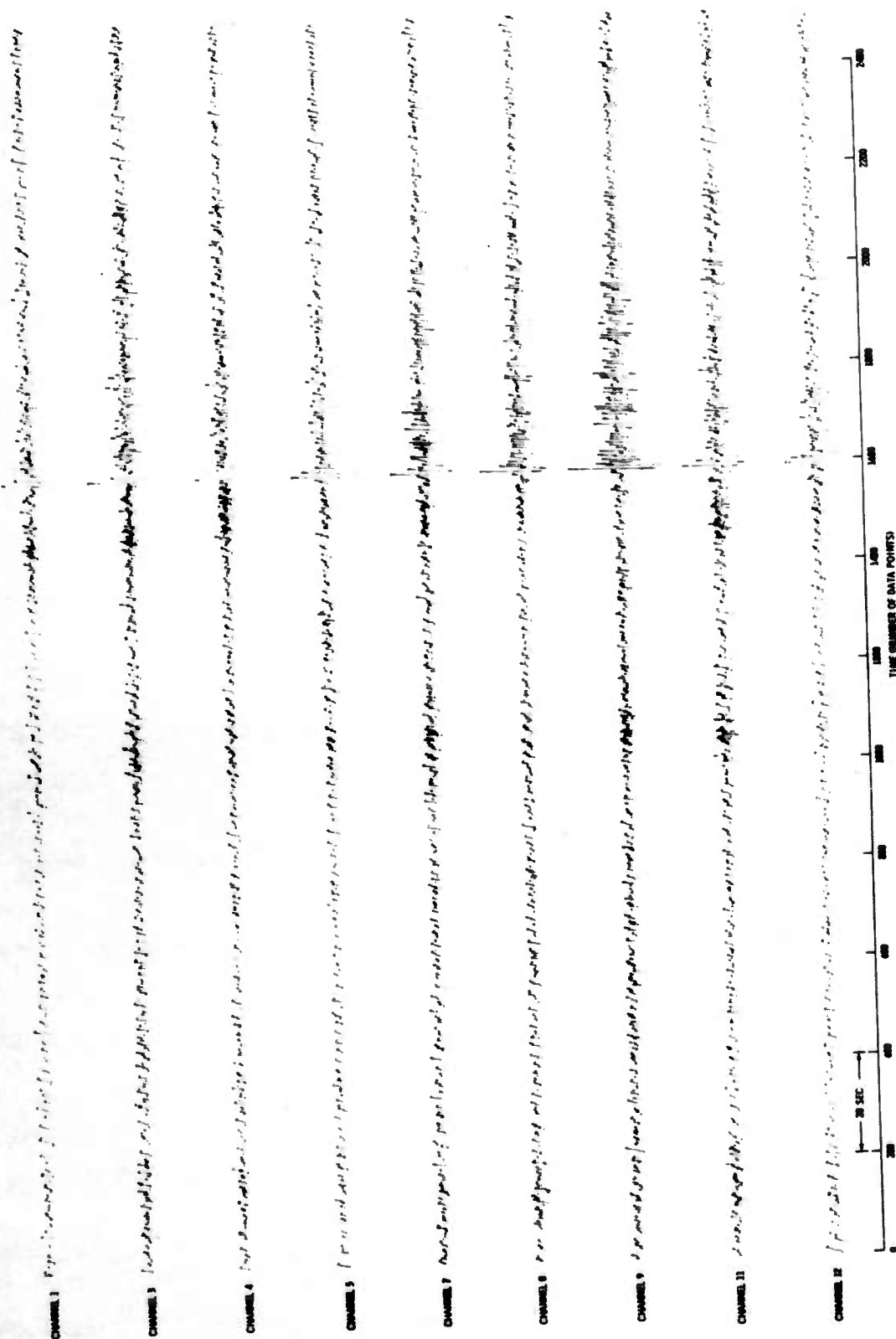


Figure III-1. Bandpass-Filtered (0.5 to 3.0 Hz) and Aligned Data for LASA Subarray C1, Aleutian Islands Event

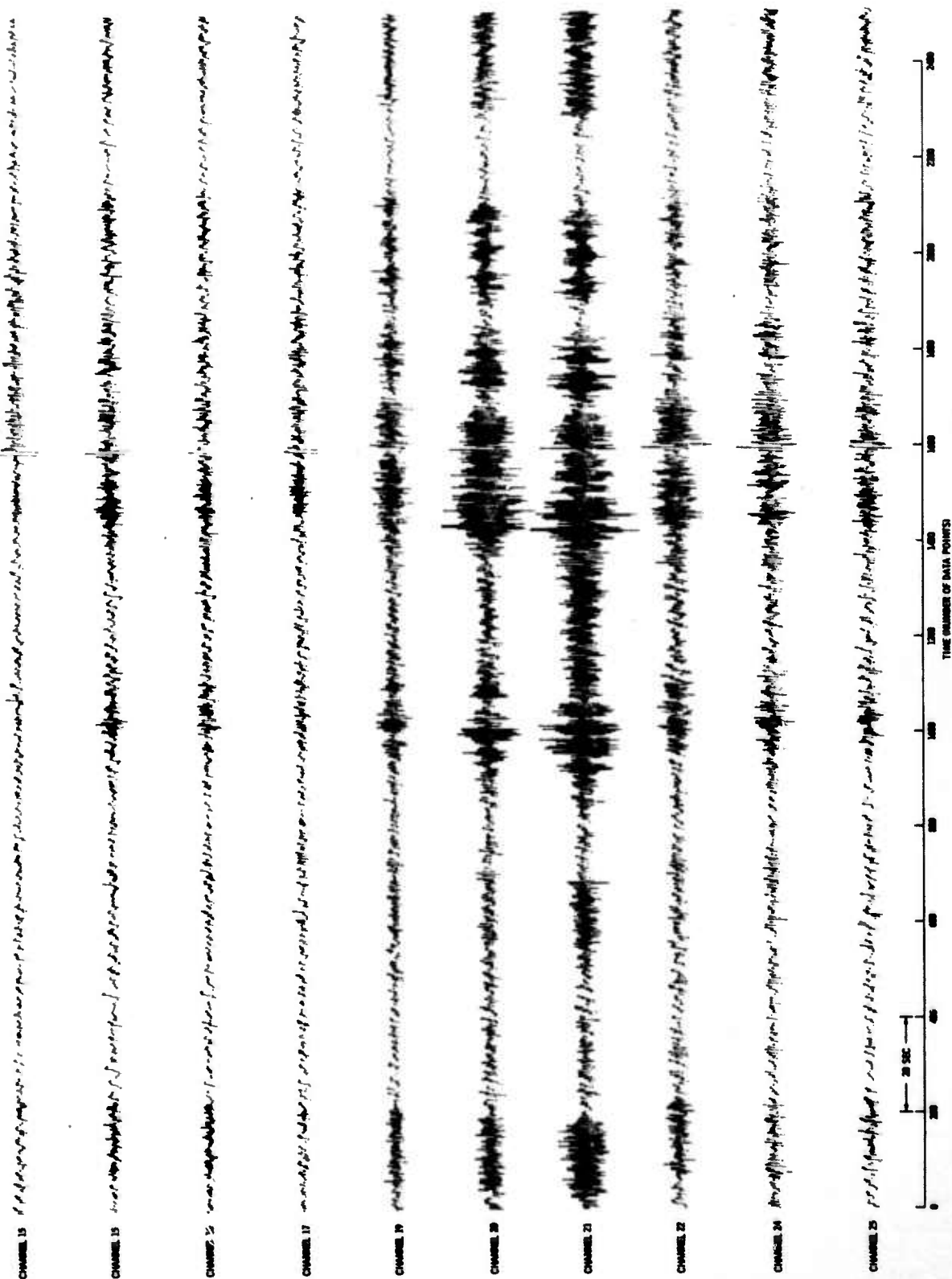


Figure III-1. (Contd)

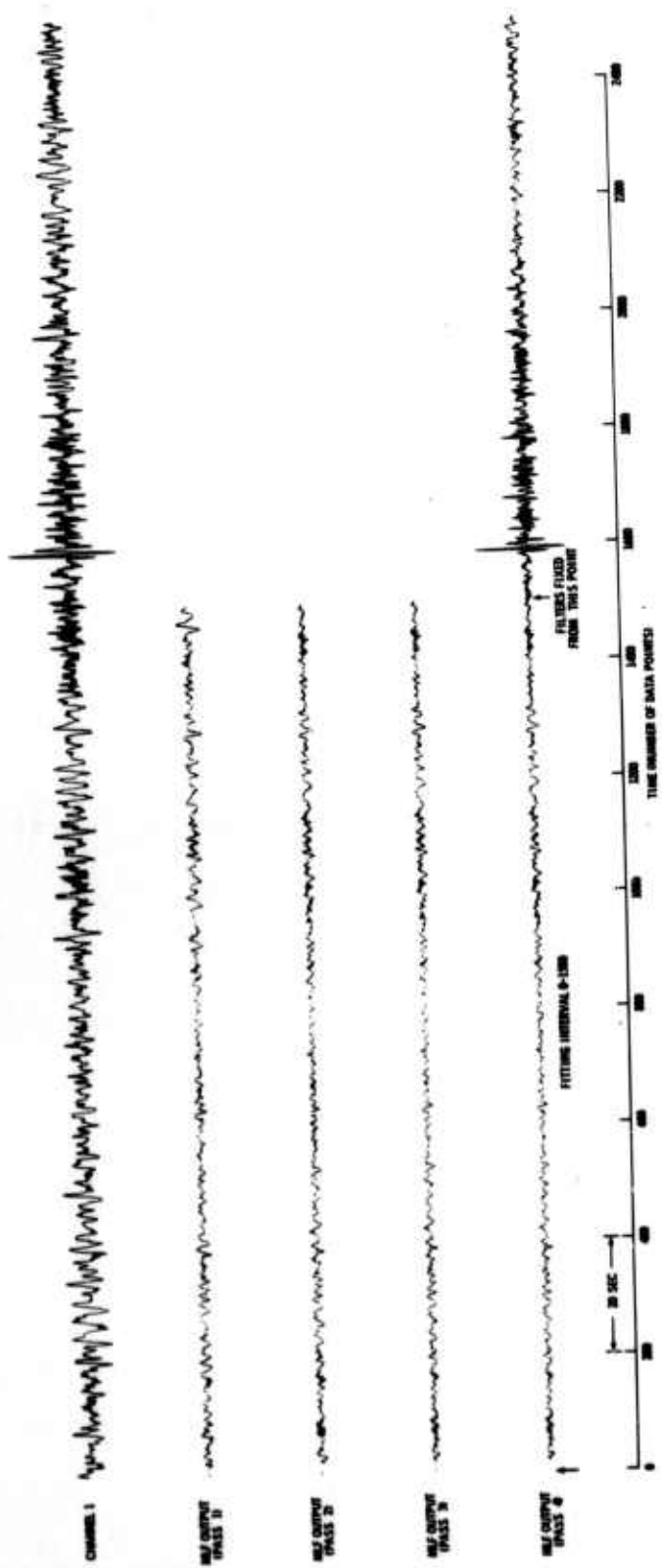


Figure III-2. Adaptive Design of Maximum-Likelihood Filters



The theoretical signal used here was generated by taking the inverse Fourier transform of the average amplitude spectra of 60 teleseismic events recorded at CPO.⁴ The Fourier transform from the frequency domain to the time domain is a periodic function in time. The period of the function of time was 11.4 sec, 158 sample points with a Δt of 72 msec. Thus, the large-amplitude waveform at the beginning of the 250-point transform appears again at 158 points, or 11.4 sec later, giving two nearly identical large-amplitude waveforms in the 250-point signal model. The 12 points immediately preceding the maximum signal amplitude at point 158 were added in front of the signal to smooth its beginning. This double-wavelet signal model was chosen because it gives an indication of the degree of filter distortion resulting from a transient signal. If no filter distortion results from the first high-amplitude signal waveform, then the second one should come through the filtering process looking like the first. Any difference between the first and second waveforms in the filter output, therefore, is evidence of filter distortion by the first waveform, the degree of difference indicating the degree of distortion.

1. Case 1 — Noise Rejection

Figure III-3 shows one of the noise channels and the outputs of a summation, MCF 3, full-gradient MLF, and reduced-gradient MLF. For the first pass through the data in the full-gradient MLF case, the 25 filter coefficients for each channel were set equal to 0 except for the center ones which were set to 1/19. Thus, the maximum-likelihood constraint equations were satisfied initially. On the remaining four passes, coefficients were initialized at their values at the end of the previous pass. Values of k_s for the five passes were 0.00005, 0.00005, 0.000005, 0.000005, and 0.000005.

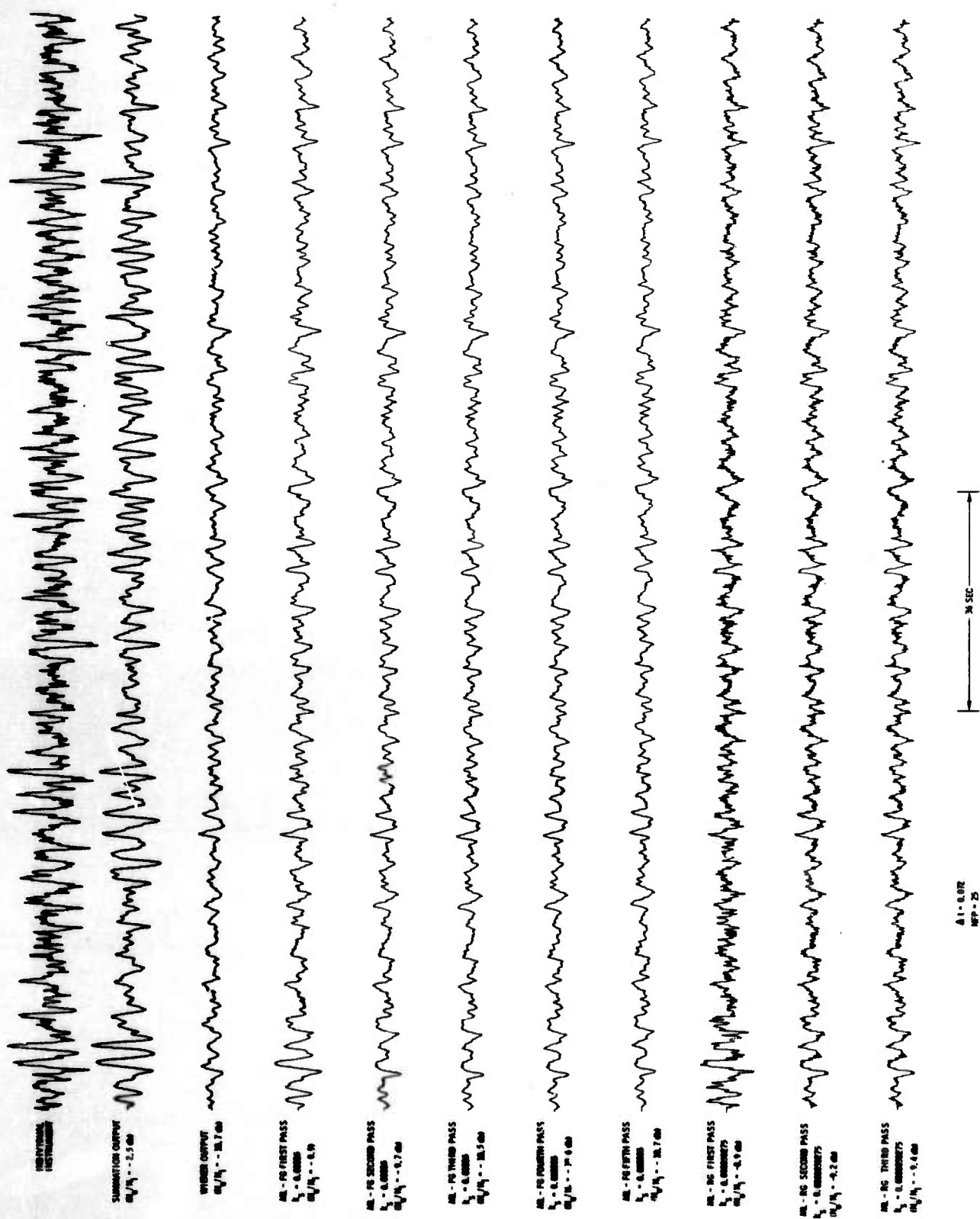


Figure III-3. Adaptive Processing of a 19-Channel CPO Noise Sample



Three passes through the data were made in the reduced-gradient MLF case, with k_g values of 0.00005275, 0.000005275, and 0.0000005275. k_g was scaled by 19/18 to give the same time constants in the 18-channel problem as those in the 19-channel problem. The 25 filter coefficients for each of the 18 difference traces (channel 10 being the reference trace) were set to 0 to begin the first pass and to their values at the end of the previous pass to begin passes 2 and 3.

Power spectra of channel 1, mean across channels, channel 1 minus mean, and the full-gradient MLF output from pass 5 are shown in Figure III-4. Figure III-5 is the spectra of channel 1, channel 10 minus channel 1, and the reduced-gradient MLF output from pass 3.

Noise rejection by the full-gradient method over the last 1000 points of the fifth pass was -10.7 db, which was equal to the noise rejection of MCF 3 over the same interval. Only the last 1000 points were used to compute noise rejection thereby reducing any start-up effects which might be present at the beginning of each adaptive pass.

The reduced-gradient MLF did not match the noise-rejection level of MCF 3 in its three passes. However, since five passes were required to match MCF 3 with the full-gradient algorithm, it cannot be concluded that the reduced gradient algorithm would not have done so well after five passes with similar values of k_g .

2. Case 2 — Infinite-Velocity Signal (SNR = 1.0)

The theoretical signal was added to the 2500-point noise sample of case 1 in the 2001- to 2250-point interval on all traces. The signal was scaled so that one-half of its maximum peak-to-trough displacement was equal to the rms value of the noise on channel 1. The resulting data then were processed by summing, Wiener filtering (MCF 3), and full-gradient maximum-likelihood filtering. Processing was identical to that for case 1 except that only three adaptive passes were made, with k_g being 0.00005, 0.00005, and 0.000005. The signal, channel 19 of the data, and the processing outputs are shown in Figure III-6.

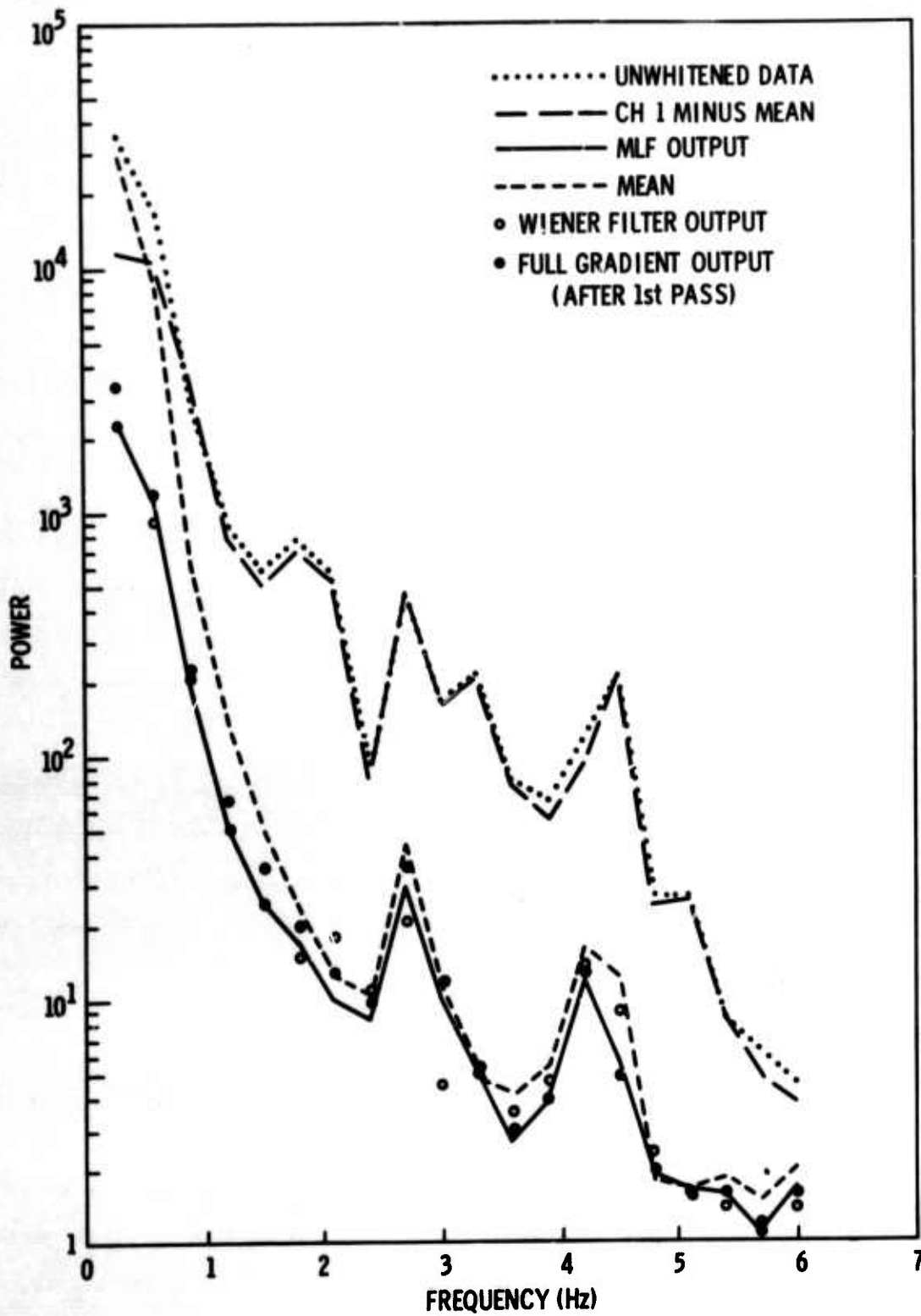


Figure III-4. Adaptive Processing of the CPO Noise Sample with Full-Gradient Power Output

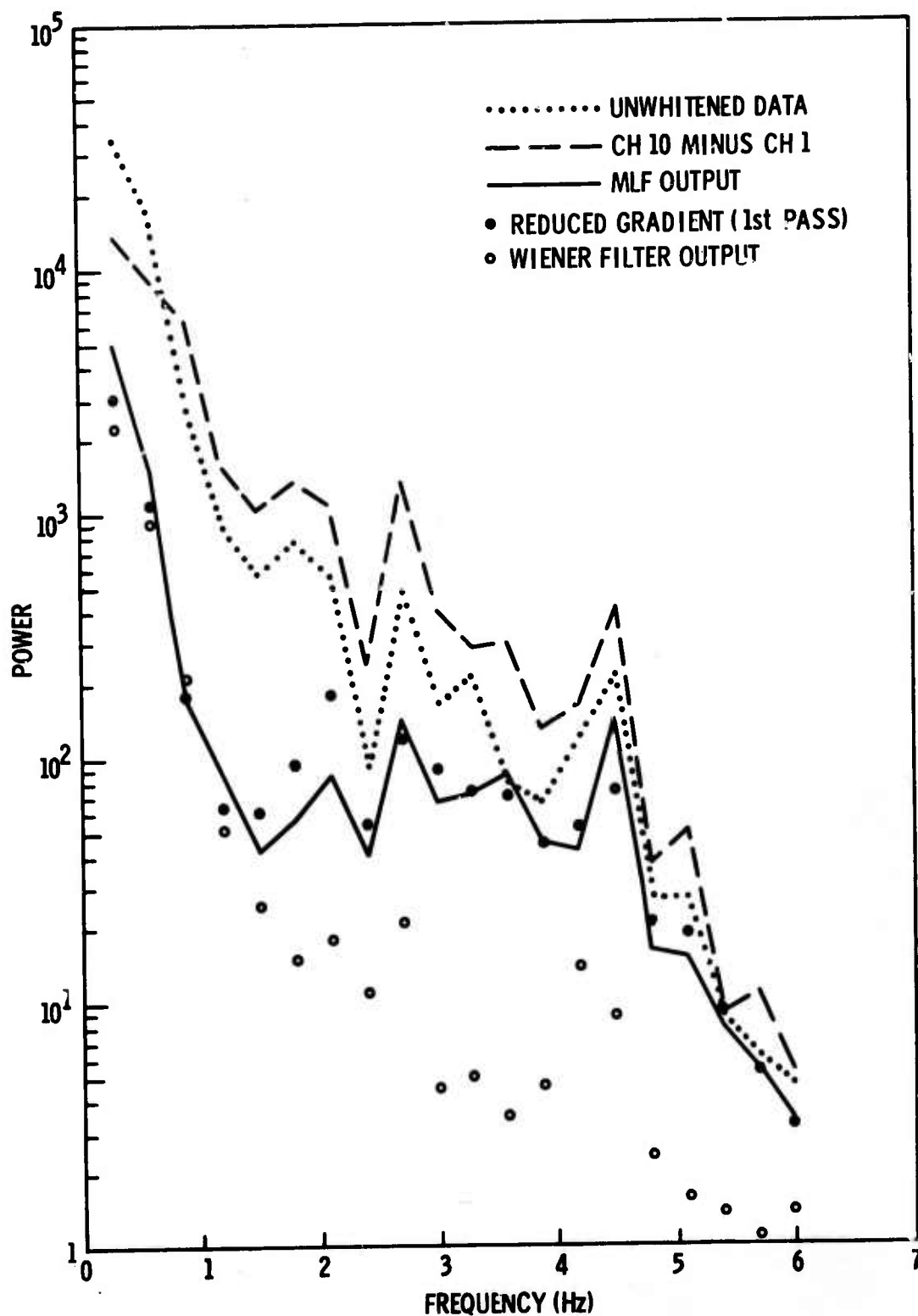


Figure III-5. Adaptive Processing of the CPO Noise Sample with Reduced-Gradient Power Output

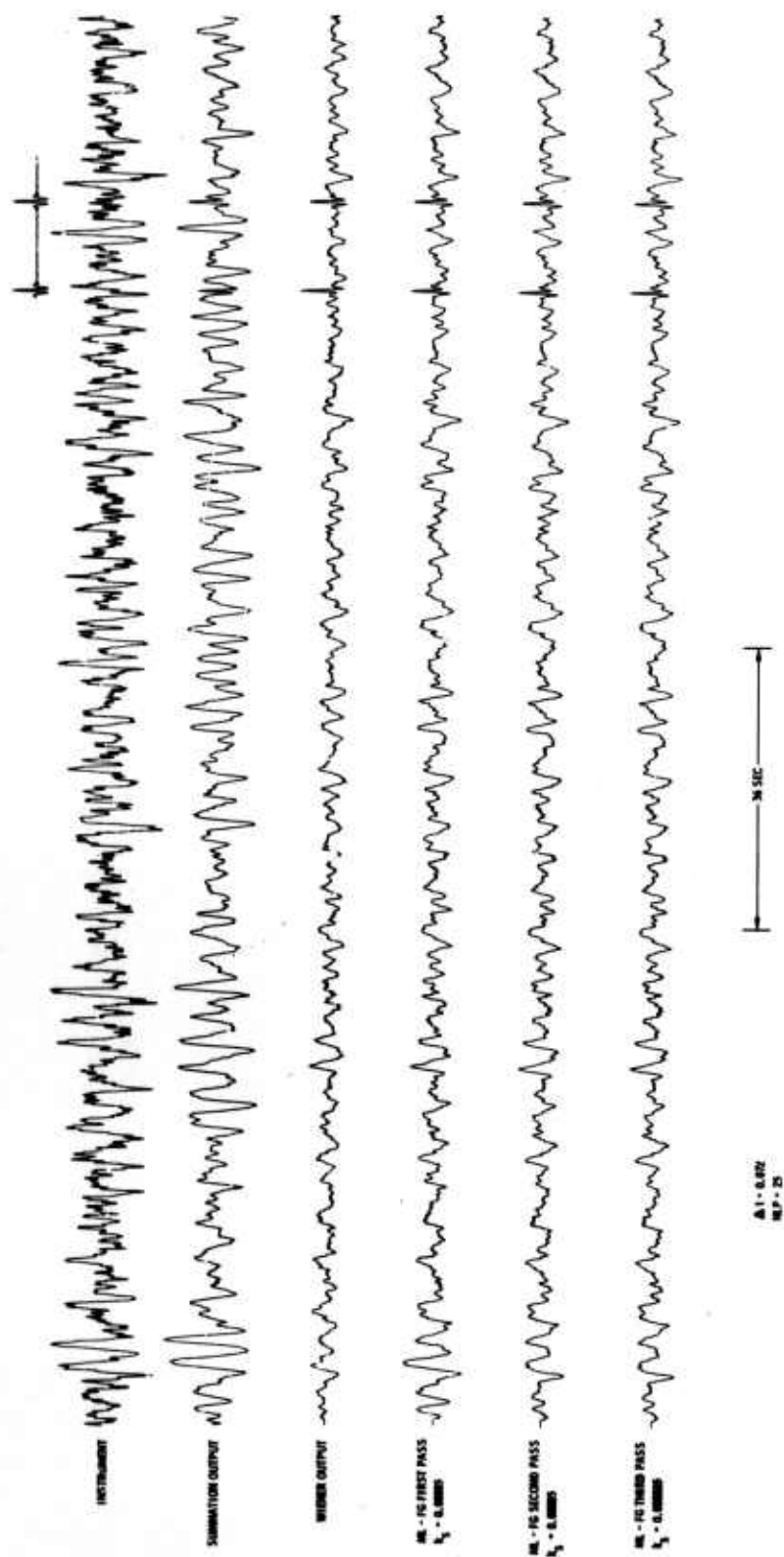


Figure III-6. Adaptive Processing of a 19-Channel Infinite-Velocity Synthetic Signal Plus Noise (SNR = 1.0)



3. Case 3 — Infinite-Velocity Signal (SNR = 10.0)

The signal of case 2 was scaled up by 10 and added as before to the noise data of case 1. The processing of case 2 was duplicated here. A representative data channel and the processing results are given in Figure III-7.

4. Case 4 — 12 km/sec Signal (SNR = 1.0)

Data and processing for this case duplicates case 2 except that the signal was not added in at the same place on all channels but was time-shifted on each channel to represent a signal traveling across the array at 12 km/sec. Results for this case are shown in Figure III-8.

5. Case 5 — 12 km/sec Signal (SNR = 10.0)

The signal of case 4 was scaled by 10 and added once again to the noise data, with a velocity of 12 km/sec. The processing results for this case, shown in Figure III-9, were obtained by procedures identical to the previous case.

C. DESIGN PROBLEM FOR FIVE SAMPLES

1. Summary

A composite of five noise samples from a short-period surface array was chosen to compare adaptive maximum-likelihood filters to Wiener filters. The Wiener filters were designed from the stacked correlations, infinite-velocity signal model, SNR = 4 with gain variability, and applied to the first 1000 points of each of the five noise samples.

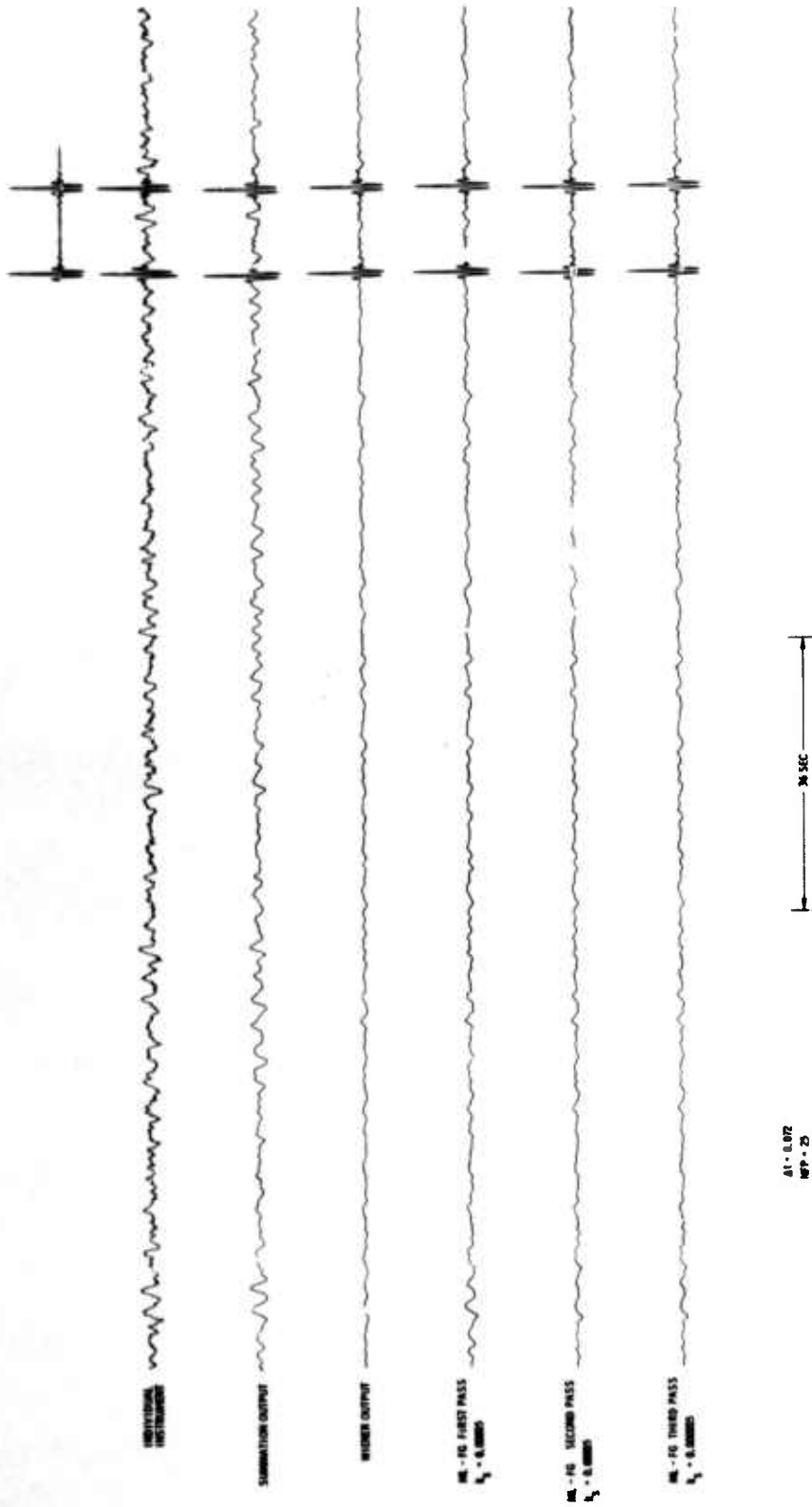


Figure III-7. Adaptive Processing of a 19-Channel Infinite-Velocity Synthetic Signal Plus Noise (SNR = 10.0)

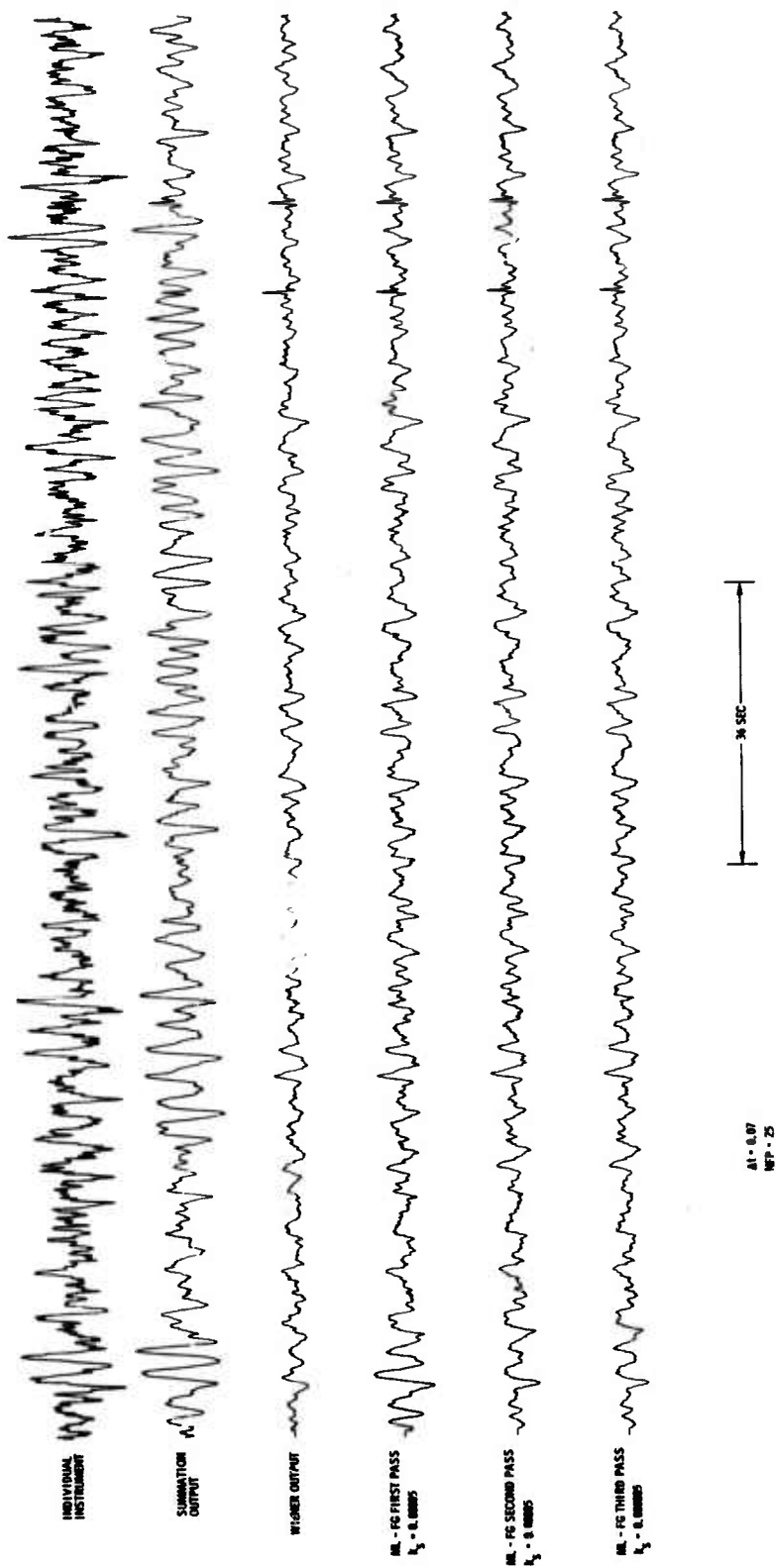


Figure III-8. Adaptive Processing of a 19-Channel 12 km/sec Synthetic Signal Plus Noise (SNR = 1.0)

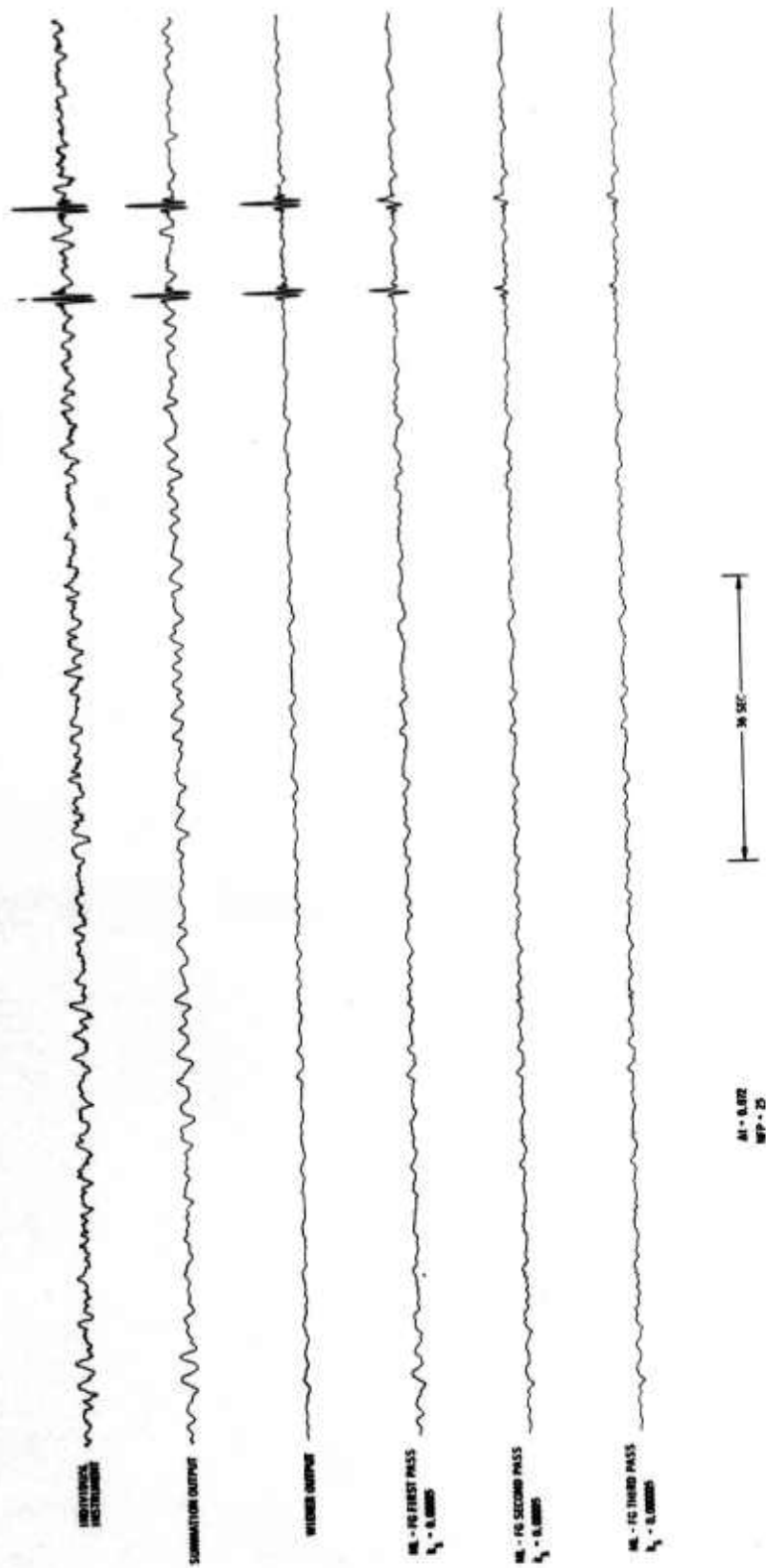


Figure III-9. Adaptive Processing of a 19-Channel 12 km/sec Synthetic Signal Plus Noise (SNR = 10.0)



The maximum-likelihood filters were adaptively designed by obtaining a starting set of filters from the first noise sample using a large value of k_g . The first half of each noise sample then was processed in the order 1 to 5 using a smaller value of k_g ; finally, the last half of each noise sample was processed in the order 5 to 1 with an extremely small value of k_g . These adaptively designed filters then were fixed and applied to the first 1000 points of each noise sample. For comparison, a straight stack and large- k_g adaptive outputs also were computed.

Spectra of the error traces indicate that the Wiener filter is better (2 db) at 0.5 Hz with a crossover at approximately 1 Hz and that the adaptively designed maximum-likelihood filter performs better (up to 15 db) over the 2- to 5-Hz band. The fixed-adaptive and large k_g performed alike except for frequencies above 2 Hz, where an improvement up to 10 db implies a consistent time-varying high-frequency component.

2. Method

The twofold purpose of this experiment is to illustrate the application of the adaptive method to the problem of filter design on a composite of noise and to compare the behavior of online adaptive filters to fixed Wiener and adaptively designed maximum-likelihood filters.

Five 216-sec noise samples of 72-mil data from 16 short-period seismometers were used to determine the noise correlations from which a 29-point infinite-velocity Wiener filter was computed. This work was performed previously under a separate contract and the results borrowed to make the comparison between conventional and adaptive filters.⁵

Prior to any adaptive processing, the entire set of data was normalized by a scale factor determined from channel 1 of sample 1. Design of the composite maximum-likelihood filters was accomplished by the procedure illustrated in Figure III-10. Starting with an infinite-velocity beam-steer set of filters, an "initialize" run on sample 1 through 500 points was

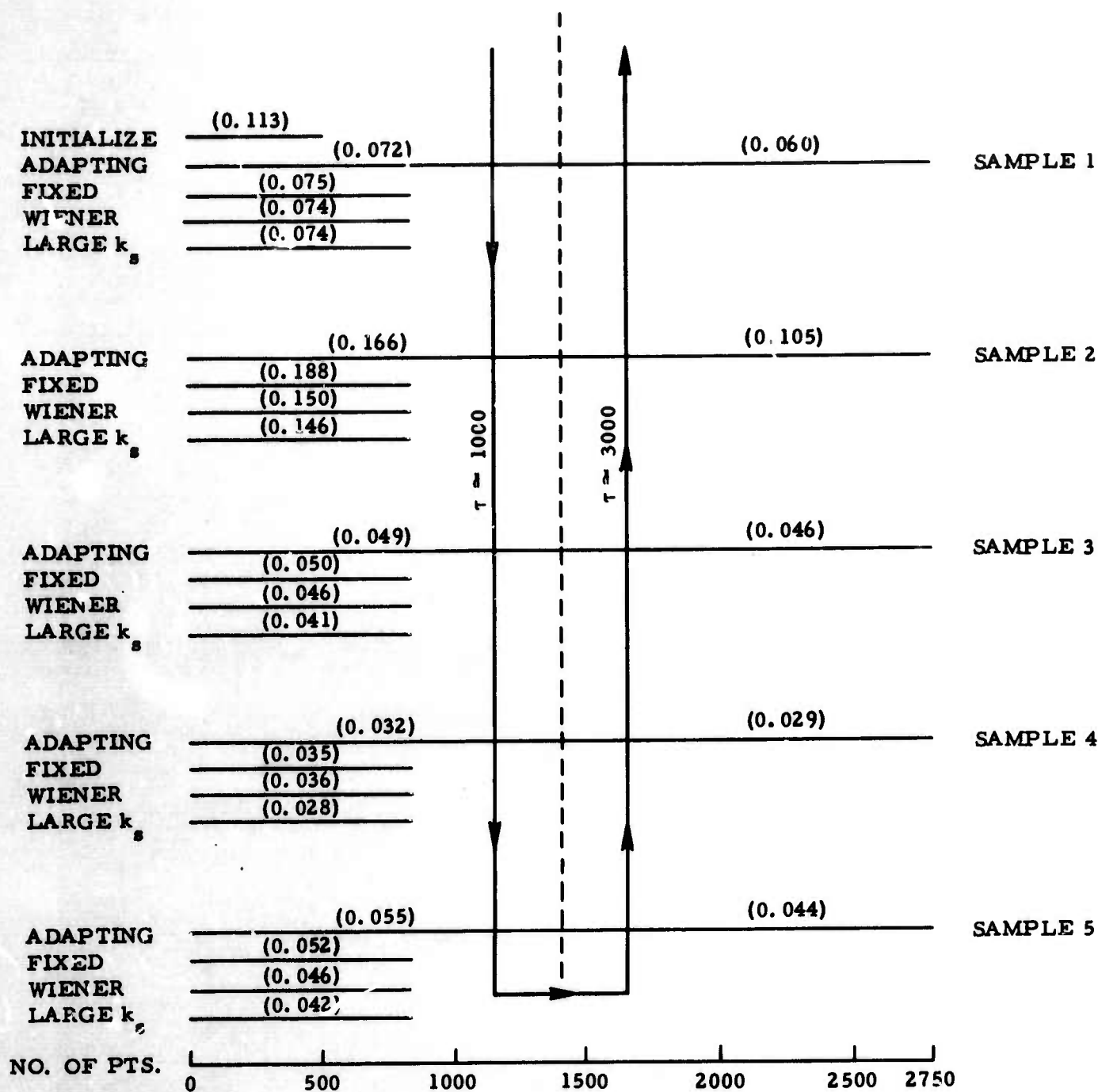


Figure III-10. Five-Sample Maximum-Likelihood Design Problem



made with a large value of k_g (0.00025), indicated by the first line of Figure III-10. Values in parentheses are mean-square-error over the indicated length of data, with the type of filters at the left of the page.

The filters at the end of the initial run then were used as starting filters in the design problem. Each data sample was split as indicated by the dashed line of Figure III-10 and processed in the order indicated by the arrowed line. The k_g values of 18×10^{-7} and 6×10^{-7} were used throughout the first-half and second-half processing, respectively.

Actual outputs for four types of filters applied to the first 1000 points of the five noise samples are shown in Figures III-11 through III-15. Power spectra of these error traces are given in Figures III-16 through III-20.

3. Discussion

The maximum-likelihood fixed or adaptive filter is approximately equivalent to the Wiener filter for frequencies between 0.75 and 1.5 Hz. Wiener filters perform better at low frequency and the maximum-likelihood filters better at high frequency. Additional improvement is shown in the high-frequency region for the adaptive large- k_g maximum-likelihood filter.

First, attempts were made to explain the low-frequency phenomenon on the basis of different frequency response to high-velocity data for the designed Wiener and maximum-likelihood filters. The response of the Wiener filter was down only 1 db at 0.1 Hz and 0.5 db at 1.0 Hz, whereas the maximum-likelihood filter response was not influenced by roundoff error. Thus, the differences in frequency response are not sufficient to explain the results. No theoretical reasons why the optimum filters have different error powers as a function of frequency could be determined; however, at present, the following explanation of the results is favored.



The optimum Wiener filter and maximum-likelihood filters produce highly comparable error-power curves. Maximum-likelihood filters produced by the method cited in this report are almost equal to the optimum Wiener filter in total mean-square-error, but this error has a radically different frequency distribution. This difference in frequency occurs because the filters are updated at each point in time by $x_{ij} - \bar{x}_j$ and subtracting the mean over channels acts as a low-cut frequency filter. Thus, the filters are influenced more by the high-frequency data than by the low-frequency data.

It would appear from processing results on the design data that the adaptive procedure will produce good filters based on broadband mean-square-error more cheaply than the Wiener procedure. Response plots in $f-\bar{k}$ space, however, indicate that although the adaptively designed maximum-likelihood filter performed well on the design data in terms of total mean-square-error, it is not likely to perform well on-line on low-frequency energy coming from a large subset of K -space. Response of the fixed adaptive maximum-likelihood and Wiener filters at 0.25 Hz are compared in Figures III-21 and III-22. Although this may be a problem in considering the adaptive method as a procedure for designing fixed filters, it is definitely not a problem in considering the adaptive method as an online procedure.

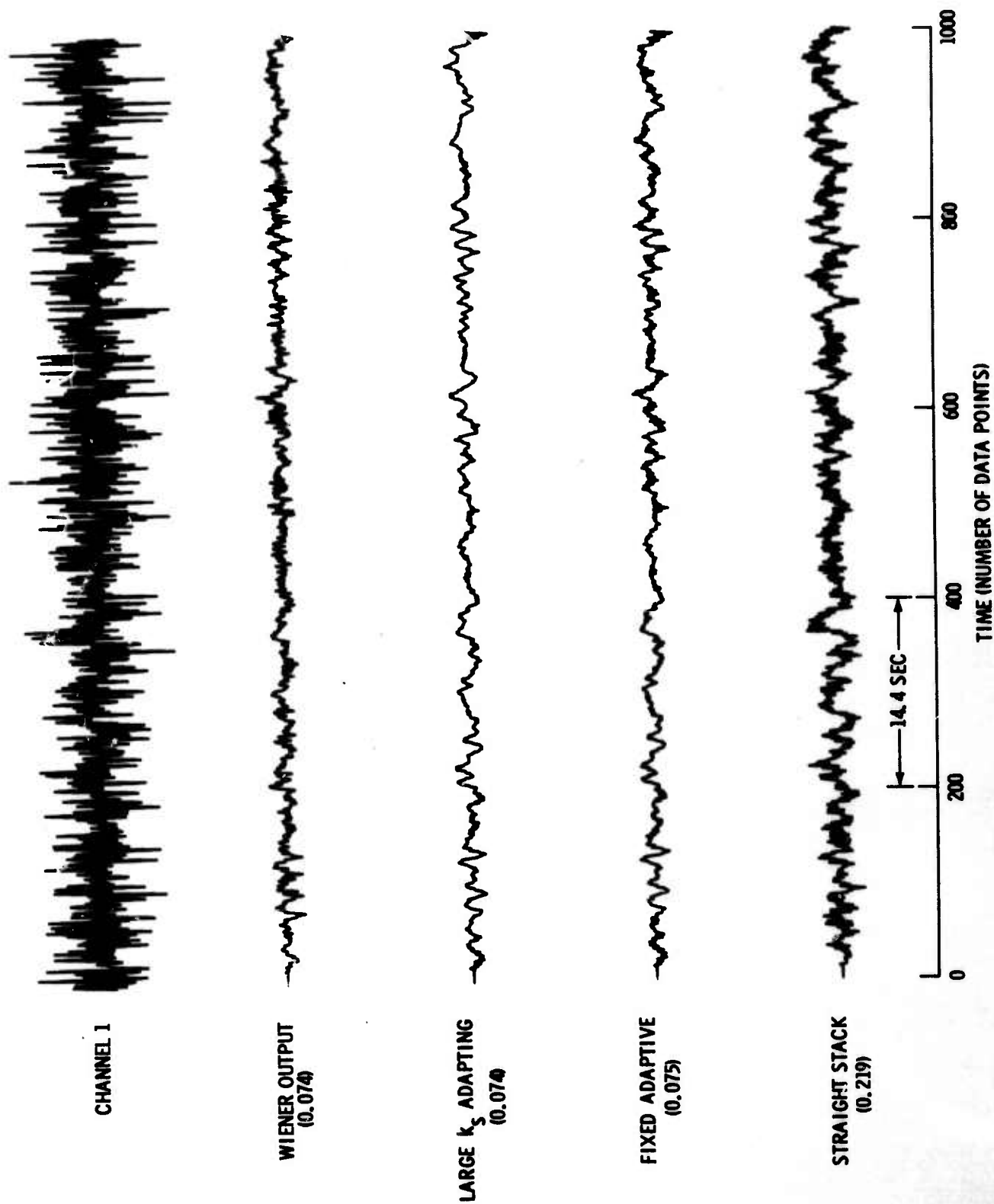


Figure III-11. Outputs for Compared Filter-Design Techniques, Noise Sample 1

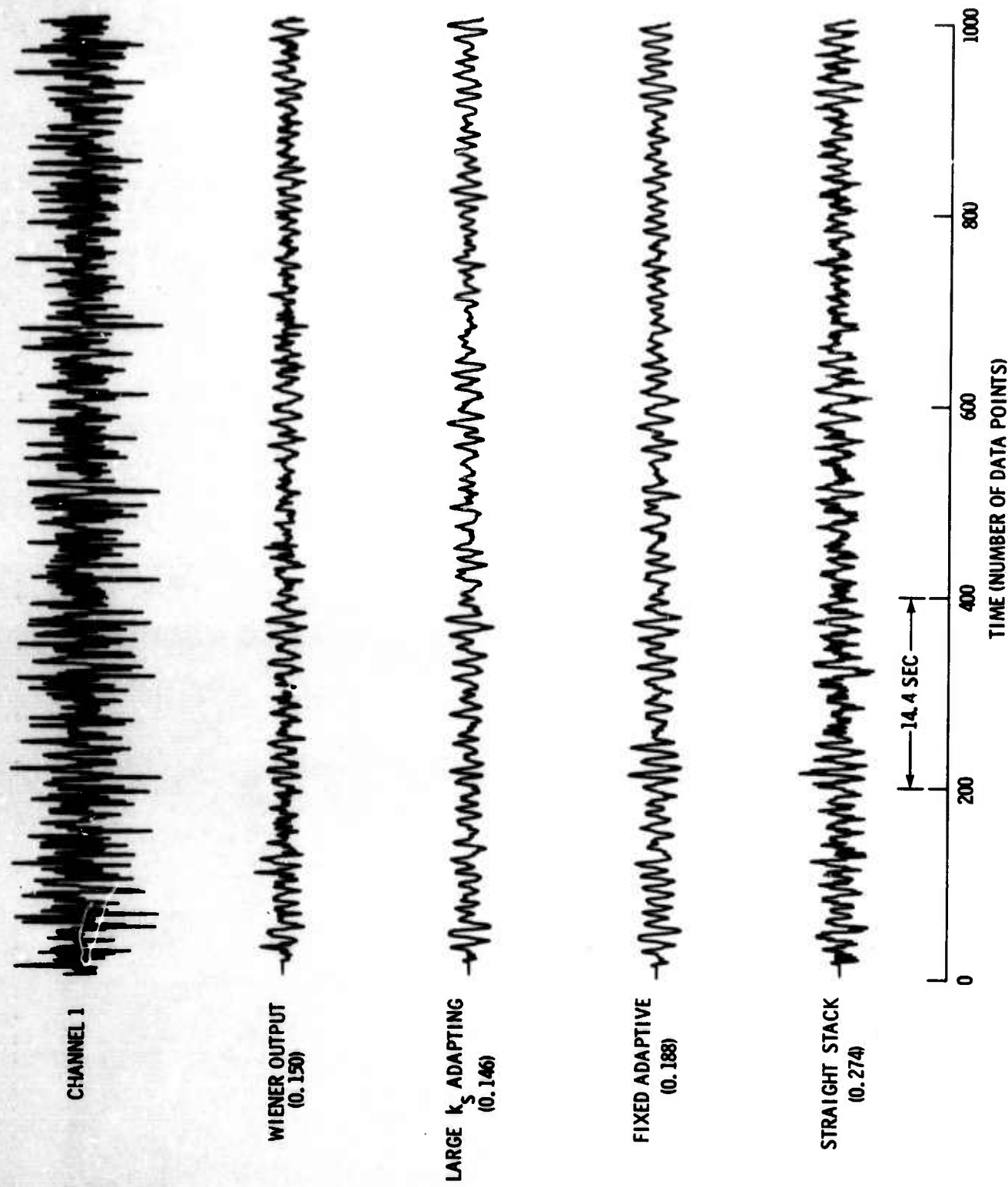


Figure III-12. Outputs for Compared Filter-Design Techniques, Noise Sample 2

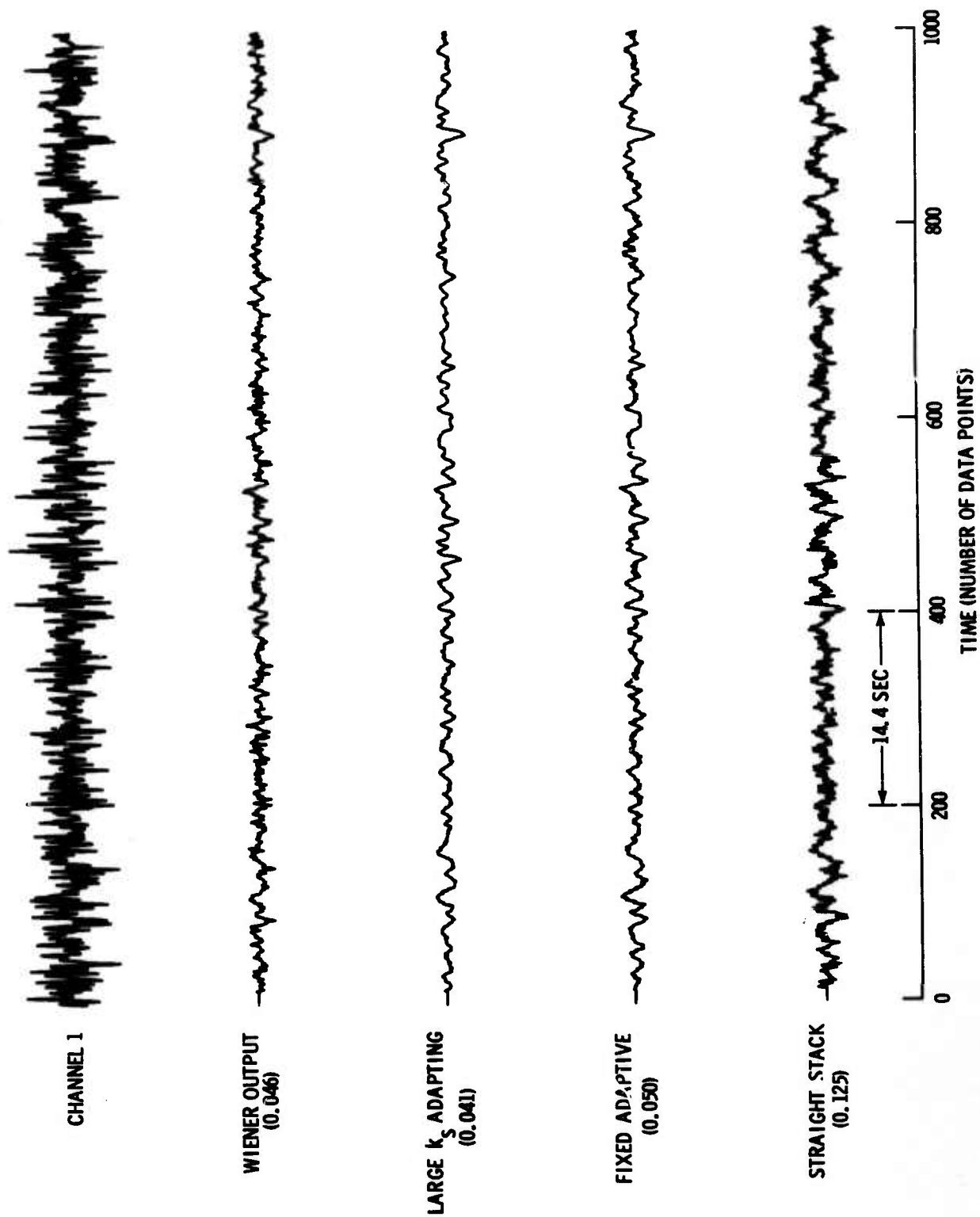


Figure III-13. Outputs for Compared Filter-Design Techniques, Noise Sample 3

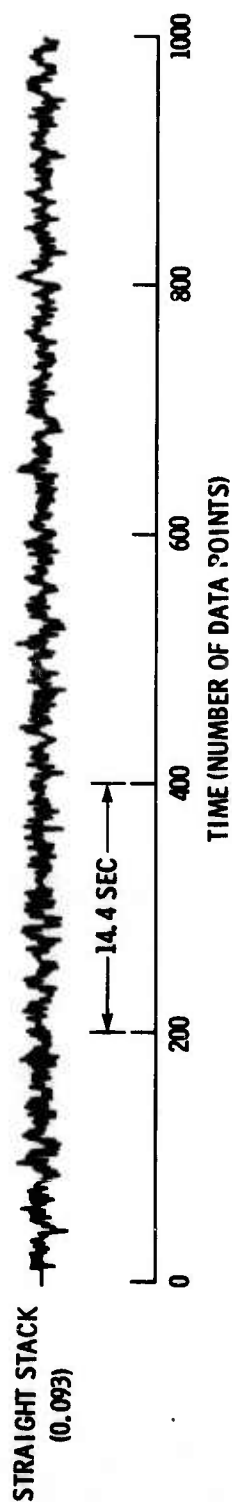


Figure III-14. Outputs for Compared Filter-Design Techniques, Noise Sample 4

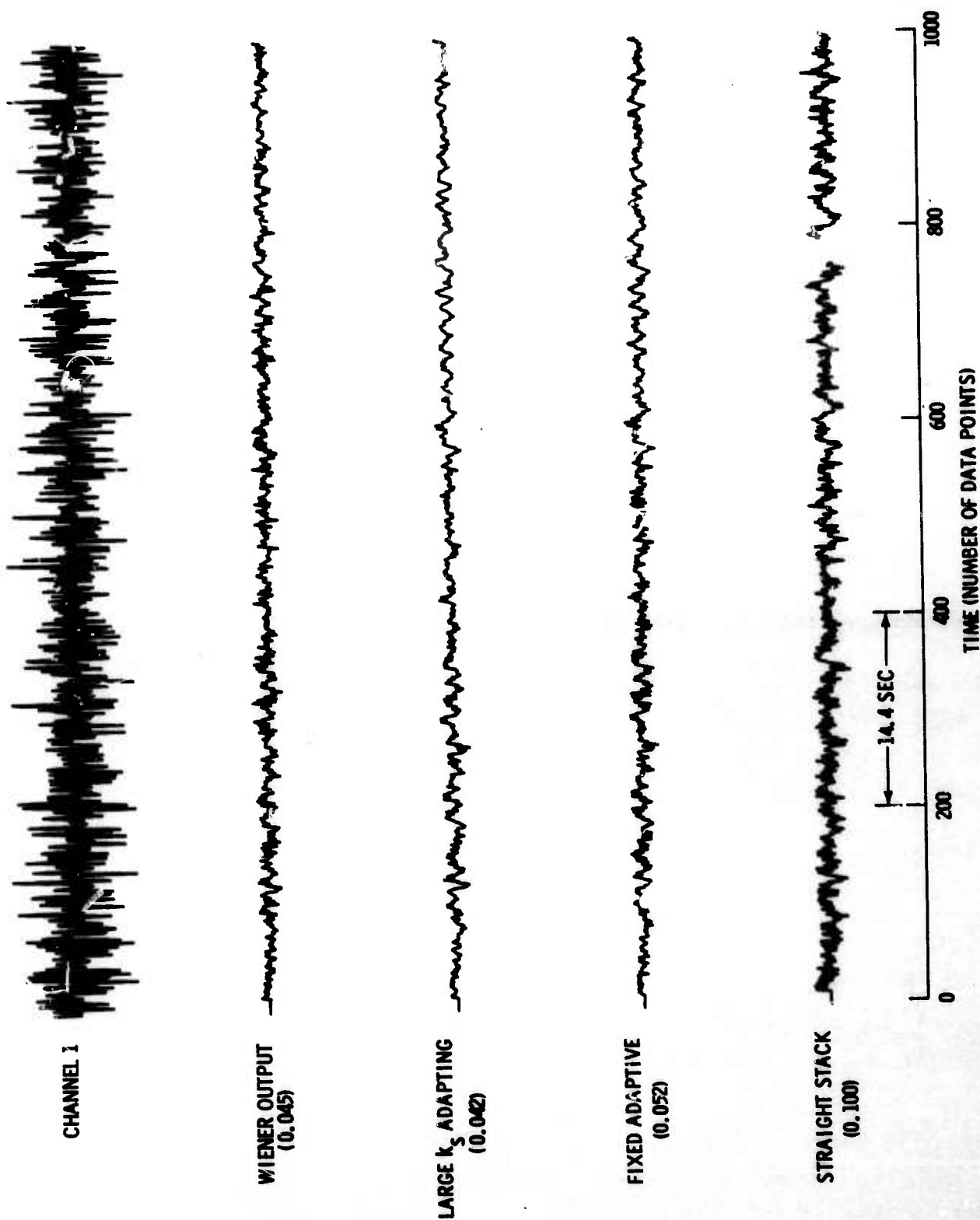


Figure III-15. Outputs for Compared Filter-Design Techniques, Noise Sample 5

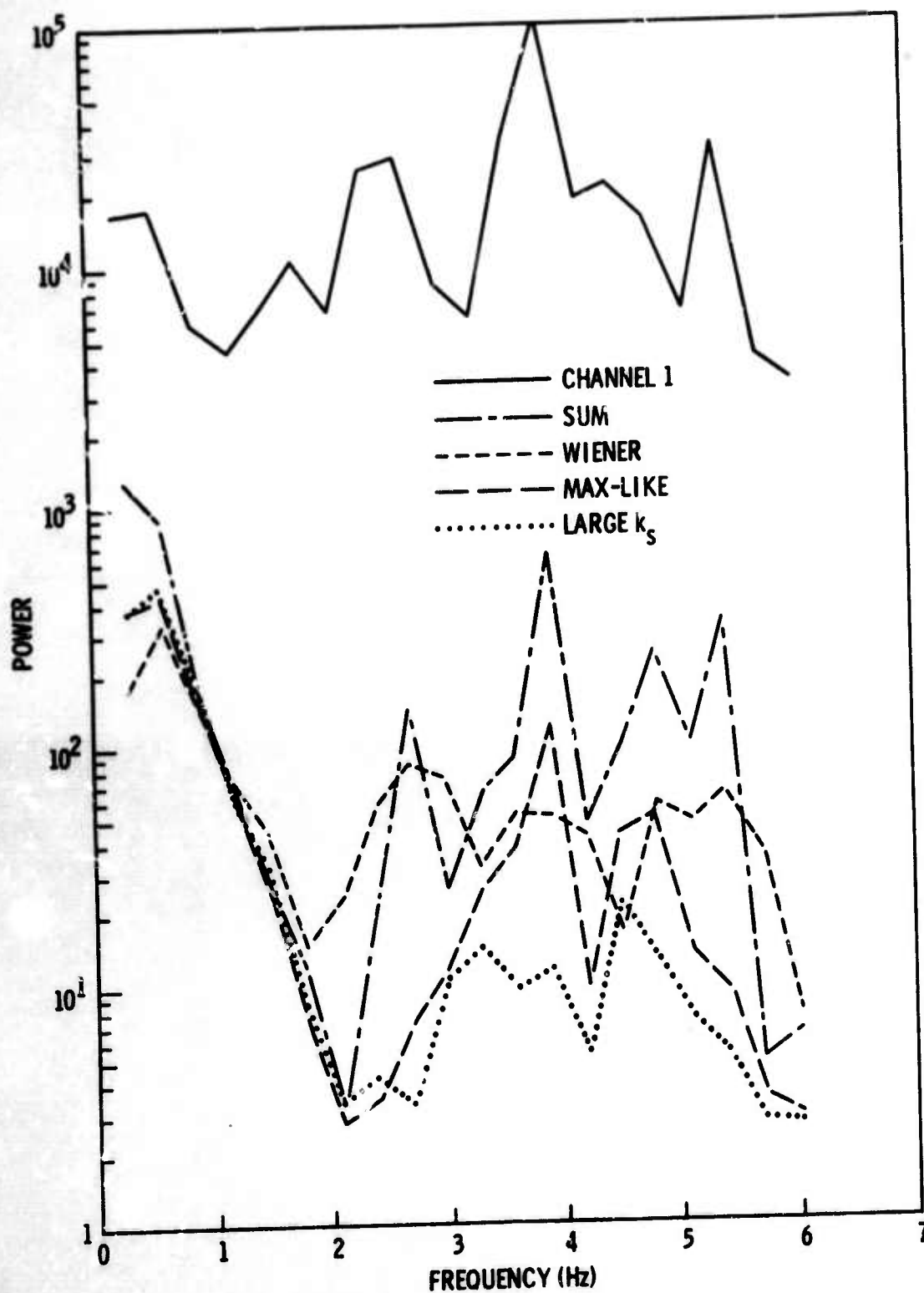


Figure III-16. Error Power Spectra for Compared Filter-Design Techniques, Noise Sample 1

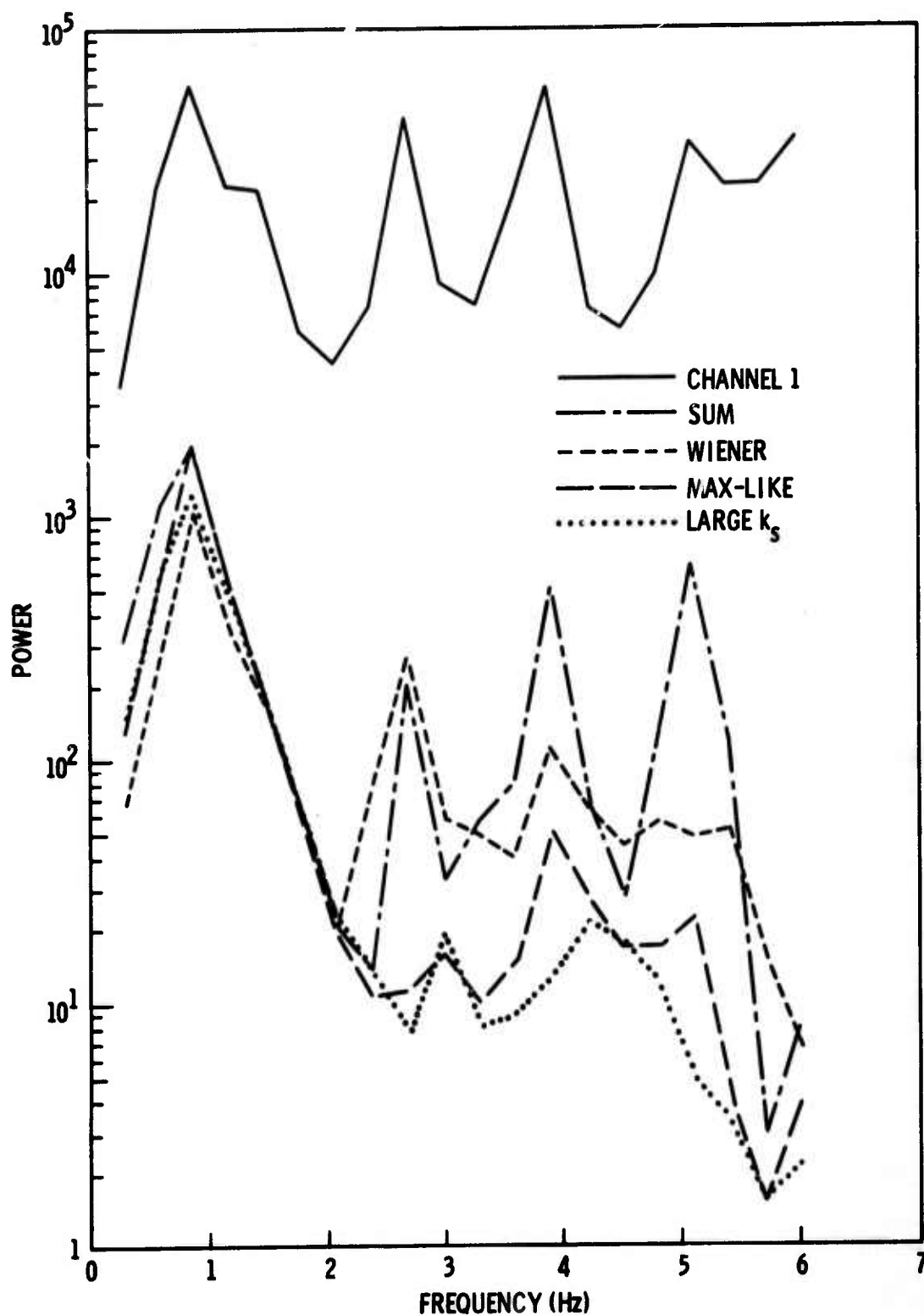


Figure III-17. Error Power Spectra for Compared Filter-Design Techniques, Noise Sample 2

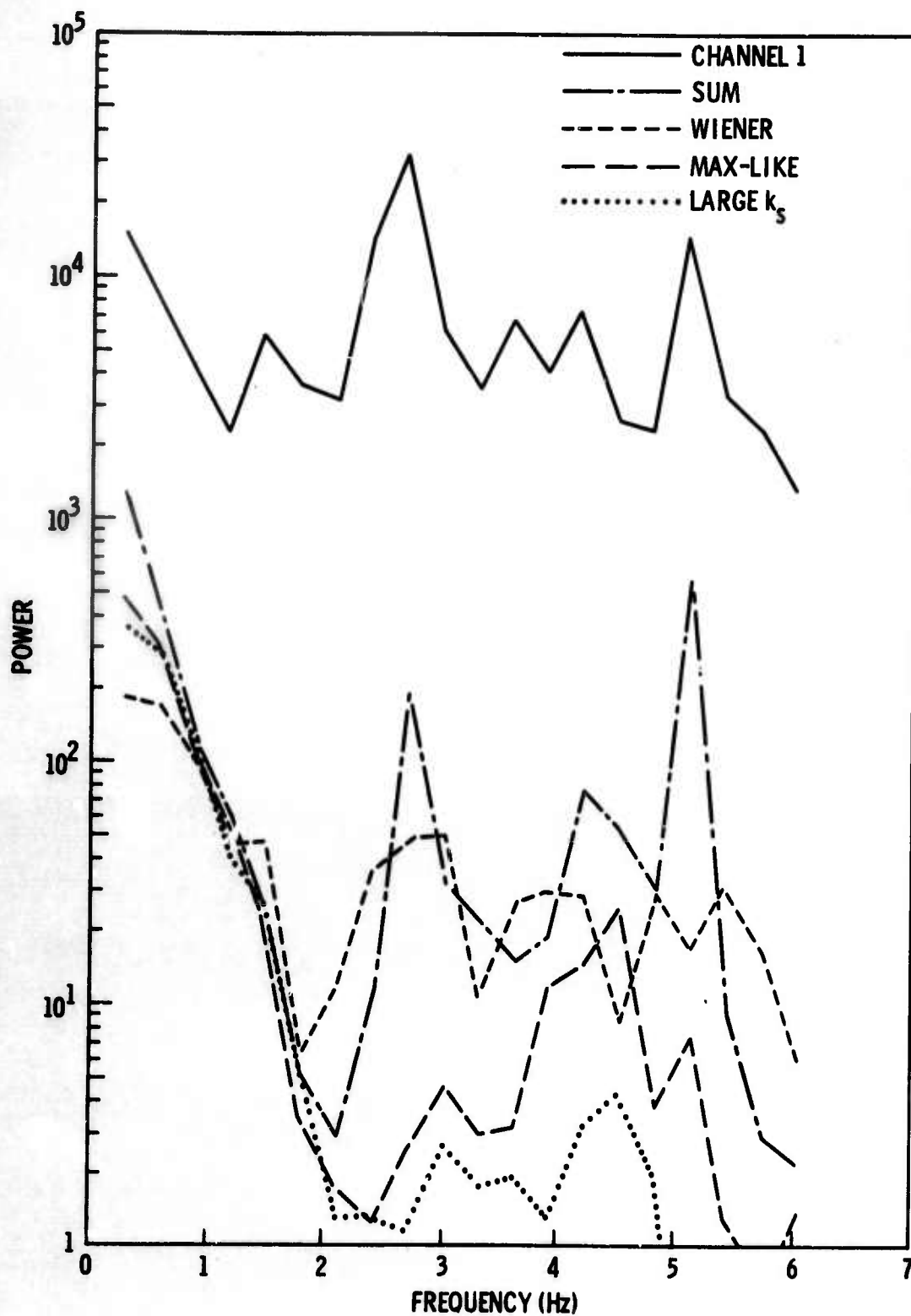


Figure III-18. Error Power Spectra for Compared Filter-Design Techniques, Noise Sample 3

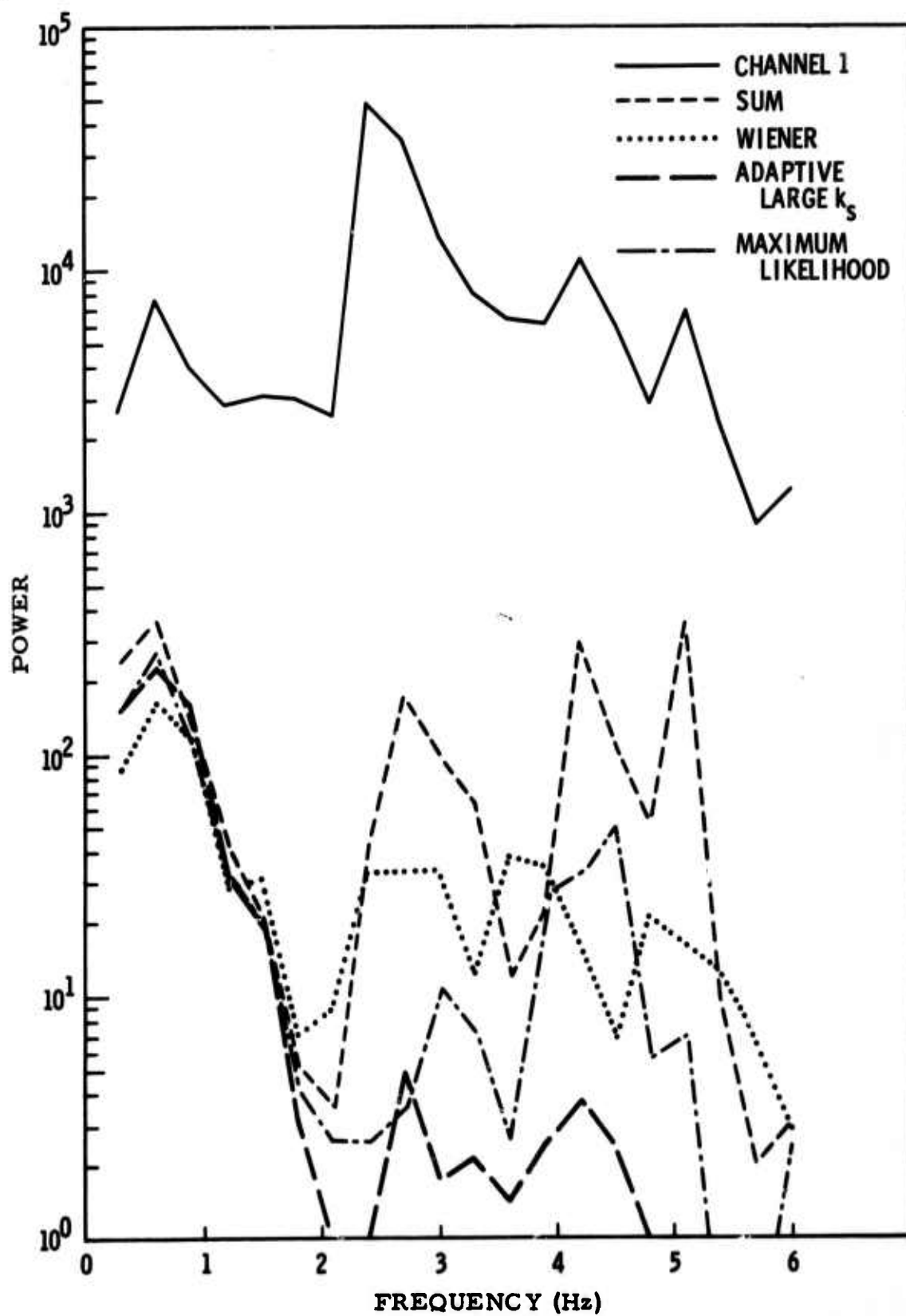


Figure III-19. Error Power Spectra for Compared Filter-Design Techniques, Noise Sample 4

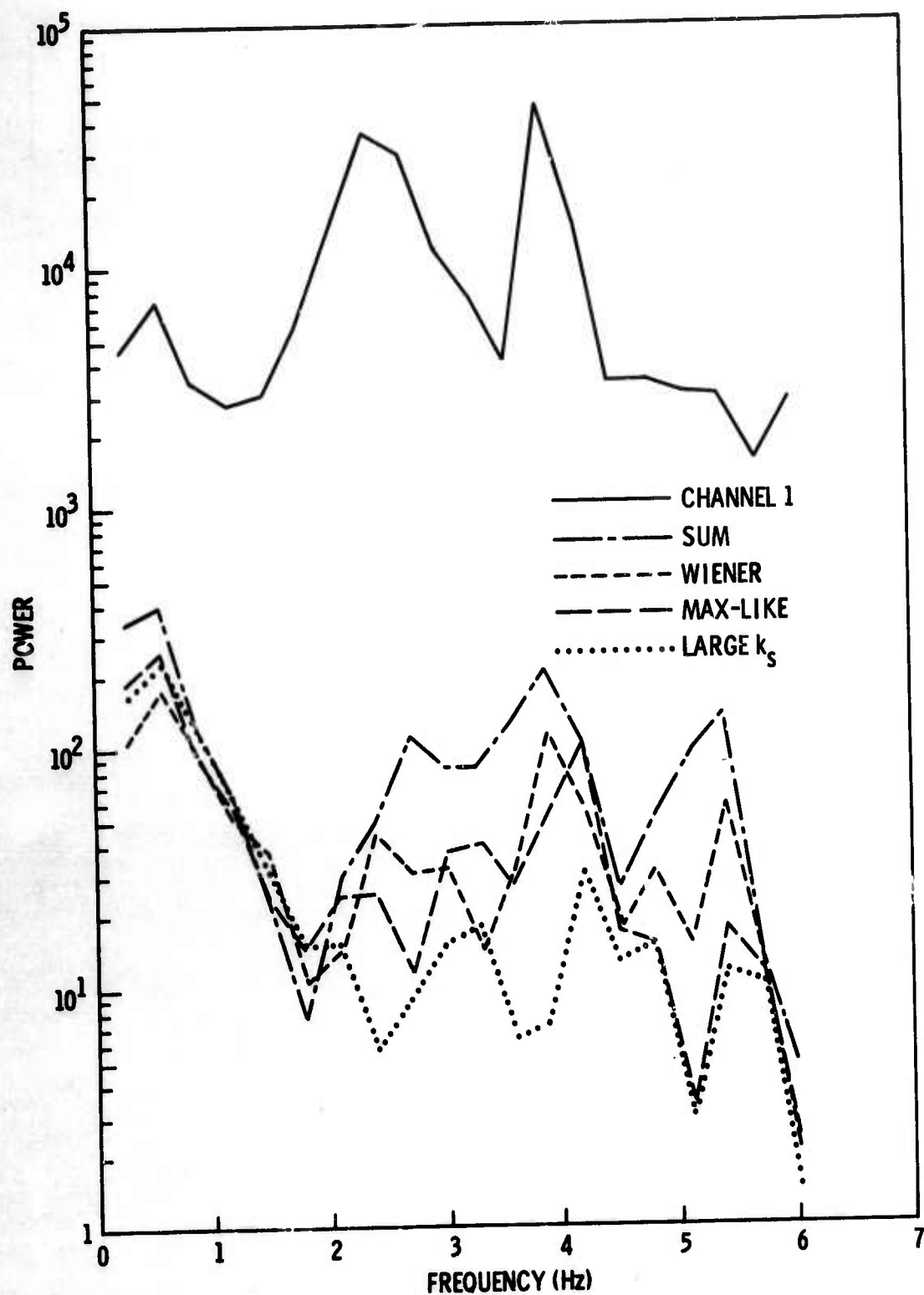


Figure III-20. Error Power Spectra for Compared Filter-Design Techniques, Noise Sample 5

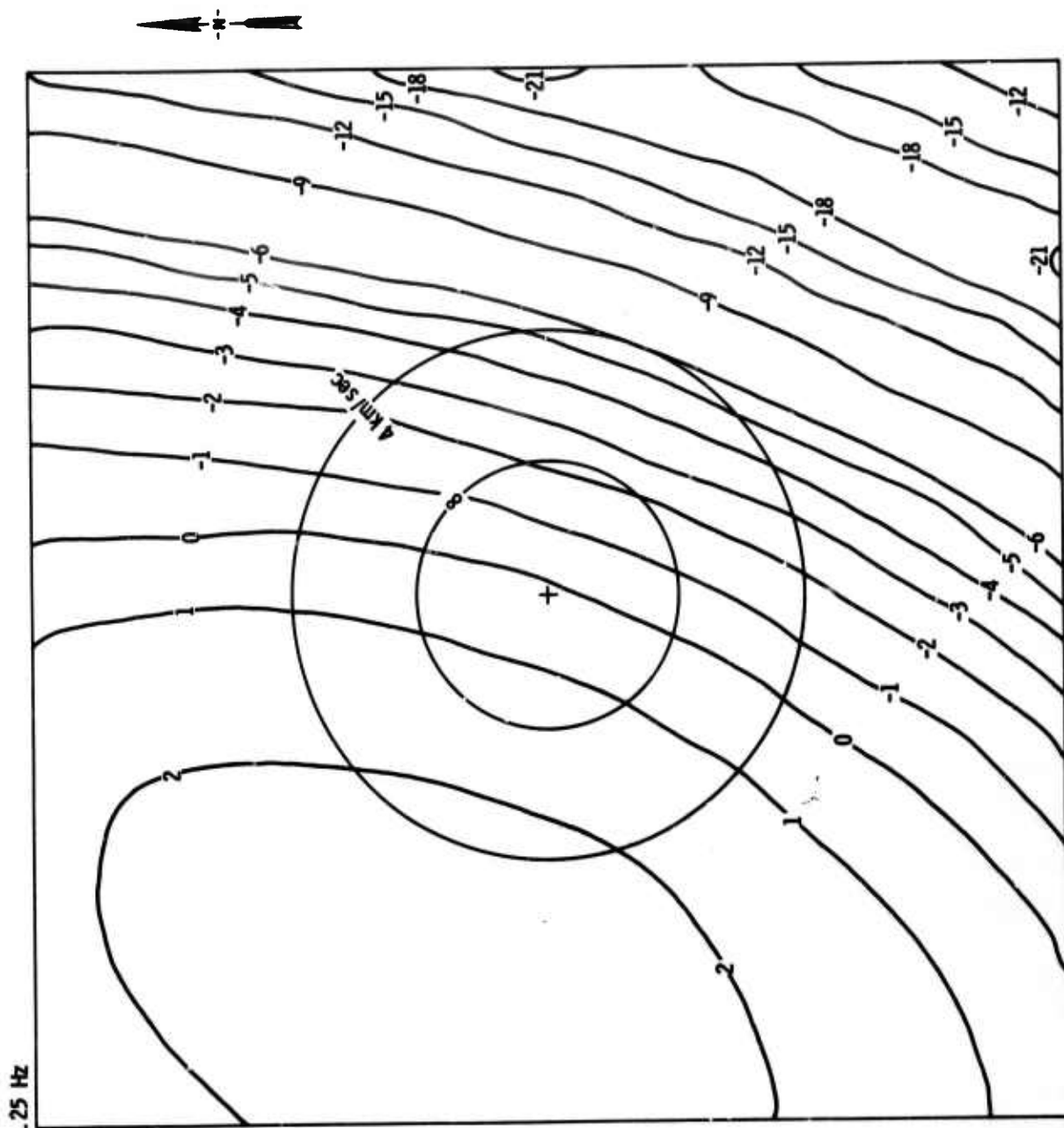


Figure III-21. Fixed Adaptive Maximum-Likelihood Filter Response

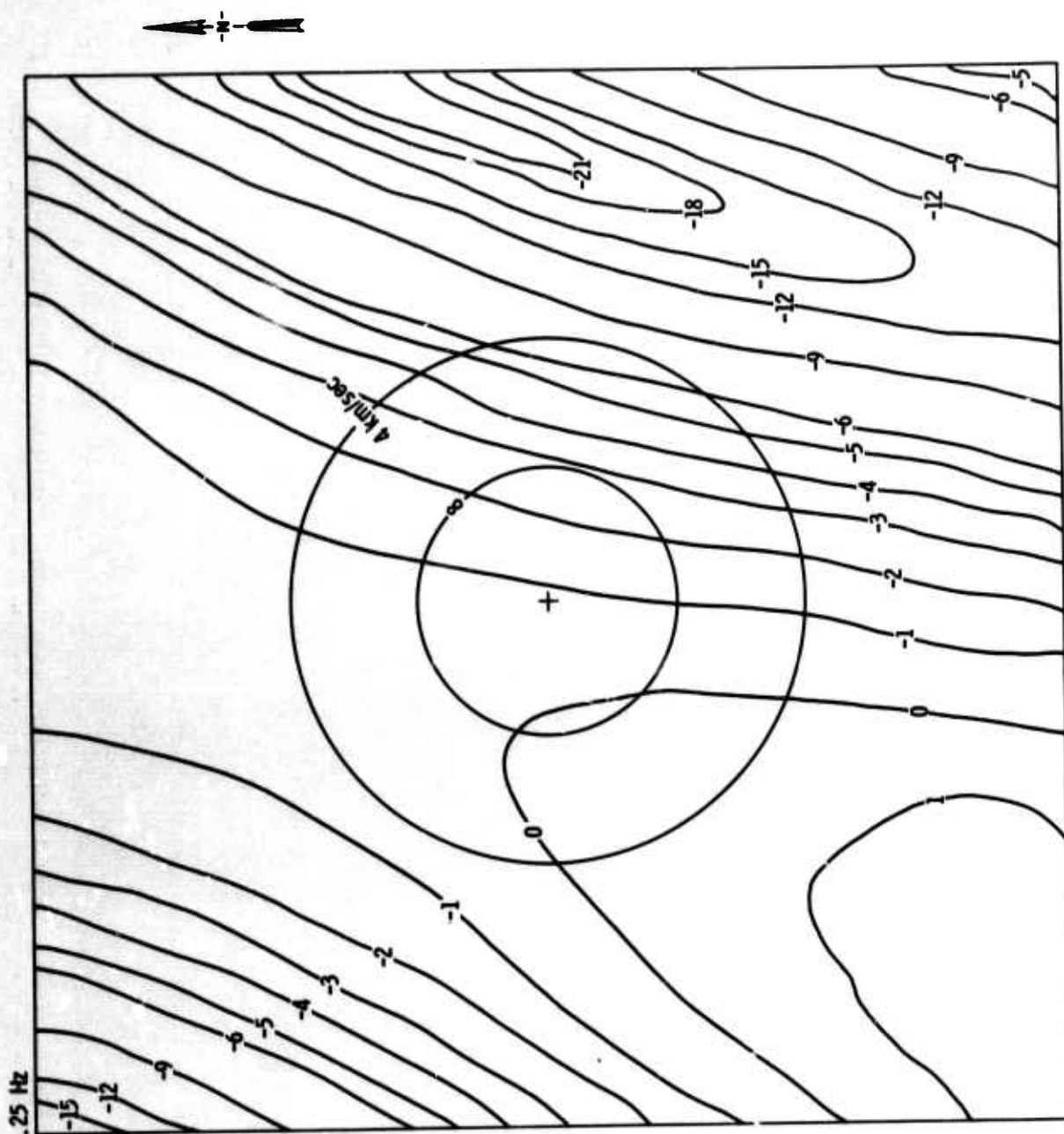


Figure III-22. Wiener Filter Response



SECTION IV

REFERENCES

1. Texas Instruments Incorporated, 1967: Adaptive Filtering of Seismic Array Data, Advanced Array Research Spec. Rpt. No. 1, Contract F33657-67-C-0708-P001, 18 Sep.
2. Stanford Electronics Laboratories, 1966: Adaptive Filters I: Fundamentals, Tech. Rpt. No. 6764-6, Contract DA-01-021 AMC-900-5(Y), Dec.
3. Texas Instruments Incorporated, 1968: Theoretical Considerations in Adaptive Processing, Advanced Array Research Spec. Rpt. No. 13, Contract F33657-67-C-0708-P001, 28 Feb.
4. Texas Instruments Incorporated, 1967: Study of Teleseisms Recorded at Cumberland Plateau Observatory, Array Research Spec. Rpt. No. 25, Contract AF 33(657)-12747, 28 Feb.
5. Teledyne, Inc., 1966: Two Examples of Maximum-Likelihood Filtering of LASA Seismograms, Contract AF 33(657)15919, 8 Jun.

UNCLASSIFIED

Security Classification

DOCUMENT CONTROL DATA - RAD

(Security classification of title, body of abstract and indexing annotation must be entered when the overall report is classified)

1. ORIGINATING ACTIVITY (Corporate author)

Texas Instruments Incorporated
Science Services Division
P. O. Box 5621, Dallas, Texas 75222

2a. REPORT SECURITY CLASSIFICATION

Unclassified

2b. GROUP

3. REPORT TITLE

PREDICTION ERROR AND ADAPTIVE MAXIMUM-LIKELIHOOD PROCESSING
ADVANCED ARRAY RESEARCH - SPECIAL REPORT NO. 10

4. DESCRIPTIVE NOTES (Type of report and inclusive dates)

Special

5. AUTHOR(S) (Last name, first name, initial)

Booker, Aaron H.
Holyer, Ronald J.

6. REPORT DATE

28 February 1968

7a. TOTAL NO. OF PAGES

122

7b. NO. OF REFS

5

8a. CONTRACT OR GRANT NO.

F33657-67-C-0708-P001

8b. PROJECT NO.

VELA T/7701

8c. ORIGINATOR'S REPORT NUMBER(S)

9b. OTHER REPORT NO(S) (Any other numbers that may be assigned this report)

10. AVAILABILITY/LIMITATION NOTICES

This document is subject to special export controls and each transmittal to foreign governments or foreign nationals may be made only with prior approval of Chief, AFTAC.

11. SUPPLEMENTARY NOTES

ARPA Order No. 624

12. SPONSORING MILITARY ACTIVITY

Advanced Research Projects Agency
Department of Defense
The Pentagon, Washington, D. C. 20301

13. ABSTRACT

Adaptive multichannel prediction-error filtering is compared to conventional optimum Wiener filtering for 10 types of array data. Adaptive maximum-likelihood signal extraction is compared to Wiener filtering for three sets of data; the three sets are composed of actual signal, artificial signal with varying magnitude and velocity, and a composite of noise data. Comparison of the two methods is based on total mean-square-error and the distribution of the error power with frequency. Online adaptive processing will solve problems with slowly time-varying noise fields such as UBO road noise. The adaptive method is also simpler and more economical than the Wiener method as an off-line filter design procedure for array data known to be approximately time stationary. The two methods will produce essentially equivalent filters with respect to total mean-square-error; however, relatively large differences in the actual filter response characteristics are possible.

14. KEY WORDS	LINK A		LINK B		LINK C	
	ROLE	WT	ROLE	WT	ROLE	WT
Advanced Array Research Prediction Error Adaptive Maximum-Likelihood Processing						

INSTRUCTIONS

1. **ORIGINATING ACTIVITY:** Enter the name and address of the contractor, subcontractor, grantee, Department of Defense activity or other organization (corporate author) issuing the report.

2a. **REPORT SECURITY CLASSIFICATION:** Enter the overall security classification of the report. Indicate whether "Restricted Data" is included. Marking is to be in accordance with appropriate security regulations.

2b. **GROUP:** Automatic downgrading is specified in DoD Directive 5200.10 and Armed Forces Industrial Manual. Enter the group number. Also, when applicable, show that optional markings have been used for Group 3 and Group 4 as authorized.

3. **REPORT TITLE:** Enter the complete report title in all capital letters. Titles in all cases should be unclassified. If a meaningful title cannot be selected without classification, show title classification in all capitals in parentheses immediately following the title.

4. **DESCRIPTIVE NOTES:** If appropriate, enter the type of report, e.g., interim, progress, summary, annual, or final. Give the inclusive dates when a specific reporting period is covered.

5. **AUTHOR(S):** Enter the name(s) of author(s) as shown on or in the report. Enter last name, first name, middle initial. If military, show rank and branch of service. The name of the principal author is an absolute minimum requirement.

6. **REPORT DATE:** Enter the date of the report as day, month, year; or month, year. If more than one date appears on the report, use date of publication.

7a. **TOTAL NUMBER OF PAGES:** The total page count should follow normal pagination procedures, i.e., enter the number of pages containing information.

7b. **NUMBER OF REFERENCES:** Enter the total number of references cited in the report.

8a. **CONTRACT OR GRANT NUMBER:** If appropriate, enter the applicable number of the contract or grant under which the report was written.

8b, 8c, & 8d. **PROJECT NUMBER:** Enter the appropriate military department identification, such as project number, subproject number, system numbers, task number, etc.

9a. **ORIGINATOR'S REPORT NUMBER(S):** Enter the official report number by which the document will be identified and controlled by the originating activity. This number must be unique to this report.

9b. **OTHER REPORT NUMBER(S):** If the report has been assigned any other report numbers (either by the originator or by the sponsor), also enter this number(s).

10. **AVAILABILITY/LIMITATION NOTICES:** Enter any limitations on further dissemination of the report, other than those

imposed by security classification, using standard statements such as:

- (1) "Qualified requesters may obtain copies of this report from DDC."
- (2) "Foreign announcement and dissemination of this report by DDC is not authorized."
- (3) "U. S. Government agencies may obtain copies of this report directly from DDC. Other qualified DDC users shall request through _____."
- (4) "U. S. military agencies may obtain copies of this report directly from DDC. Other qualified users shall request through _____."
- (5) "All distribution of this report is controlled. Qualified DDC users shall request through _____."

If the report has been furnished to the Office of Technical Services, Department of Commerce, for sale to the public, indicate this fact and enter the price, if known.

11. **SUPPLEMENTARY NOTES:** Use for additional explanatory notes.

12. **SPONSORING MILITARY ACTIVITY:** Enter the name of the departmental project office or laboratory sponsoring (paying for) the research and development. Include address.

13. **ABSTRACT:** Enter an abstract giving a brief and factual summary of the document indicative of the report, even though it may also appear elsewhere in the body of the technical report. If additional space is required, a continuation sheet shall be attached.

It is highly desirable that the abstract of classified reports be unclassified. Each paragraph of the abstract shall end with an indication of the military security classification of the information in the paragraph, represented as (TS), (S), (C), or (U).

There is no limitation on the length of the abstract. However, the suggested length is from 150 to 225 words.

14. **KEY WORDS:** Key words are technically meaningful terms or short phrases that characterize a report and may be used as index entries for cataloging the report. Key words must be selected so that no security classification is required. Identifiers, such as equipment model designation, trade name, military project code name, geographic location, may be used as key words but will be followed by an indication of technical context. The assignment of links, rules, and weights is optional.